

# **From Harmony to Dissonance**

**An organoid-based study of chromosomal instability and  
aneuploidy in colorectal cancer progression**

Richard H. van Jaarsveld

**ISBN:** 978-94-6375-306-7

**Copyright:** © 2019 by Richard H. van Jaarsveld

**Printed by:** Ridderprint

**Cover design by:** R.H. van Jaarsveld & Ridderprint

The cover shows an edited picture taken from a human colorectal cancer derived organoid line which was filmed as part of the research described in this thesis.

# **From Harmony to Dissonance**

## **An organoid-based study of chromosomal instability and aneuploidy in colorectal cancer progression**

Van Harmonie naar Dissonantie: Een op organoids gebaseerde studie  
naar chromosomale instabiliteit en aneuploidie in colorectale kanker  
progressie

(met een samenvatting in het Nederlands)

### **Proefschrift**

ter verkrijging van de graad van doctor aan de Universiteit Utrecht op gezag van  
de rector magnificus, prof. dr. H.R.B.M. Kummeling, ingevolge het besluit van het  
college voor promoties in het openbaar te verdedigen op dinsdag 5 maart 2019 des  
ochtends te 10.30 uur

door

**Richard Hermanus van Jaarsveld**

geboren op 3 juni 1987 te Woerden

**Promotor: Prof. dr. G.J.P.L. Kops**



Opgedragen aan Harry van Jaarsveld (1953 - 2006)

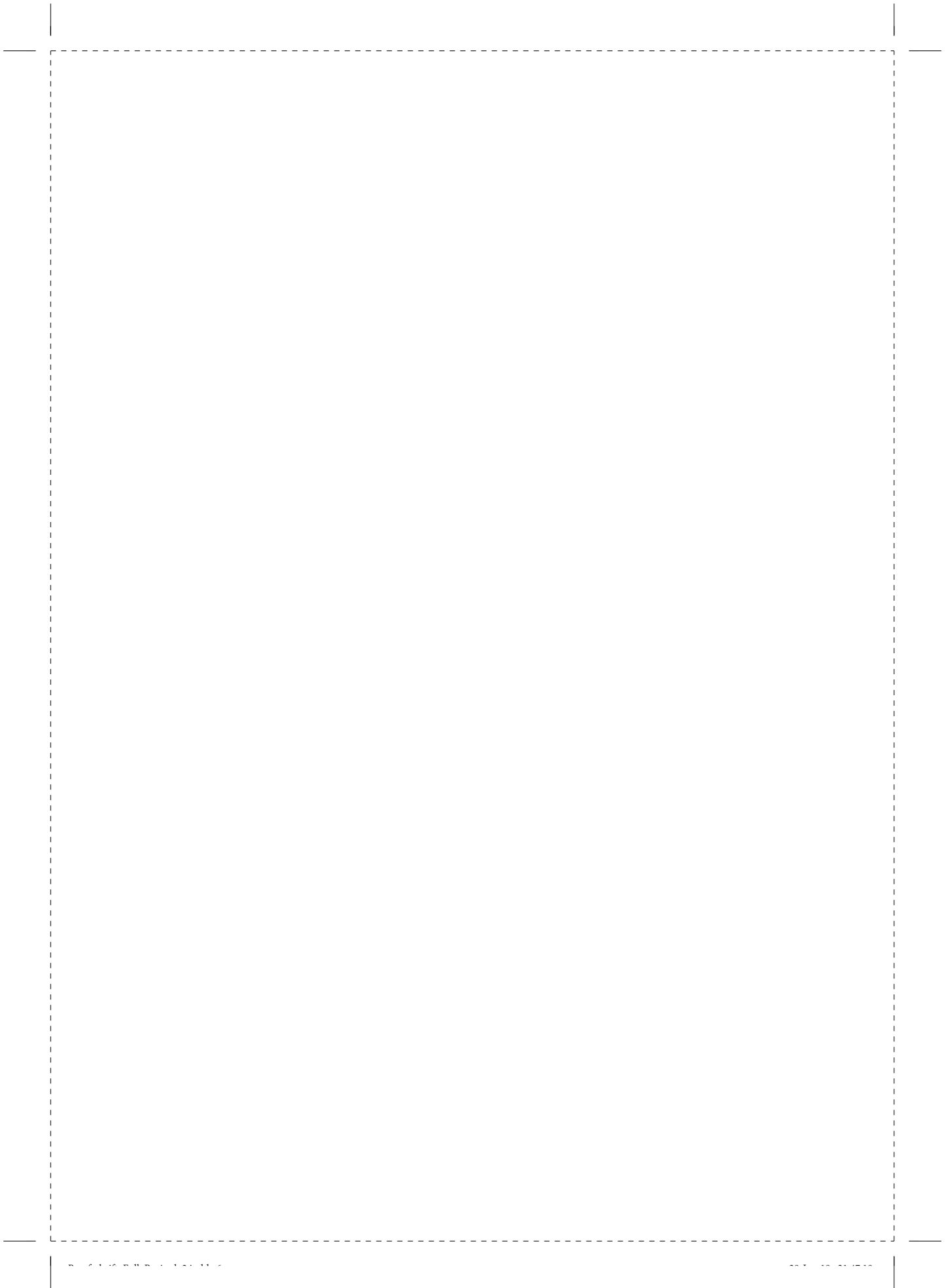
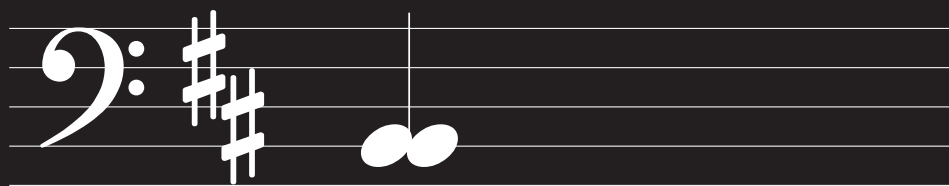


# Table of Contents

<b>Chapter 1</b>	<b>9</b>
Introduction	
<b>Chapter 2</b>	<b>25</b>
Difference Makers: Chromosomal instability versus aneuploidy in cancer	
<b>Chapter 3</b>	<b>47</b>
Sequential cancer mutations in cultured human intestinal stem cells	
<b>Chapter 4</b>	<b>77</b>
p38 restrains chromosomal instability upon p53 loss in human colon organoid cultures	
<b>Chapter 5</b>	<b>103</b>
The onset of chromosomal instability is associated with oncogenic transformation in colorectal cancer	
<b>Chapter 6</b>	<b>125</b>
Individual chromosomes differ in propensity for missegregation in SAC-compromised cells	
<b>Chapter 7</b>	<b>143</b>
Summary & Discussion	
<b>Addendum</b>	<b>157</b>
Nederlandse Samenvatting	
Nederlands Curriculum Vitae	
List of Publications	
Dankwoord	



# Chapter 1

## Introduction

## Cancer: Mutations and Genetic Instability

Cancer arises when healthy cells acquire features that enables them to proliferate in an uncontrolled fashion outside of their normal environment. The acquisition of such features is facilitated by mutations in the genome that obscure the normal functions of genes. Mutations that lead to the activation of oncogenes or the inactivation of tumor-suppressor genes and thereby contribute to oncogenic transformation are termed 'driver' mutations. The number of driver mutations needed for full malignant transformation is estimated between 1-10 per tumor, but likely differs between specific tumor types and between patients [1]. Despite this limited number of mutations needed for malignant transformation, the amount of mutations found in tumors is generally a multitude of that number, up to a mutation frequency of 1,000/Mb [2]. The majority of these mutations are believed to not contribute to oncogenic transformation and are termed 'passengers'.

The high abundance of passenger mutations in human cancer is attributed to an elevated mutation rate that arises during -or possibly even causes- oncogenesis. This mutator phenotype is believed to be necessary to generate sufficient driver mutations through a stochastic process [3]. Many mutational processes have been identified to date, and they leave specific footprints in the tumor's DNA [4]. Ongoing mutagenesis in cancer cells is referred to as genetic instability, a feature that is now recognized as a hallmark of cancer [5]. Genetic instability can present in many forms, ranging from base substitutions, to epigenetic changes and to copy number alterations (CNAs). Interestingly, tumors generally harbor one dominant form of instability and the level of instability is believed to have an optimum where the mutagenesis level is beneficial for tumor evolution but limited in order to prevent genotoxicity [6-9].

## Aneuploidy and Chromosomal Instability

One of the most dramatic manifestations of genome instability in cancer is aneuploidy. Aneuploidy describes a state in which a cell harbors a set of chromosomes that is not an exact multiple of the haploid set and can present in multiple forms. Aneuploid karyotypes can harbor whole chromosome gains and losses or structural aberrations, including fusions, inversions, translocations and intra-chromosomal duplications and deletions. The majority of human tumors are aneuploid [10] and aneuploidy can therefore be considered a hallmark of cancer. The gains and losses of chromosomes are considered to contribute to oncogenic transformation by increasing the expression of oncogenes and decreasing expression or providing loss-of-heterozygosity for tumor suppressors, respectively [11-15].

Aneuploidy results from chromosome segregation errors during mitosis [12, 14]. Faithful chromosome segregation depends on a number of conditions (Figure 1). First, all chromosomes have to be fully and correctly duplicated during S-phase. Incomplete duplication leaves chromosomes intertwined and pulling forces during anaphase results in stretching and potentially breakage of these chromosomes [16, 17] (Figure 1B).

To ensure correct and complete genome duplication, multiple pathways are in place to monitor the process [18]. Second, the duplicated chromosomes have to be equally divided over the daughter cells during mitosis. To achieve this, all chromosome pairs have to attach to the mitotic spindle in a bipolar fashion, i.e. each sister chromatid has to attach to opposite sides of the mitotic spindle (Figure 1A). Chromosome attachment to the spindle is facilitated by protein-rich structures located at the centromeres known as kinetochores. An example of erroneous attachment is merotelic attachment (Figure 1B). This occurs when microtubules from opposing sides attach to the same kinetochore which results in pulling of the chromatid towards both sides, causing a lagging chromosome during anaphase if the erroneous attachment is not resolved (Figure 1B). To prevent chromosome missegregation, the attachment status of kinetochores to the mitotic spindle is monitored by two main surveillance mechanisms:

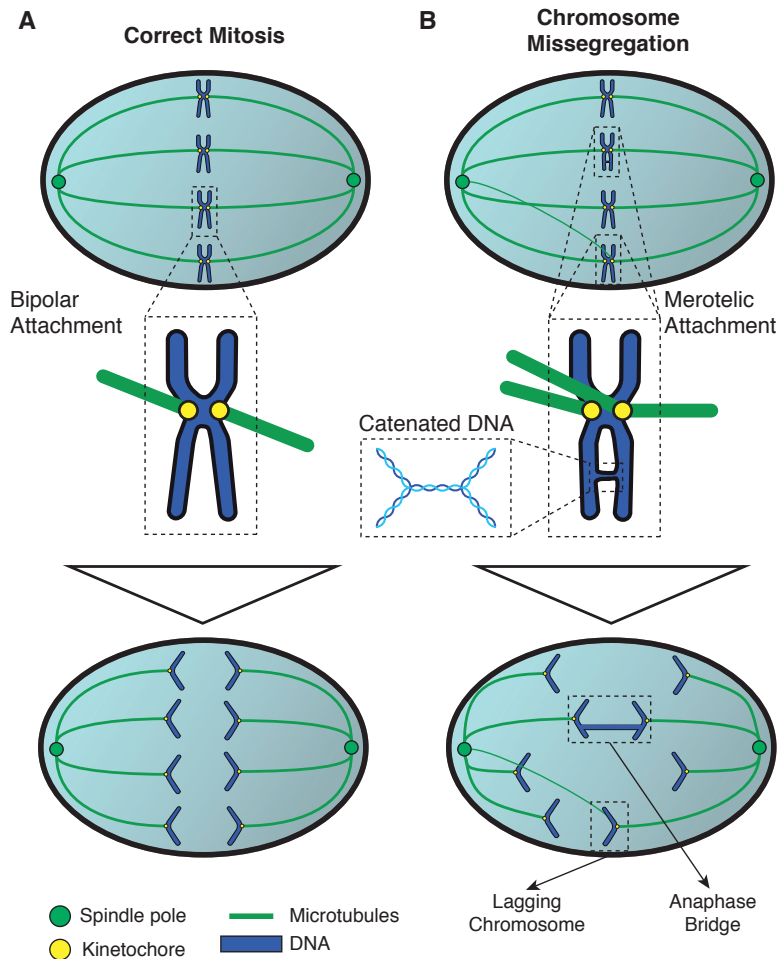


**Figure 1: Conditions to achieve correct chromosome segregation.** A) During mitosis, all chromosome pairs have to align to the metaphase plate (top panel) and attach to the mitotic spindle (microtubules in green) in a bipolar fashion. This means that each kinetochore pair (yellow circles) has to attach to opposite spindle poles (green circles) so that each sister chromatid will be pulled to opposite sides during anaphase (bottom panel). B) Chromosome missegregation can occur when cells enter mitosis while not all chromosomes have been fully duplicated. Under replicated regions remain as intertwined or catenated DNA that results in an anaphase bridge when the chromatids are pulled apart (bottom panel). DNA catenates can also result from other aberrant DNA structures such as DNA-damage repair foci. Lagging chromosomes result from erroneous attachments of the mitotic spindle to kinetochores. Shown is a merotelic attachment, which is formed when one kinetochore is attached to opposite sides of the spindle. Other attachment errors can be syntelic (both sister kinetochores are attached to the same side) or monotelic (only one kinetochore is attached).



the spindle-assembly checkpoint (SAC) and the error-correction pathway. Defects in those mechanisms can lead to premature anaphase onset and subsequent chromosome missegregation [19, 20]. Elevated levels of chromosome missegregation occur human cancer and this phenotype is referred to as chromosomal instability (CIN) [21].

CIN can constantly generate new karyotypes and can thus be considered a form of genetic instability. The genetic consequences of CIN are however not limited to gross CNAs. Chromosome missegregation can lead to DNA-damage, likely by means of chromosome breakage during cytokinesis [22, 23]. Missegregated chromosomes can furthermore end up in micronuclei which can lead to additional DNA-damage and extensive genome rearrangements such as chromothripsis [24–27]. DNA-damage foci in turn can result in subsequent chromosome missegregation [17, 28, 29], and thus one missegregation event can potentially induce a vicious cycle of DNA-damaging events. Furthermore, chromosome missegregation can disrupt cytokinesis, giving rise to polyploid cells due to failure of abscission or cytokinetic furrow regression [30, 31].

The influences of CIN on tumorigenesis have been widely studied with a variety of mouse models [32]. These models generally harbor germline mutations in SAC genes that cause attenuated checkpoint signaling to induce elevated chromosome missegregation rates. When combined with tumor prone mouse models, CIN can increase tumor burden or accelerate tumorigenesis. For instance, heterozygous deletion of *Mad211* caused increased tumor frequencies in *Tp53<sup>-/-</sup>* mice [33]. However, combination with *Bub3<sup>-/-</sup>* mice show no differences in tumor incidence in a *Tp53<sup>-/-</sup>* background [34]. Similar discrepancies have been reported regarding spontaneous tumor development in CIN models. Whereas *Plk1<sup>-/-</sup>* mice spontaneously develop a variety of tumors, *Bub1b* hypomorph mice do not develop cancer [35, 36]. This variety of observations might be due to differences in gene specific functions (possibly non-mitotic) or mouse strains. Another explanation however might be that the level of missegregation determines the tumorigenic potential of CIN, according to an optimum level of genetic instability. Indeed, combination of *Cenpe<sup>-/-</sup>* and *Mad211<sup>-/-</sup>* increased missegregation rates but decreased tumor burden as compared to the single mutants [37].

In addition to its influence on tumor formation, CIN has been implicated in different aspects of cancer biology as well. For instance, CIN increases the metastatic potential of cancer cells [38, 39] and has been implicated in therapy resistance and tumor relapse [40, 41]. On the contrary, CIN can present therapeutic opportunities by increasing the missegregation levels to an extent where the resulting aneuploidies and DNA-damage are no longer compatible with survival [8, 9]. Indeed, elevated CIN levels reduce tumorigenesis and elevated CIN levels can kill cancer cells [37, 42].

Despite its central role in shaping tumor karyotypes and its contributions to oncogenic transformation, the underlying mechanisms leading to CIN in human cancer remain obscure. Correct chromosome segregation however depends on many pathways, and therefore it is unlikely there is one common mechanisms that leads to CIN. Indeed, many mechanisms have been reported to give rise to CIN, including replication stress [17], altered microtubule dynamics [43], centrosome amplification [44-46] and weakened cohesion [47, 48]. Besides the causes for CIN, it is furthermore unclear when CIN arises during tumor progression and whether CIN is constantly present over the course of tumorigenesis. Understanding the causes and consequences of CIN during tumorigenesis might aid in cancer prevention, detection and in developing anti-cancer therapies.

## Thesis outline

### **Organoids to study CIN in colorectal cancer development**

This thesis aims to contribute to our understanding of CIN in tumorigenesis. To that aim, we employed studies based on a recently developed culturing technique known as organoids to study CIN in colorectal cancer (CRC) development. This approach was based on a number of considerations. First, we chose to study CRC development since it is well described in terms of molecular and pathological tumorigenesis and CIN is well studied in the context of CRC [21, 49-53]. Second, we conduct organoid studies since organoids are a closer resemblance of the tissue of origin than conventional cell lines and can be grown directly from a variety of lesion

biopsies or resections [54, 55]. The latter is an important advantage over classical two-dimensional cell lines since there is no cell line available that represents pre-malignant lesions in CRC. Finally, organoids from healthy and cancerous intestinal tissues are available and well characterized [55–60] and so CRC is the optimal tumor type to study cancer progression based on organoid cultures.

### Basics of intestinal epithelium renewal

The epithelial layer covering the intestinal tract is organized into crypts and villi. The epithelium renews every four to five days [61], which is facilitated by proliferation of progenitor cells that reside within the crypts [62]. At the bottom of the crypts remain the stem cells, which provide the regenerative capacity of the intestine. Intestinal stem cells are marked by the R-spondin receptor *Lgr5*, which serves for amplifying Wnt signaling, the main pathway controlling stemness in the intestine [63]. Wnt signaling facilitates the stabilization of the  $\beta$ -catenin transcription factor by sequestering its negative regulator APC. Stem cells generate trans amplifying (TA) cells that subsequently give rise to the differentiated cell types that cover the villus. Proliferation in the crypts is thus essential for self-renewal of the intestine and is, besides the Wnt pathway, driven by EGFR-signaling [64]. EGFR binds its ligand EGF to activate a MAPK signaling cascade that includes KRAS, MEK and ERK kinases to drive a transcriptional program that facilitates proliferation and other functions [65]. Finally, the crypt-villus organization is maintained by controlling BMP signaling. Activated BMP signaling facilitates the formation of crypts and is therefore inhibited in the villus compartment by its negative regulator NOGGIN [66].

### Colorectal cancer development

CRC can be classified into two distinct forms according to the mutational landscape of the tumor. First, about 15% of CRCs harbor high burdens of point mutations and are referred to as hypermutated [67]. The accumulation of base substitutions in those tumors is attributed to mutations in the mismatch repair machinery (MMR, e.g. *MLH1* and *MSH3* [68]) or the proofreading domains of DNA polymerases (e.g. *POLE*) [69]. Defects in MMR cause a specific form of genetic instability known as

microsatellite instability (MSI or MIN) [70]. Germline mutations in genes like *MLH1* and other MMR genes cause a hereditary cancer syndrome known as hereditary nonpolyposis CRC (HNPCC) also known as Lynch syndrome [71]. HNPCC patients have a lifetime risk of 80% to develop CRC.

The remainder (~85%) of CRCs is characterized by high levels of CNAs in the genome of the tumor and relatively low burden of point mutations and are therefore referred to as non-hypermutated [67]. Based on the highly aberrant karyotypes found in these tumors and to distinguish them from MIN tumors, they are often referred to as CIN. It is however important to notice here that this terminology can be confusing, since their aneuploid karyotypes do not necessarily mean these tumors have elevated missegregation rates. For a detailed discussion on this topic, readers are referred to **Chapter 2**. The karyotypes found in these tumors show many common characteristics. Common gains include chromosomes 7, 8q, 13 and 20 [67]. Whereas chromosomes 7, 8q and 20 are commonly found amplified in other tumor types as well, the gain of chromosome 13 is specific for CRC since this chromosome is commonly lost in tumors originating from other organs [72]. Common chromosome losses include 8p and 18. The most commonly gene mutated in non-hypermutated CRC is the *APC* gene [67]. Germline mutations in *APC* are associated with a hereditary CRC syndrome known as familial adenomatous polyposis (FAP) [73]. FAP patients develop high burdens of adenomas in the colon and ultimately develop CRC. The adenoma burden in Lynch syndrome patients however is much lower [74]. It thus appears there are two distinct routes to develop CRC based on the genetic instability mechanism involved: hypermutation or CIN.

Two main models for CRC development have been described. The first states that CRC progress gradually according to a stepwise development known as the adenoma-to-carcinoma sequence [51]. Healthy tissue first transforms into less organized, hyperproliferative tissue to form an adenoma which generally presents as a polyp. Later in the development of the tumor, cells start invading neighboring tissues and ultimately become malignant. Based on the prevalence of driver mutations in the different steps, the adenoma-to-carcinoma sequence has been proposed to

occur via distinct, successive genetic alterations that drive the progression of the tumor [51]. This model involves mutations in *APC*, *TP53*, *KRAS* and *SMAD4*, mutations mostly associated with non-hypermuted tumors [67] and therefore likely describes the development of CIN tumors specifically. An alternative model for CRC development, known as the big bang model, has recently been proposed based on in-depth analysis of multiregional sequencing of adenomas and carcinomas [52]. According to this model, the tumor is formed by a defining moment of crisis in which all mutations needed for full malignant transformation are acquired. Instead of gradually developing by a multi-step nature, the metastatic potential of a tumor is thus defined at the beginning of tumorigenesis. Acquisition of only part of the mutations needed for full malignant transformations during the genomic crisis therefore limits the malignant potential of the tumor and this provides an alternative explanation for the mutation prevalence at different tumor stages that initially formed the core observations to develop the adenoma-to-carcinoma model. In concordance with limiting malignant potential, the majority of colorectal adenomas do not develop into invasive carcinomas [75].

Since it is unknown whether CIN is present in pre-malignant lesions, the contribution of CIN to the development of CRC remains unknown. The presence of CRC associated aneuploidies in FAP patient adenomas [76] however suggests that CIN arises at or before the adenoma stage according to the stepwise model. The alternative explanation could be that chromosome missegregation at the moment of genetic crisis contributes to forming the metastatic potential of the tumor but has limited influence of the remainder of tumor growth. CIN would thus be present at the early stages of CRC development but is not necessarily needed for further development of the tumor. The presence of CIN in end-stage tumors might therefore be merely a remainder of the moment of genetic crisis (in case mitotic fidelity has not been regained after the crisis), which might point to a more severe crisis moment and might therefore hint towards higher malignant potential. Understanding the role of CIN in CRC development might therefore aid in the assessment of risk to develop CRC.

## Organoids

Organoids are three-dimensional, stem cell-based cultures that closely represent the tissue of origin [54, 55, 58]. Culturing and maintaining organoids is based on the expansion of stem cells by means of providing stem cell niche factors via the growth medium [77]. In the case of intestinal organoids, the medium contains the growth factors RPSO1 (R-spondin1), NOGGIN and EGF. R-Spondin1 is an Lgr-5 ligand that amplifies Wnt signaling which is essential for intestinal stemness [63]. NOGGIN is an inhibitor of BMP signaling and serves to facilitate crypt formation [66]. Finally, EGF activates EGFR signaling to increase proliferation rates. Depending on the species (mouse or human) and tissue of origin (small intestine, colon or rectum), the medium might furthermore contain Wnt3A and some small-molecule inhibitors to reduce stress responses or maintain stemness. Seeding of the cells in basement-membrane-extract-based gels provides a protein rich matrix that allows for the three-dimensional growth and formation of tissue-resembling structures. Organoids can be manipulated by standard techniques such as plasmid transfection and viral infection, making them an outstanding model for investigating tissue homeostasis and pathology.

## Thesis Contents

The thesis presented here contains a collection of studies that aim to understand the causes and consequences of CIN in CRC development. **Chapter 2** gives an overview of current literature on CIN and aneuploidy and their influence on cancer evolution and therapy response. Furthermore, it argues that CIN should be measured independently of aneuploidy and CIN levels should be based on visualization of chromosome missegregation during anaphase. **Chapter 3** describes the generation of an artificial recreation of the adenoma-to-carcinoma sequence by means of CRISPR/Cas9 mutagenesis in organoids derived from healthy intestinal tissues. We find that CIN coincides with the loss of p53 and continue in **Chapter 4** to characterize the role of p53 in preventing CIN. We describe how loss of p53 renders CRC cells dependent on p38 activity to prevent chromosome missegregation and how combined loss of p53 and p38 leads to the formation of a specific type of anaphase bridges. To investigate the onset of CIN in naturally occurring tumors as opposed to the artificial tumorigenesis in Chapters 3 and 4, **Chapter 5** presents the first analysis of CIN in human adenomas

and additional analysis of CIN in human CRC-derived organoids, revealing that CIN is associated with oncogenic transformation. Finally, the study presented in **Chapter 6** reveals that not all chromosomes have an equal chance to missegregate when the spindle-assembly checkpoint is impaired. The thesis ends with an in-depth discussion on how the results presented in this thesis relate to previous observations and how the conclusions of this thesis open the way for translating CIN research to clinically valuable insights.

## References

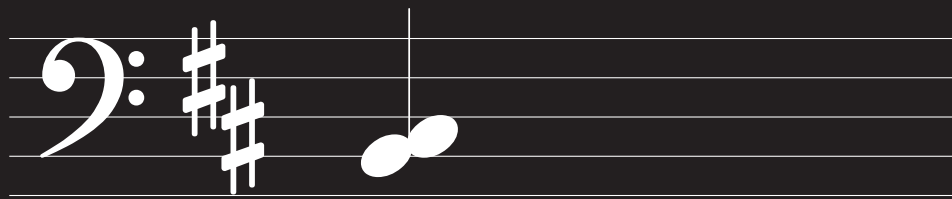
1. Martincorena, I., et al., *Universal Patterns of Selection in Cancer and Somatic Tissues*. Cell, 2017. **171**(5): p. 1029-1041 e21.
2. Campbell, B.B., et al., *Comprehensive Analysis of Hypermutation in Human Cancer*. Cell, 2017. **171**(5): p. 1042-1056 e10.
3. Loeb, L.A., *Mutator Phenotype May Be Required for Multistage Carcinogenesis*. Cancer Research, 1991. **51**(12): p. 3075-3079.
4. Alexandrov, L.B., et al., *Signatures of mutational processes in human cancer*. Nature, 2013. **500**(7463): p. 415-21.
5. Hanahan, D. and R.A. Weinberg, *Hallmarks of Cancer: The Next Generation*. Cell, 2011. **144**(5): p. 646-674.
6. Alexandrov, L.B. and M.R. Stratton, *Mutational signatures: the patterns of somatic mutations hidden in cancer genomes*. Curr Opin Genet Dev, 2014. **24**: p. 52-60.
7. Andor, N., et al., *Pan-cancer analysis of the extent and consequences of intratumor heterogeneity*. Nat Med, 2016. **22**(1): p. 105-13.
8. Janssen, A. and R.H. Medema, *Genetic instability: tipping the balance*. Oncogene, 2013. **32**(38): p. 4459-4470.
9. van Jaarsveld, R.H. and G.J.P.L. Kops, *Difference Makers: Chromosomal Instability versus Aneuploidy in Cancer*. Trends Cancer, 2016. **2**(10): p. 561-571.
10. Duijf, P.H.G., N. Schultz, and R. Benezra, *Cancer cells preferentially lose small chromosomes*. International Journal of Cancer, 2012. **132**(10): p. 2316-2326.
11. Santaguida, S. and A. Amon, *Short- and long-term effects of chromosome mis-segregation and aneuploidy*. Nature reviews. Molecular cell biology, 2015. **16**(8): p. 473-485.
12. Kops, G.J.P.L., B.A.A. Weaver, and D.W. Cleveland, *On the road to cancer: aneuploidy and the mitotic checkpoint*. Nature reviews. Cancer, 2005. **5**(10): p. 773-785.
13. Orr, B., K.M. Godek, and D. Compton, *Aneuploidy*. Current Biology, 2015. **25**(13): p. R538-R542.
14. Gordon, D.J., B. Resio, and D. Pellman, *Causes and consequences of aneuploidy in cancer*. Nat Rev Genet, 2012. **13**(3): p. 189-203.
15. Weaver, B.A.A. and D.W. Cleveland, *Does aneuploidy cause cancer?* Current Opinion in Cell Biology, 2006. **18**(6): p. 658-667.
16. Mankouri, H.W., D. Huttner, and I.D. Hickson, *How unfinished business from S-phase affects mitosis and beyond*. The EMBO Journal, 2013. **32**(20): p. 2661-2671.
17. Burrell, R.A., et al., *Replication stress links structural and numerical cancer chromosomal instability*. Nature, 2013. **494**(7438): p. 492-496.
18. Blackford, A.N. and S.P. Jackson, *ATM, ATR, and DNA-PK: The Trinity at the Heart of the DNA Damage Response*. Mol Cell, 2017. **66**(6): p. 801-817.
19. Sacristan, C. and G.J. Kops, *Joined at the hip: kinetochores, microtubules, and spindle assembly checkpoint signaling*. Trends Cell Biol, 2015. **25**(1): p. 21-8.
20. Musacchio, A., *The Molecular Biology of Spindle Assembly Checkpoint Signaling Dynamics*. Curr Biol, 2015. **25**(20): p. R1002-18.
21. Lengauer, C., K.W. Kinzler, and B. Vogelstein, *Genetic instability in colorectal cancers*. Nature, 1997. **386**(6625): p. 623-627.
22. Janssen, A., et al., *Chromosome segregation errors as a cause of DNA damage and structural chromosome aberrations*. Science, 2011. **333**(6051): p. 1895-1898.
23. Crasta, K., et al., *DNA breaks and chromosome pulverization from errors in mitosis*. Nature, 2012. **482**(7383): p. 53-58.
24. Zhang, C.-Z., et al., *Chromothripsis from DNA damage in micronuclei*. Nature, 2015. **522**(7555): p. 179-184.
25. Terradas, M., et al., *DNA lesions sequestered in micronuclei induce a local defective-damage response*. DNA Repair (Amst), 2009. **8**(10): p. 1225-34.
26. Terradas, M., et al., *Nuclear envelope defects impede a proper response to micronuclear DNA lesions*. Mutat Res, 2012. **729**(1-2): p. 35-40.
27. Hoffelder, D.R., et al., *Resolution of anaphase bridges in cancer cells*. Chromosoma, 2004. **112**(8): p. 389-97.
28. Bakhoun, S.F., et al., *DNA-Damage Response during Mitosis Induces Whole-Chromosome Missegregation*. Cancer discovery, 2014. **4**(11): p. 1281-1289.
29. Chan, Y.W., K. Fugger, and S.C. West, *Unresolved recombination intermediates lead to ultra-fine anaphase bridges, chromosome breaks and aberrations*. Nat Cell Biol, 2018. **20**(1): p. 92-103.
30. Steigemann, P., et al., *Aurora B-mediated abscission checkpoint protects against tetraploidization*. Cell, 2009. **136**(3): p. 473-84.



31. Mullins, J.M. and J.J. Biesele, *Terminal phase of cytokinesis in D-98s cells*. J Cell Biol, 1977. **73**(3): p. 672-84.
32. Schvartzman, J.-M., R. Sotillo, and R. Benezra, *Mitotic chromosomal instability and cancer: mouse modelling of the human disease*. Nature reviews. Cancer, 2010. **10**(2): p. 102-115.
33. Chi, Y.H., et al., *Spindle assembly checkpoint and p53 deficiencies cooperate for tumorigenesis in mice*. Int J Cancer, 2009. **124**(6): p. 1483-9.
34. Kalitsis, P., et al., *Increased chromosome instability but not cancer predisposition in haploinsufficient Bub3 mice*. Genes Chromosomes Cancer, 2005. **44**(1): p. 29-36.
35. Lu, L.Y., et al., *Polo-like kinase 1 is essential for early embryonic development and tumor suppression*. Mol Cell Biol, 2008. **28**(22): p. 6870-6.
36. Baker, D.J., et al., *BubR1 insufficiency causes early onset of aging-associated phenotypes and infertility in mice*. Nat Genet, 2004. **36**(7): p. 744-9.
37. Silk, A.D., et al., *Chromosome missegregation rate predicts whether aneuploidy will promote or suppress tumors*. Proc Natl Acad Sci U S A, 2013. **110**(44): p. E4134-41.
38. Bakhom, S.F., et al., *Chromosomal instability drives metastasis through a cytosolic DNA response*. Nature, 2018. **553**(7689): p. 467-472.
39. Godek, K.M., et al., *Chromosomal Instability Affects the Tumorigenicity of Glioblastoma Tumor-Initiating Cells*. Cancer Discov, 2016.
40. Ryan, S.D., et al., *Up-regulation of the mitotic checkpoint component Mad1 causes chromosomal instability and resistance to microtubule poisons*. Proc Natl Acad Sci U S A, 2012. **109**(33): p. E2205-14.
41. Sotillo, R., et al., *Mad2-induced chromosome instability leads to lung tumour relapse after oncogene withdrawal*. Nature, 2010. **464**(7287): p. 436-440.
42. Janssen, A., G.J. Kops, and R.H. Medema, *Elevating the frequency of chromosome mis-segregation as a strategy to kill tumor cells*. Proc Natl Acad Sci U S A, 2009. **106**(45): p. 19108-13.
43. Bakhom, S.F., G. Genovese, and D.A. Compton, *Deviant kinetochore microtubule dynamics underlie chromosomal instability*. Curr Biol, 2009. **19**(22): p. 1937-42.
44. Godinho, S.A., et al., *Oncogene-like induction of cellular invasion from centrosome amplification*. Nature, 2014: p. 1-18.
45. Fukasawa, K., et al., *Abnormal centrosome amplification in the absence of p53*. Science, 1996. **271**(5256): p. 1744-7.
46. Ganem, N.J. and D. Pellman, *Linking abnormal mitosis to the acquisition of DNA damage*. J Cell Biol, 2012. **199**(6): p. 871-81.
47. Zhang, N., et al., *Overexpression of Separase induces aneuploidy and mammary tumorigenesis*. Proc Natl Acad Sci U S A, 2008. **105**(35): p. 13033-8.
48. Barber, T.D., et al., *Chromatid cohesion defects may underlie chromosome instability in human colorectal cancers*. Proc Natl Acad Sci U S A, 2008. **105**(9): p. 3443-8.
49. Rajagopalan, H., et al., *The significance of unstable chromosomes in colorectal cancer*. Nature reviews. Cancer, 2003. **3**(9): p. 695-701.
50. Shih, I.M., et al., *Evidence that genetic instability occurs at an early stage of colorectal tumorigenesis*. Cancer Research, 2001. **61**(3): p. 818-822.
51. Fearon, E.R. and B. Vogelstein, *A genetic model for colorectal tumorigenesis*. Cell, 1990. **61**(5): p. 759-767.
52. Sottoriva, A., et al., *A Big Bang model of human colorectal tumor growth*. Nature genetics, 2015. **47**(3): p. 209-216.
53. Pino, M.S. and D.C. Chung, *The Chromosomal Instability Pathway in Colon Cancer*. Gastroenterology, 2010. **138**(6): p. 2059-2072.
54. Drost, J. and H. Clevers, *Organoids in cancer research*. Nat Rev Cancer, 2018. **18**(7): p. 407-418.
55. Sato, T., et al., *Long-term Expansion of Epithelial Organoids From Human Colon, Adenoma, Adenocarcinoma, and Barrett's Epithelium*. Gastroenterology, 2011. **141**(5): p. 1762-1772.
56. Fujii, M., et al., *A Colorectal Tumor Organoid Library Demonstrates Progressive Loss of Niche Factor Requirements during Tumorigenesis*. Cell Stem Cell, 2016.
57. Matano, M., et al., *Modeling colorectal cancer using CRISPR-Cas9-mediated engineering of human intestinal organoids*. Nature Medicine, 2015. **21**(3): p. 256-262.
58. Sato, T., et al., *Single Lgr5 stem cells build crypt-villus structures in vitro without a mesenchymal niche*. Nature, 2009. **459**(7244): p. 262-265.
59. van de Wetering, M., et al., *Prospective derivation of a living organoid biobank of colorectal cancer patients*. Cell, 2015. **161**(4): p. 933-945.
60. Drost, J., et al., *Sequential cancer mutations in cultured human intestinal stem cells*. Nature, 2015. **521**(7550): p. 43-47.
61. van der Flier, L.G. and H. Clevers, *Stem cells, self-renewal, and differentiation in the intestinal epithelium*. Annu Rev Physiol, 2009. **71**: p. 241-60.
62. Clevers, H., *The intestinal crypt, a prototype stem cell compartment*. Cell, 2013. **154**(2): p. 274-84.

63. de Lau, W., et al., *The R-spondin/Lgr5/Rnf43 module: regulator of Wnt signal strength*. Genes Dev, 2014. **28**(4): p. 305-16.
64. Marchbank, T., et al., *Luminal epidermal growth factor is trophic to the small intestine of parenterally fed rats*. Clin Sci (Lond), 1995. **89**(2): p. 117-20.
65. Chen, J., et al., *Expression and Function of the Epidermal Growth Factor Receptor in Physiology and Disease*. Physiological Reviews, 2016. **96**(3): p. 1025-1069.
66. Haramis, A.P., et al., *De novo crypt formation and juvenile polyposis on BMP inhibition in mouse intestine*. Science, 2004. **303**(5664): p. 1684-6.
67. Cancer Genome Atlas, N., *Comprehensive molecular characterization of human colon and rectal cancer*. Nature, 2012. **487**(7407): p. 330-337.
68. Vilar, E. and S.B. Gruber, *Microsatellite instability in colorectal cancer—the stable evidence*. Nat Rev Clin Oncol, 2010. **7**(3): p. 153-62.
69. Palles, C., et al., *Germline mutations affecting the proofreading domains of POLE and POLD1 predispose to colorectal adenomas and carcinomas*. Nat Genet, 2013. **45**(2): p. 136-44.
70. Thibodeau, S.N., G. Bren, and D. Schaid, *Microsatellite instability in cancer of the proximal colon*. Science, 1993. **260**(5109): p. 816-9.
71. Sinicrope, F.A., *Lynch Syndrome-Associated Colorectal Cancer*. N Engl J Med, 2018. **379**(8): p. 764-773.
72. Hoadley, K.A., et al., *Multiplatform analysis of 12 cancer types reveals molecular classification within and across tissues of origin*. Cell, 2014. **158**(4): p. 929-944.
73. Jasperson, K.W., S.G. Patel, and D.J. Ahnen, *APC-Associated Polyposis Conditions*, in *GeneReviews*(R), M.P. Adam, et al., Editors. 1993, University of Washington, Seattle. GeneReviews is a registered trademark of the University of Washington, Seattle: Seattle WA.
74. Kalady, M.F., et al., *Defining the adenoma burden in lynch syndrome*. Dis Colon Rectum, 2015. **58**(4): p. 388-92.
75. Brenner, H., et al., *Risk of progression of advanced adenomas to colorectal cancer by age and sex: estimates based on 840,149 screening colonoscopies*. Gut, 2007. **56**(11): p. 1585-9.
76. Borrás, E., et al., *Genomic Landscape of Colorectal Mucosa and Adenomas*. Cancer Prev Res (Phila), 2016. **9**(6): p. 417-27.
77. Clevers, H., *Modeling Development and Disease with Organoids*. Cell, 2016. **165**(7): p. 1586-1597.





# Chapter 2

## Difference Makers: Chromosomal instability versus aneuploidy in cancer

R.H. van Jaarsveld<sup>1,2</sup> and G.J.P.L. Kops<sup>1,2,3</sup>

<sup>1</sup> Hubrecht Institute – KNAW (Royal Netherlands Academy of Arts and Sciences) Uppsalalaan 8, 3584 CT Utrecht, The Netherlands.

<sup>2</sup> Cancer Genomics Netherlands, and <sup>3</sup>Center for Molecular Medicine, University Medical Center Utrecht, 3584 CG, Utrecht, The Netherlands.

Trends in Cancer, 2016. 2(10): p. 561-571

## Abstract

Human cancers harbor great numbers of genomic alterations. One of the most common is aneuploidy, an imbalance at the chromosome level. Some aneuploid cancer cell populations show varying chromosome copy number alterations over time, a phenotype known as ‘chromosomal instability’ (CIN). Chromosome segregation errors in mitosis are the most common cause for CIN *in vitro*, and these are also thought to underlie the aneuploidies seen in clinical cancer samples. CIN and aneuploidy are however different traits and they are likely to have distinct impacts on tumor evolution and clinical tumor behavior. Here we discuss these differences and describe scenarios in which distinguishing them can be clinically relevant.

## Aneuploidy and chromosomal instability in cancer

The development of neoplastic lesions is accompanied by the accumulation of genomic mutations [1]. Recent sequencing efforts greatly enhanced our understanding of cancer genomes and their evolution. These studies strongly suggest that elevated mutation rates combined with evolutionary dynamics ultimately ensure clonal expansion of tumor cells, giving rise to heterogeneous tumors [2, 3].

One of the most dramatic manifestations of genomic alterations in cancer is aneuploidy. Aneuploidy describes a karyotype that deviates from an exact multiple of the haploid set of chromosomes, resulting in genetic imbalances. The presence of aneuploidy in cancer is widespread and diverse [4], with great heterogeneity within tumors [5-7] and between different tumor types. For instance, about 65% of lung tumors [8] and 91% of glioblastomas [9] are reported to be aneuploid, whereas aneuploidy is rare in early stage prostate cancer [10, 11]. A recent study estimated that approximately 70% of all human tumors are aneuploid [9]. In addition, on average, ~30% of the genome of a tumor shows copy number alterations [12].

Cancer genomes are generally dynamic, owing to underlying genetic instability phenotypes and changes in selective pressures in the course of tumorigenesis [1, 13]. Different mechanisms of genomic instability have been described and each can be recognized by specific mutational signatures [13, 14]. Instability is also observed at the whole chromosome level and was first described to be present in cell lines derived from colorectal tumors [15]. By determining the copy-number of specific chromosomes in single cells, it was shown that the chromosomal content within certain cell populations varied over time. This phenotype was named 'Chromosomal Instability' (CIN), and was proposed to result from errors in chromosome segregation during mitosis. Indeed CIN cell lines typically show decreased mitotic fidelity [16-18]. CIN can have additional causes, including erroneous or unfinished replication [19], and entosis [20]. For simplicity's sake we refer to cells that evolve novel karyotypes over time as CIN, irrespective of underlying mechanisms, but note that it

most commonly relates to errors during mitotic chromosome segregation.

Confusingly, the term CIN has been widely used not only to describe the tendency for mitotic errors in cells that lead to karyotype divergence, but also in the classification of aneuploid tumors to distinguish them from hypermutated tumors. As such, 'CIN' is a term used to describe fundamentally different traits. Recent advances however led to plausible hypotheses on how aneuploidy and CIN may differentially affect tumor behavior, therapy response and tumor relapse. We therefore argue that considering them as distinct traits is relevant for cancer research and therapy. In this essay we highlight data that underscores the differences between aneuploidy and mitotic infidelity and provide scenarios in which the distinction can be clinically relevant.

## **Chromosomal traits: definitions, differences and interplay**

Aneuploidy, karyotype divergence and CIN are thus closely linked but not identical traits (Our operational definitions of the three chromosomal traits -aneuploidy, CIN and karyotype divergence- are clarified in Box 1). In principle, karyotype divergence can result solely from evolutionary dynamics in a heterogeneously aneuploid population and therefore, although CIN at one time caused the heterogeneity, CIN is not necessarily present in such populations (Fig. 1a). The evolutionary dynamics are likely driven by selection for optimal karyotypes, but might also result from genetic drift (Fig. 1a, population 3 to 4 and 2 to 3, respectively). An example of such dynamics is the Big Bang model of colorectal cancer evolution, in which catastrophic events (possibly mitotic errors) in a primordial tumor cell generates a population of cells with a high level of genetic variation. This population then expands to generate intermixed subclones, which changes over time as a result of evolutionary dynamics [21]. Interestingly, this model has recently been proposed to explain punctuated karyotype evolution in triple-negative breast tumors [22]. Karyotype divergence can thus be present in the absence of CIN. One important implication from this notion is that the level of CIN cannot be inferred from karyotype measurements. This concept



is further clarified in figure 1a, which shows the progression of a cell population from homogeneously diploid (Fig. 1a, population 1) to heterogeneously aneuploid (populations 2, 3 & 4) but with distinct causes for karyotype changes at different stages in the life of the population. Importantly, karyotype measurements from the populations 2, 3 and 4 will show karyotype divergence, and CIN may falsely be inferred.

Several observations support the notion that CIN and aneuploidy are not necessarily directly correlated. A case in point is the human colorectal carcinoma cell line HCT 116 that is aneuploid but mitotically stable. In addition, single cell sequencing (SCSing) of breast cancers suggested that in those patients aneuploid rearrangements occurred early but were then maintained stably since there were little karyotypic variances between cells [22-24]. The breast cancer cells may thus not be CIN. Finally, a recent study showed that non-regenerating tissues in a CIN mouse strain are highly aneuploid while regenerating tissues were not [25]. Aneuploidy measurements thus do not directly relate to the level of mitotic errors in these mice.

#### Text Box 1: Operating definitions of aneuploidy, karyotype divergence and CIN

In order to clearly discriminate between the chromosomal traits, we here provide our operational definitions as used throughout this essay:

Aneuploidy is the state of having a karyotype that deviates from an exact multiple of the haploid set of chromosomes and thus refers to the *genotype*. The level of aneuploidy refers to the number of imbalanced chromosomes.

Karyotype divergence is a *population phenotype* in which fractions of cells with specific karyotypes change over time. The level of divergence refers to the changes in size and number of fractions over time.

CIN is the acquired elevated chance of unequal distribution of genomic content over two daughter cells, and is thus a *cellular phenotype*. The level of CIN refers to the frequency and severity of these errors over successive cell division cycles.

Although the three traits are intimately linked, they are fundamentally different. Therefore, the presence of one does not necessarily require the presence of another at a given point in time. For instance, CIN leads to aneuploid progeny and karyotypically divergent populations, but an aneuploid cell or cells within divergent populations do not necessarily remain CIN (Fig. 1a). The CIN phenotype can be temporary (e.g. due to environmental factors) and the resulting aneuploid progeny may regain the ability for high fidelity mitotic cell divisions.

In conclusion, aneuploidy, karyotype divergence and CIN are linked but distinct traits. Importantly, since unstable aneuploidies in a population can result from ongoing mitotic errors but also from evolutionary dynamics, a CIN phenotype cannot be directly inferred from static karyotype measurements in experimental or clinical samples.

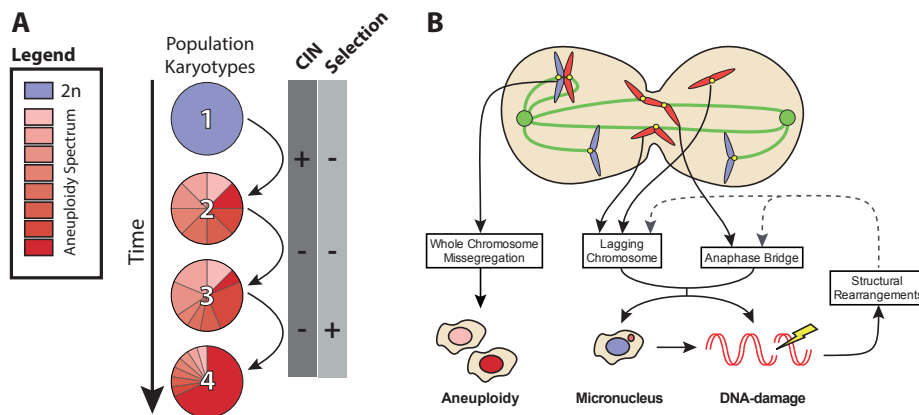


**Figure 1: Distinguishing aneuploidy, karyotype divergence and chromosomal instability.** A) During the generation of a heterogeneously aneuploid population (for example a tumor), the karyotypes in the population are initially caused by chromosomal instability (CIN) and subsequently selected for via evolutionary mechanisms. Once a heterogeneous population has been formed, CIN is no longer essential to cause karyotype divergence. The level of aneuploidy or karyotype divergence therefore does not necessarily reflect the level of CIN. Pie chart depict cell populations; the colors reflect diploid (blue) or different aneuploid (shades of red) karyotypes. B) Chromosome missegregation can occur in different forms. Whole chromosome missegregation leads to aneuploid progeny. Lagging chromosomes and anaphase bridges can cause the formation of micronuclei and DNA-damage. Erroneous repair can subsequently result in chromosome rearrangements that in turn can give rise to lagging chromosomes and anaphase bridges.

## CIN vs. aneuploidy on cellular fitness and proliferation

Although debated for liver and brain [26–32], aneuploidy is rare in adult tissues. This is in agreement with the incompatibility of constitutional aneuploidies with organismal development: In humans all autosomal aneuploidies, with the exception of trisomies 13, 18 and 21, are embryonic lethal [33]. Some patients with somatic mosaic and

variegated aneuploidies on the other hand can survive until well into childhood, but suffer from mental and growth retardation and delayed development [34].

In accordance with the problems that present at the organismal level, aneuploidy decreases fitness at the cellular level. Both mammalian and yeast cells have reduced proliferation rates when aneuploid [35–38], mainly resulting from general aneuploidy-induced proteotoxic and metabolic stresses [35, 39, 40]. The association of aneuploidy with decreased cellular fitness on the one hand and cancer on the other appears counterintuitive. In fact, cancer cells are the only cell type known to maintain or even increase their proliferation rate while being aneuploid. This ‘*aneuploidy paradox*’ in cancer has raised questions regarding the causative roles of mitotic errors and aneuploidy in oncogenesis [37]. The aneuploidy paradox is not yet resolved, but it seems likely that cancer cells have acquired aneuploidy tolerance, either by mutations or by altered environments that favor the proliferation of aneuploid cells. The acquisition of aneuploidy tolerance was shown to be a plausible scenario in yeast [41, 42].

Mitotic errors lead to aneuploid progeny and therefore impaired fitness. In addition, chromosome missegregation events can induce DNA-damage and thereby activate DNA-damage response mechanisms that generally lead to p53-mediated cell-cycle arrest or apoptosis [43–46]. The nature of the CIN phenotype, however, potentially enables acquisition of compensatory mutations that allow cell cycle progression of aneuploid cells. For example, disruption of p53 function is a widely used approach to ensure cell-cycle progression of cells after a mitotic error. Therefore, if the error itself affects the p53 locus, cells may be able to escape cell-cycle arrest or apoptosis. The CIN phenotype may thus overcome at least the direct problems associated with aneuploidy.

## CIN vs. aneuploidy on genome integrity

The consequence of aneuploidy for the genome is mostly limited to alterations in gene copy numbers. In stark contrast, mitotic errors can have extensive secondary effects on genome integrity (Fig. 1b). Although the underlying causes are still unclear and probably not limited to one mechanism, laboratory CIN cancer cell lines show specific forms of mitotic errors known as lagging chromosomes and anaphase-bridges [16-18]. These are chromosomes that are not migrating with either of the two packs of chromosomes during anaphase. As a result they are trapped in the cleavage furrow or form a separate micronucleus in one of the daughter cells [46, 47] (Fig. 1b). Trapped chromosomes can acquire double strand DNA breaks that are repaired by the error-prone non-homologous end joining (NHEJ) pathway in G1, resulting in structural rearrangements like translocations [46]. Such genomic rearrangements have also been observed in tumors of a CIN mouse model [48].

Micronuclei too can give rise to DNA damage and genomic rearrangements. The chromosomes in micronuclei suffer from replication stress and are additionally damaged when their fragile nuclear envelope collapses, exposing the DNA to the hostile cytoplasm [47, 49]. The catastrophic chromosome fragmentation results in various kinds of genome rearrangements, including chromothripsis [50-52]. In the longer term, when cells harboring rearranged chromosomes are allowed to continue to proliferate, a subset of those cells may engage in a breakage-fusion-bridge (BFB) cycle [53, 54], thus creating a vicious cycle of chromosome missegregation and genome insults (Fig. 1b, dashed lines).

While aneuploidy is a logical aberration in CIN cells, the reverse may also occur. Several studies have suggested that aneuploidy can predispose to additional aneuploidies, genome rearrangements, and increased mutational burden on the nucleotide level [37, 55-59]. Aneuploidy may thus cause a CIN phenotype, adding another layer to the vicious cycle described above. However, other studies have contradicted this [18, 60] and the presence of stably aneuploid cancer cell lines (like HCT-116) implies CIN is not an obligatory outcome of aneuploidy.

## CIN vs. aneuploidy on the course of tumor evolution

Given that CIN cells frequently reshuffle their genomes and aneuploidy is a static state, the two are predicted to influence the evolutionary dynamics of a developing tumor in distinct ways. During tumorigenesis, CIN increases population plasticity by stochastically providing genomic variants that are subsequently enriched or purged via evolutionary dynamics (Fig. 1a). Accordingly, CIN could be a promoter of tumorigenesis, and indeed CIN can act to enhance or even initiate tumorigenesis in several mouse models [61] while stable aneuploidies impair embryonic development [36, 62]. CIN mouse models usually have decreased mitotic fidelity due to germ line mutations in genes that regulate mitosis. Therefore, elevated mitotic errors are present already from conception onwards. Since CIN might have different influences on tumorigenesis in different tissues and at different points during tumor evolution, conditional CIN animal models will advance our understanding of CIN in tumor progression.

CIN levels in tumors are frequently inferred from karyotype analyses, which (as outlined above) cannot distinguish between ongoing mitotic errors and selection on karyotypes. Whether CIN is an early-acquired phenotype of tumor cells and whether CIN is present throughout tumor evolution is therefore currently unknown. In fact even the presence of aneuploidy in the tumor cannot speak to whether CIN is or has been present during the development of the tumor. The missegregation rate of healthy cells in 2D cell culture is estimated at ~0.025% per chromosome per division [18]. In certain instances, the aneuploid cells may remain in the population and can acquire more complex aneuploidies over time. *In silico* modeling has provided support for this, as aneuploidy tolerance in the absence of CIN was sufficient to explain the lower-grade aneuploidies observed in tumors, and CIN was only important to generate higher-grade aneuploidies [63]. Direct measurement of CIN will thus give answers regarding the presence of CIN in human tumors (see Box 2).

Whereas a CIN phenotype provides the ability to continuously reshape genomic content, allowing adaptation to changing environmental conditions, aneuploidy enables at best only a temporary advantage. Predominant aneuploidies within a tumor reflect the favored oncogenic karyotypes resulting from mitotic errors. These aneuploid karyotypes are thus not only the result of mitotic errors, but also from selection. This is illustrated by a number of observations. First, tumors generally harbor dominant karyotypic traits shared by the majority of tumor cells, which was recently shown to be also true in a CIN mouse model [64]. Second, different tumor types are characterized by different karyotypic traits, implying that specific genes on these chromosomes exert tissue-specific oncogenic benefits. For example, intestinal tumors typically gain copies of chromosome 13q [65–67] and glioblastoma multiform is generally characterized by gains of chromosome 7 and loss of 10 [68, 69]. Such differences enable discrimination between tumors originating from different tissue lineages, as well as specific tumor types [70]. Third, predisposition to certain types of cancer in hereditary aneuploidy patients depends on the specific karyotype involved [71]. Finally, increasing aneuploidy levels are generally correlated with later tumor stages, for example in breast [72] and colon cancer [73], suggesting that several rounds of selection accumulate different karyotypic changes during tumor evolution.

## **CIN vs. aneuploidy in therapy response and relapse**

Since therapeutic agents can be regarded as new selection pressures, CIN and aneuploidy might differentially influence therapy response and tumor relapse in ways similar to their impact on tumor evolution. The cellular plasticity provided by a CIN phenotype will therefore not only accelerate tumorigenesis, but also the outgrowth of resistant clones and thus tumor relapse. Aneuploidy, too, can have profound impact on therapy by similar mechanisms but with a different outlook after relapse and different options for combination therapies.

Let us consider two hypothetical tumors (Fig. 2). Both are karyotypically heterogeneous and have moderate to high aneuploidy tolerance. One however contains predominantly CIN cells while the other is mitotically stable. Note that both tumors show karyotype divergence, but that the divergence in the mitotically stable tumor is the result of evolutionary dynamics. When faced with a therapeutic

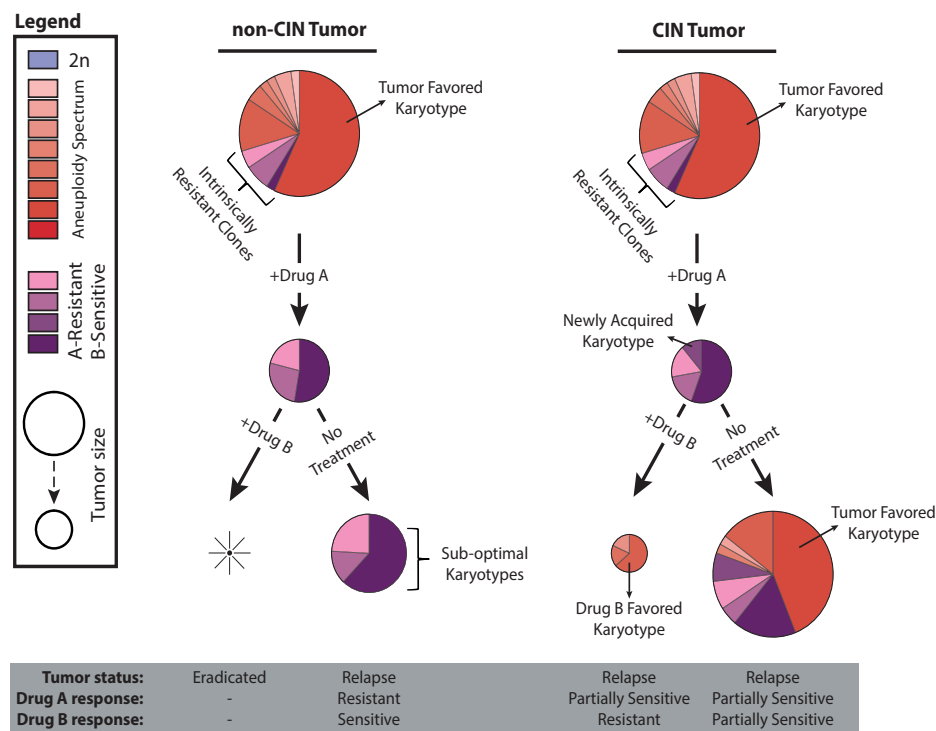


**Figure 2: Influences of CIN on response to therapy and tumor relapse.** Two karyotypically identical tumors, one of which contains cells with the chromosomal instability (CIN) phenotype (right side) are both treated with drug A. Intrinsically resistant clones in each tumor will survive. Additionally, CIN cells can generate new resistant karyotypes. The karyotypic characteristics that confer therapy resistance to drug A simultaneously induce sensitivity towards drug B. The tumor is now efficiently eradicated since only sensitive karyotypes populate the tumor, as these are selected for by drug A. The CIN tumor cells however can generate new resistant karyotypes and so this tumor will again present resistant clones. If no second treatment is applied after drug A, both tumors will relapse. In the non-CIN tumor only the selected clones will regrow, whereas in the CIN tumor new clones will be generated that can again gain the optimal karyotype for tumor growth. CIN can thus both enhance drug resistance and tumor relapse. Pie chart depict cell populations; the colors reflect diploid (blue) or different aneuploid (shades of red) karyotypes; red karyotypes are sensitive to drug A and resistant to drug B; orange depicts cells with karyotypes that are resistant to drug A and sensitive to drug B.

agent (Fig. 2; Drug A), most cells in both tumors will die but a small population will prove resistant as a result of certain karyotypes within that population. Heterogeneity in the surviving population will be greatly reduced. Interestingly, this population in the mitotically stable tumor is amenable to the ‘evolution trap’ approach, in which a second drug (Fig. 2; Drug B) specifically targets the karyotype that survived the first agent [74]. All tumor cells are eventually eradicated by the second line treatment. However, if the surviving cells are CIN they are likely to generate novel resistant karyotypes (i.e. acquired resistance). The relapsed tumor, while potentially resensitized to the original drug, is not amenable to the evolution trap approach. Although the scenario delineated above is at present purely theoretical, it illustrates the need for individual assessment of CIN, karyotype divergence and aneuploidy when addressing such therapeutic approaches. In the given example, karyotype measurements will not suffice in selecting the right populations.

In addition to enhanced resistance, CIN potentially also accelerates tumor relapse. The non-CIN tumor will regrow with sub-optimal karyotypes and is unable to quickly regain new karyotypes. The CIN cells in the other tumor can however accelerate the appearance of karyotypes optimal for tumor growth (Fig. 2). This enhanced tumor relapse has been observed *in vivo*, where induction of CIN by overexpression of Mad2 accelerated tumor relapse in a Ras-withdrawal lung cancer model [75].

In summary, both CIN and aneuploidy can theoretically provide therapy resistance via evolutionary mechanisms. But whereas aneuploid populations may harbor intrinsic resistant clones, CIN additionally provides cellular plasticity and might thereby promote acquired resistance and tumor relapse.

## CIN vs. aneuploidy in choice of therapy

Anti-mitotic agents like vinca alkaloids and taxanes are important clinical cancer therapy drugs. Both types of drugs interfere with microtubule dynamics and are well known inducers of mitotic delays. In 2D cultures, cells treated with taxol either undergo mitotic catastrophe or mitotic slippage [76]. A recent study examining the



**Text Box 2: Measuring CIN and aneuploidy**

Assessment of aneuploidy and CIN status in tumor samples will be required to test feasibility of therapeutic options described here. Although aneuploidy status can relatively quickly be determined by various karyotyping or FISH-based methods, such techniques have several limitations. Karyotyping generally requires trapping cells in mitosis and is therefore biased to fast-cycling cells. FISH can be performed on interphase nuclei but can only analyse a limited number of loci. Recent advances in SCSing approaches will aid in overcoming such limitations. Practical and economic arguments currently preclude widespread use of SCSing, but this may be the approach of choice when such issues are overcome [97]. SCSing gives genome-wide information at single-cell resolution and thereby allows estimation of intra-tumor heterogeneity and thus possibly additional clues regarding therapy sensitivity.

Determining the level of CIN in clinical samples is more challenging, since the rate and level of errors during cell divisions need to be assessed. Although not ideal in terms of quantification of all parameters, visual inspection of anaphases in H&E stained tumor sections may be sufficient to determine the severity and rate of segregation errors. The generally low mitotic indices in tumors may however complicate such approaches. To truly determine CIN, visualization of chromosome segregation over subsequent generations is required. In fundamental research settings, this is most commonly achieved by fluorescent labeling of histones and subsequent live-cell imaging. Although doable with simple and affordable imaging systems, various practical reasons complicate its use for patient material. A potential solution is the use of non-toxic DNA dyes such as SiR-DNA that can be added directly to the sample prior to imaging [98]. Another challenge is the need for living tumor material. This may be facilitated by recent developments in culturing stem cell based 'organoid' structures that develop *ex vivo* in membrane extract gels and in the presence of niche factors provided in the growth medium [99]. Organoids can be grown from tumors and retain the major characteristics of the original tumor, thus providing an excellent *ex vivo* intermediate model [100-104]. We have recently shown the onset of CIN in an artificial intestinal tumor progression organoid model [105], showing that imaging of mitotic errors in organoids is technically feasible. Improvements in low-cost high-resolution imaging and organoid cultures might make this type of approach a viable option for more widespread use in the future.

cytotoxic effects of paclitaxel in breast cancer reported that, at clinically relevant concentrations, the drug induces multipolar divisions [77]. Cells thus appeared to die as a result of too severe segregation errors (likely causing severe proteotoxicity and DNA damage, as outlined above). CIN cells may already have acquired substantial tolerance for segregation errors and as such may not be very sensitive to taxanes. In line with this, tumors deemed CIN by a CIN70 gene expression signature [78] were more resistant to taxanes [79], a correlation seen more widely [80]. It is unknown however if these tumors still made frequent mitotic errors, and it would be interesting to examine correlation between mitotic errors and taxane resistance.

Seemingly at odds with the observation that CIN tumors are more resistant to taxanes is the hypothesis, proposed by us and others, that CIN tumors might be sensitive to

exacerbation of mitotic errors. The sensitivity may depend on the level of increase of CIN induced by the treatment and whether this exceeds an aneuploidy-tolerance and/or DNA damage-tolerance threshold. This concept is in concordance with hormesis: The situation when a low dose of an entity is beneficial for cellular fitness while a high dose is lethal (Fig. 3). Indeed, CIN promotes tumor progression only at limited dose and is tumor suppressive at higher doses [81, 82] and these findings are supported by stochastic modeling of karyotype evolution [83, 84]. In addition, recent pan-cancer genome analysis suggested “the existence of an optimal degree of genomic instability” [85]. Increasing CIN to high levels by combining an attenuated spindle checkpoint with low doses of taxanes or inhibition of the mitotic kinesin CENP-E, killed tumor cells of various kinds *in vitro* [86, 87]. Inhibition of the spindle checkpoint was key in combination therapy studies, and drug discovery projects related to inhibition of TTK/Mps1, a crucial kinase in the spindle checkpoint, have been initiated by a number of companies. Various studies using xenograft models have verified that TTK/Mps1 inhibition can enhance the effect of taxol in treatment of, for example, triple negative breast cancer [88], glioblastoma [89, 90], and melanoma [91].

Whether the CIN hormesis concept will hold in clinical settings remains to be seen. Importantly, the efficacy of this approach relies on the ability of a given treatment to enhance CIN. Although a wide variety of drugs are capable of this [92], efficacy will vary between patients. It will therefore be important to determine CIN status when evaluating the feasibility of this approach (see Box 2). Enhancing CIN as a therapeutic strategy requires passing the ‘hormesis threshold’ and therefore CIN tolerance is an important factor. This tolerance is likely to consist of a combination of aneuploidy and DNA-damage tolerance. Interestingly, CIN tumors appear to be more sensitive to DNA damaging agents [79] and radiation therapy [93], which might be explained by exceeding the DNA damage component of CIN tolerance.

Aneuploidy may also be amenable to hormesis-based therapy, but by a different mechanism than CIN: By increasing the general stresses accompanying an unbalanced karyotype. Aneuploid cells tend to be more sensitive to inhibition of the pathways

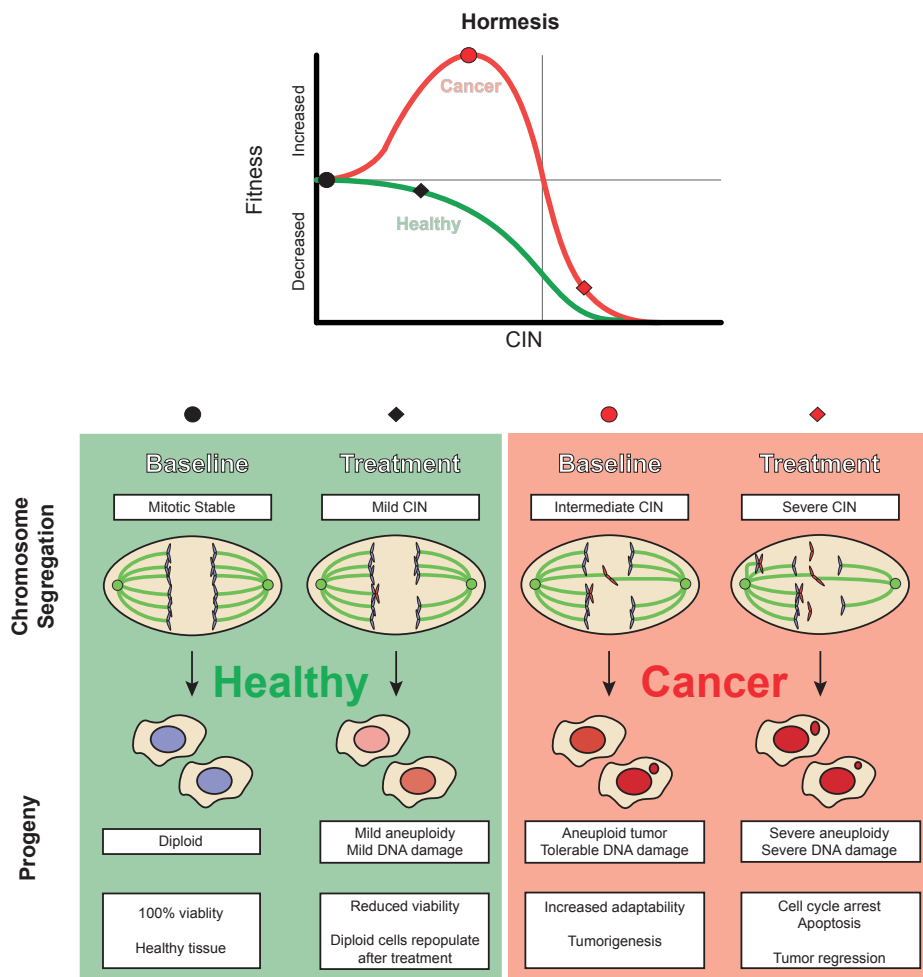


**Figure 3: Enhancing CIN as a strategy to kill CIN cells.** Chromosomal instability (CIN) probably acts according to hormesis in cancer cells, as illustrated by a hypothetical fitness curve (top). Whereas an intermediate level of CIN is beneficial for development of the tumor, higher levels will be detrimental for survival (red line). This benefit is likely absent in healthy cells (green line). Enhancing the baseline CIN level (round symbols) with a drug (square symbols) might be therapeutically beneficial. The increase of CIN in healthy cells will only mildly impair fitness of the progeny (green, left side), whereas increased mitotic errors in already CIN cells will generate severe aneuploidy and DNA damage and subsequent cell death (orange, right side). CIN levels are probably easier elevated in CIN cells, given they already contain intrinsic causes for missegregation, like dicentric chromosomes as illustrated on the right. Correct segregating chromosomes and diploid cells are depicted in blue, mis-segregating chromosomes and aneuploid cells are red.

regulating proteostasis, like protein folding and autophagy, resulting in toxic overload of these pathways [94, 95]. For a more elaborated view on aneuploidy as a therapeutic target, we refer interested readers to an excellent recent review [96].

Therapeutically exploiting aneuploidy will likely depend on the mechanism and level of aneuploidy tolerance in those cells. Since aneuploidy tolerance might be a bottleneck for increasing karyotypic divergence, low divergence might predict higher sensitivity towards such therapeutic strategies. They will obviously benefit from an absence of CIN (and thus cellular plasticity) as elaborated on above. Aneuploidy targeting strategies are thus likely most successful in mitotically stable, aneuploid tumors that show little divergence and thus this hypothesis again highlights the importance of individual assessment of CIN, aneuploidy and karyotypic divergence.

## Concluding Remarks

Whole-genome sequencing efforts in the past years made clear that no tumor is the same. Major improvements in cancer therapy will thus come from carefully matching individual patients with specific drugs, an approach referred to as personalized medicine. In order to select the best therapy, there is a great need for biomarkers, i.e. an identifiable, tumor specific feature that can predict drug response.

Here, we underpin the notion that more systemic alterations, i.e. CIN and aneuploidy, can impact tumor evolution and therapy response. This in turn may provide guidance in therapy-of-choice selection, and prompt the development of therapies that exploit vulnerabilities presented by either one. A broad empirical evidence basis to translate these insights to the clinic is currently lacking, and will require more careful assessment of CIN and aneuploidy in various cancer samples (Box 2), and assessment of correlation between this and the differential responses to therapies. Finally, distinguishing CIN from aneuploidy in cancers may help to address the long-standing questions as depicted in the Outstanding Questions section.

**Outstanding Questions:**

- 1: What are the main causes for CIN in human tumors?
- 2: Do human tumors retain a CIN phenotype, and if so, when during oncogenic transformation does CIN occur and does severity of CIN change during tumor progression?
- 3: How do CIN and aneuploidy influence tumor aggressiveness and therapy response?
- 4: Can CIN and/or aneuploidy be exploited in cancer therapy?
- 5: How do cancer cells benefit from and circumvent problems associated with aneuploidy?

**References**

1. Vogelstein, B., et al., *Cancer Genome Landscapes*. Science, 2013. **339**(6127): p. 1546–1558.
2. Hanahan, D. and R.A. Weinberg, *Hallmarks of Cancer: The Next Generation*. Cell, 2011. **144**(5): p. 646–674.
3. Greaves, M. and C.C. Maley, *Clonal evolution in cancer*. Nature, 2012. **481**(7381): p. 306–13.
4. Helm, S. and F. Mitelman, *Nonrandom Chromosome Abnormalities in Cancer—An Overview*. 2010: p. 25–43.
5. Furuya, T., et al., *Relationship between chromosomal instability and intratumoral regional DNA ploidy heterogeneity in primary gastric cancers*. Clin Cancer Res, 2000. **6**(7): p. 2815–20.
6. Di Vinci, A., et al., *Intratumor heterogeneity of chromosome 1, 7, 17, and 18 aneusomies obtained by FISH and association with flow cytometric DNA index in human colorectal adenocarcinomas*. Cytometry, 1999. **35**(4): p. 369–75.
7. Orndal, C., et al., *Cytogenetic intratumor heterogeneity in soft tissue tumors*. Cancer Genet Cytogenet, 1994. **78**(2): p. 127–37.
8. Choma, D., et al., *Aneuploidy and prognosis of non-small-cell lung cancer: a meta-analysis of published data*. Br J Cancer, 2001. **85**(1): p. 14–22.
9. Duijff, P.H.G., N. Schultz, and R. Benezra, *Cancer cells preferentially lose small chromosomes*. International Journal of Cancer, 2012. **132**(10): p. 2316–2326.
10. Shankey, T.V., et al., *Consensus review of the clinical utility of DNA content cytometry in prostate cancer*. Cytometry, 1993. **14**(5): p. 497–500.
11. Koivisto, P., *Aneuploidy and rapid cell proliferation in recurrent prostate cancers with androgen receptor gene amplification*. Prostate Cancer Prostatic Dis, 1997. **1**(1): p. 21–25.
12. Beroukhim, R., et al., *The landscape of somatic copy-number alteration across human cancers*. Nature, 2010. **463**(7283): p. 899–905.
13. Lengauer, C., K.W. Kinzler, and B. Vogelstein, *Genetic instabilities in human cancers*. Nature, 1998. **396**(6712): p. 643–649.
14. Alexandrov, L.B., et al., *Signatures of mutational processes in human cancer*. Nature, 2013. **500**(7463): p. 415–21.
15. Lengauer, C., K.W. Kinzler, and B. Vogelstein, *Genetic instability in colorectal cancers*. Nature, 1997. **386**(6625): p. 623–627.
16. Bakhom, S.F., et al., *The mitotic origin of chromosomal instability*. Current biology : CB, 2014. **24**(4): p. R148–9.
17. Tanno, Y., et al., *The inner centromere–shugoshin network prevents chromosomal instability*. Science, 2015. **349**(6253): p. 1237–1240.
18. Thompson, S.L. and D.A. Compton, *Examining the link between chromosomal instability and aneuploidy in human cells*. The Journal of cell biology, 2008. **180**(4): p. 665–672.
19. Burrell, R.A., et al., *Replication stress links structural and numerical cancer chromosomal instability*. Nature, 2013. **494**(7438): p. 492–496.
20. Krajcovic, M., et al., *A non-genetic route to aneuploidy in human cancers*. Nature cell biology, 2011. **13**(3): p. 324–330.
21. Sottoriva, A., et al., *A Big Bang model of human colorectal tumor growth*. Nature genetics, 2015. **47**(3): p. 209–216.
22. Gao, R., et al., *Punctuated copy number evolution and clonal stasis in triple-negative breast cancer*. Nat

- Genet, 2016.
23. Navin, N., et al., *Tumour evolution inferred by single-cell sequencing*. Nature, 2012. **472**(7341): p. 90–94.
  24. Wang, Y., et al., *Clonal evolution in breast cancer revealed by single nucleus genome sequencing*. Nature, 2014. **512**(7513): p. 155–160.
  25. Pfau, S.J., et al., *Aneuploidy impairs hematopoietic stem cell fitness and is selected against in regenerating tissues in vivo*. Genes Dev, 2016.
  26. McConnell, M.J., et al., *Mosaic copy number variation in human neurons*. Science, 2013. **342**(6158): p. 632–7.
  27. Knouse, K.A., et al., *Single cell sequencing reveals low levels of aneuploidy across mammalian tissues*. Proc Natl Acad Sci U S A, 2014. **111**(37): p. 13409–14.
  28. van den Bos, H., et al., *Single-cell whole genome sequencing reveals no evidence for common aneuploidy in normal and Alzheimer's disease neurons*. Genome Biol, 2016. **17**(1): p. 116.
  29. Duncan, A.W., et al., *Frequent Aneuploidy Among Normal Human Hepatocytes*. Gastroenterology, 2012. **142**(1): p. 25–28.
  30. Pack, S.D., et al., *Individual adult human neurons display aneuploidy: detection by fluorescence in situ hybridization and single neuron PCR*. Cell cycle (Georgetown, Tex.), 2005. **4**(12): p. 1758–1760.
  31. Rehen, S.K., et al., *Constitutional aneuploidy in the normal human brain*. The Journal of neuroscience : the official journal of the Society for Neuroscience, 2005. **25**(9): p. 2176–2180.
  32. Yurov, Y.B., et al., *Aneuploidy and confined chromosomal mosaicism in the developing human brain*. PLoS ONE, 2007. **2**(6): p. e558.
  33. Cohen, J., *Sorting out chromosome errors*. Science, 2002. **296**(5576): p. 2164–6.
  34. Garcia-Castillo, H., et al., *Clinical and genetic heterogeneity in patients with mosaic variegated aneuploidy: delineation of clinical subtypes*. Am J Med Genet A, 2008. **146A**(13): p. 1687–95.
  35. Torres, E.M., et al., *Effects of aneuploidy on cellular physiology and cell division in haploid yeast*. Science, 2007. **317**(5840): p. 916–924.
  36. Williams, B.R., et al., *Aneuploidy affects proliferation and spontaneous immortalization in mammalian cells*. Science, 2008. **322**(5902): p. 703–709.
  37. Sheltzer, J.M. and A. Amon, *The aneuploidy paradox: costs and benefits of an incorrect karyotype*. Trends in Genetics, 2011. **27**(11): p. 446–453.
  38. Segal, D.J. and E.E. McCoy, *Studies on Down's syndrome in tissue culture. I. Growth rates and protein contents of fibroblast cultures*. J Cell Physiol, 1974. **83**(1): p. 85–90.
  39. Bonney, M.E., H. Moriya, and A. Amon, *Aneuploid proliferation defects in yeast are not driven by copy number changes of a few dosage-sensitive genes*. Genes & Development, 2015. **29**(9): p. 898–903.
  40. Dephoure, N., et al., *Quantitative proteomic analysis reveals posttranslational responses to aneuploidy in yeast*. eLife, 2014: p. e03023.
  41. Pavelka, N., et al., *Aneuploidy confers quantitative proteome changes and phenotypic variation in budding yeast*. Nature, 2010. **468**(7321): p. 321–325.
  42. Torres, E.M., et al., *Identification of Aneuploidy-Tolerating Mutations*. Cell, 2010. **143**(1): p. 71–83.
  43. Hinchcliffe, E.H., et al., *Chromosome missegregation during anaphase triggers p53 cell cycle arrest through histone H3.3 Ser31 phosphorylation*. Nat Cell Biol, 2016.
  44. Lanni, J.S. and T. Jacks, *Characterization of the p53-dependent postmitotic checkpoint following spindle disruption*. Mol Cell Biol, 1998. **18**(2): p. 1055–64.
  45. Ganem, N.J. and D. Pellman, *Linking abnormal mitosis to the acquisition of DNA damage*. J Cell Biol, 2012. **199**(6): p. 871–81.
  46. Janssen, A., et al., *Chromosome segregation errors as a cause of DNA damage and structural chromosome aberrations*. Science, 2011. **333**(6051): p. 1895–1898.
  47. Crasta, K., et al., *DNA breaks and chromosome pulverization from errors in mitosis*. Nature, 2012. **482**(7383): p. 53–58.
  48. Sotillo, R., et al., *Mad2 overexpression promotes aneuploidy and tumorigenesis in mice*. Cancer Cell, 2007. **11**(1): p. 9–23.
  49. Hatch, E.M., et al., *Catastrophic nuclear envelope collapse in cancer cell micronuclei*. Cell, 2013. **154**(1): p. 47–60.
  50. Zhang, C.-Z., et al., *Chromothripsis from DNA damage in micronuclei*. Nature, 2015. **522**(7555): p. 179–184.
  51. Jones, M.J. and P.V. Jallepalli, *Chromothripsis: chromosomes in crisis*. Dev Cell, 2012. **23**(5): p. 908–17.
  52. Stephens, P.J., et al., *Massive genomic rearrangement acquired in a single catastrophic event during cancer development*. Cell, 2011. **144**(1): p. 27–40.
  53. McClintock, B., *The Behavior in Successive Nuclear Divisions of a Chromosome Broken at Meiosis*. Proc Natl Acad Sci U S A, 1939. **25**(8): p. 405–416.
  54. Bunting, S.F. and A. Nussenzweig, *End-joining, translocations and cancer*. Nat Rev Cancer, 2013. **13**(7): p. 443–54.
  55. Kost-Alimova, M., et al., *Microcell-mediated chromosome transfer provides evidence that polysomy*

- promotes structural instability in tumor cell chromosomes through asynchronous replication and breakage within late-replicating regions.* Genes, chromosomes & cancer, 2004. 40(4): p. 316–324.
56. Nawata, H., et al., *Dysregulation of gene expression in the artificial human trisomy cells of chromosome 8 associated with transformed cell phenotypes.* PLoS ONE, 2011. 6(9): p. e25319.
  57. Reish, O., et al., *Sporadic aneuploidy in PHA-stimulated lymphocytes of trisomies 21, 18, and 13.* Cytogenetic and genome research, 2011. 133(2–4): p. 184–189.
  58. Nicholson, J.M., et al., *Chromosome mis-segregation and cytokinesis failure in trisomic human cells.* eLife, 2015. 4.
  59. Passerini, V., et al., *The presence of extra chromosomes leads to genomic instability.* Nat Commun, 2016. 7: p. 10754.
  60. Valind, A., et al., *Whole chromosome gain does not in itself confer cancer-like chromosomal instability.* Proc Natl Acad Sci U S A, 2013. 110(52): p. 21119–23.
  61. Schwartzman, J.-M., R. Sotillo, and R. Benezra, *Mitotic chromosomal instability and cancer: mouse modelling of the human disease.* Nature reviews. Cancer, 2010. 10(2): p. 102–115.
  62. Dyban, A.P. and V.S. Baranov, *Cytogenetics of mammalian embryonic development.* 1987: Clarendon Press.
  63. Valind, A., Y. Jin, and D. Gisselsson, *Elevated tolerance to aneuploidy in cancer cells: estimating the fitness effects of chromosome number alterations by in silico modelling of somatic genome evolution.* PLoS ONE, 2013. 8(7): p. e70445.
  64. Bakker, B., et al., *Single-cell sequencing reveals karyotype heterogeneity in murine and human malignancies.* Genome Biol, 2016. 17(1): p. 115.
  65. Malkhosyan, S., et al., *Molecular karyotype (amplotype) of metastatic colorectal cancer by unbiased arbitrarily primed PCR DNA fingerprinting.* Proc Natl Acad Sci U S A, 1998. 95(17): p. 10170–5.
  66. Neklason, D.W., et al., *Colorectal adenomas and cancer link to chromosome 13q22.1-13q31.3 in a large family with excess colorectal cancer.* J Med Genet, 2010. 47(10): p. 692–9.
  67. Haan, J.C., et al., *Small bowel adenocarcinoma copy number profiles are more closely related to colorectal than to gastric cancers.* Ann Oncol, 2012. 23(2): p. 367–74.
  68. Hoadley, K.A., et al., *Multiplatform analysis of 12 cancer types reveals molecular classification within and across tissues of origin.* Cell, 2014. 158(4): p. 929–944.
  69. Cancer Genome Atlas Research, N., *Comprehensive genomic characterization defines human glioblastoma genes and core pathways.* Nature, 2008. 455(7216): p. 1061–8.
  70. Ozery-Flato, M., et al., *Large-scale analysis of chromosomal aberrations in cancer karyotypes reveals two distinct paths to aneuploidy.* Genome Biol, 2011. 12(6): p. R61.
  71. Ganmore, I., G. Smooha, and S. Izraeli, *Constitutional aneuploidy and cancer predisposition.* Hum Mol Genet, 2009. 18(R1): p. R84–93.
  72. Owainati, A.A., et al., *Tumour aneuploidy, prognostic parameters and survival in primary breast cancer.* British Journal of Cancer, 1987. 55(4): p. 449–454.
  73. Risques, R.A., et al., *Redefining the significance of aneuploidy in the prognostic assessment of colorectal cancer.* Lab Invest, 2001. 81(3): p. 307–15.
  74. Chen, G., et al., *Targeting the Adaptability of Heterogeneous Aneuploids.* Cell, 2015. 160(4): p. 771–784.
  75. Sotillo, R., et al., *Mad2-induced chromosome instability leads to lung tumour relapse after oncogene withdrawal.* Nature, 2010. 464(7287): p. 436–440.
  76. Gascoigne, K.E. and S.S. Taylor, *Cancer Cells Display Profound Intra- and Interline Variation following Prolonged Exposure to Antimitotic Drugs.* Cancer Cell, 2008. 14(2): p. 111–122.
  77. Zasadil, L.M., et al., *Cytotoxicity of Paclitaxel in Breast Cancer Is due to Chromosome Missegregation on Multipolar Spindles.* Science translational medicine, 2014. 6(229): p. 229ra43.
  78. Carter, S.L., et al., *A signature of chromosomal instability inferred from gene expression profiles predicts clinical outcome in multiple human cancers.* Nature genetics, 2006. 38(9): p. 1043–1048.
  79. Swanton, C., et al., *Chromosomal instability determines taxane response.* Proc Natl Acad Sci U S A, 2009. 106(21): p. 8671–6.
  80. A'Hern, R.P., et al., *Taxane benefit in breast cancer—a role for grade and chromosomal stability.* Nat Rev Clin Oncol, 2013. 10(6): p. 357–64.
  81. Silk, A.D., et al., *Chromosome missegregation rate predicts whether aneuploidy will promote or suppress tumors.* Proc Natl Acad Sci U S A, 2013. 110(44): p. E4134–41.
  82. Godek, K.M., et al., *Chromosomal Instability Affects the Tumorigenicity of Glioblastoma Tumor-Initiating Cells.* Cancer Discov, 2016.
  83. Laughney, A.M., et al., *Dynamics of Tumor Heterogeneity Derived from Clonal Karyotypic Evolution.* Cell Rep, 2015. 12(5): p. 809–20.
  84. Gusev, Y., V. Kagansky, and W.C. Dooley, *Long-term dynamics of chromosomal instability in cancer: A transition probability model.* Mathematical and Computer Modelling, 2001. 33(12–13): p. 1253–1273.
  85. Andor, N., et al., *Pan-cancer analysis of the extent and consequences of intratumor heterogeneity.* Nat Med, 2016. 22(1): p. 105–13.



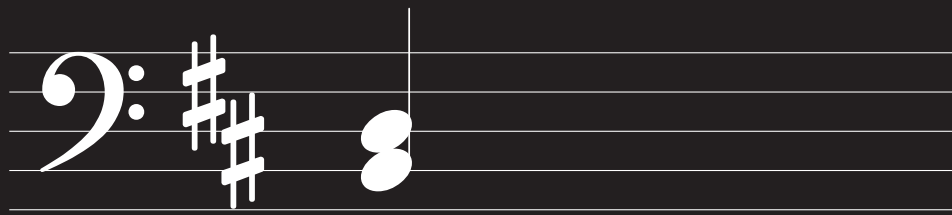
86. Janssen, A., G.J. Kops, and R.H. Medema, *Elevating the frequency of chromosome mis-segregation as a strategy to kill tumor cells*. Proc Natl Acad Sci U S A, 2009. **106**(45): p. 19108-13.
87. Ohashi, A., et al., *Aneuploidy generates proteotoxic stress and DNA damage concurrently with p53-mediated post-mitotic apoptosis in SAC-impaired cells*. Nature Communications, 2015. **6**: p. 1-16.
88. Maia, A.R., et al., *Inhibition of the spindle assembly checkpoint kinase TTK enhances the efficacy of docetaxel in a triple-negative breast cancer model*. Ann Oncol, 2015. **26**(10): p. 2180-92.
89. Maachani, U.B., et al., *Targeting MPS1 Enhances Radiosensitization of Human Glioblastoma by Modulating DNA Repair Proteins*. Mol Cancer Res, 2015. **13**(5): p. 852-62.
90. Tannous, B.A., et al., *Effects of the selective MPS1 inhibitor MPS1-IN-3 on glioblastoma sensitivity to antimitotic drugs*. J Natl Cancer Inst, 2013. **105**(17): p. 1322-31.
91. Colombo, R., et al., *Targeting the mitotic checkpoint for cancer therapy with NMS-P715, an inhibitor of MPS1 kinase*. Cancer Res, 2010. **70**(24): p. 10255-64.
92. Lee, H.S., et al., *Effects of Anticancer Drugs on Chromosome Instability and New Clinical Implications for Tumor-Suppressing Therapies*. Cancer Res, 2016.
93. Bakhoum, S.F., et al., *Numerical chromosomal instability mediates susceptibility to radiation treatment*. Nat Commun, 2015. **6**: p. 5990.
94. Tang, Y.-C., et al., *Identification of Aneuploidy-Selective Antiproliferation Compounds*. Cell, 2011. **144**(4): p. 499-512.
95. Santaguida, S., et al., *Aneuploidy-induced cellular stresses limit autophagic degradation*. Genes Dev, 2015. **29**(19): p. 2010-21.
96. Vitale, I., et al., *Karyotypic Aberrations in Oncogenesis and Cancer Therapy*. Trends in Cancer, 2015. **1**(2): p. 124-135.
97. Bakker, B., et al., *How to count chromosomes in a cell: An overview of current and novel technologies*. BioEssays : news and reviews in molecular, cellular and developmental biology, 2015. **37**(5): p. 570-577.
98. Lukinavicius, G., et al., *SiR-Hoechst is a far-red DNA stain for live-cell nanoscopy*. Nat Commun, 2015. **6**: p. 8497.
99. Sato, T., et al., *Single Lgr5 stem cells build crypt-villus structures in vitro without a mesenchymal niche*. Nature, 2009. **459**(7244): p. 262-265.
100. Sato, T., et al., *Long-term Expansion of Epithelial Organoids From Human Colon, Adenoma, Adenocarcinoma, and Barrett's Epithelium*. Gastroenterology, 2011. **141**(5): p. 1762-1772.
101. van de Wetering, M., et al., *Prospective derivation of a living organoid biobank of colorectal cancer patients*. Cell, 2015. **161**(4): p. 933-945.
102. Boj, S.F., et al., *Organoid models of human and mouse ductal pancreatic cancer*. Cell, 2015. **160**(1-2): p. 324-38.
103. Gao, D., et al., *Organoid cultures derived from patients with advanced prostate cancer*. Cell, 2014. **159**(1): p. 176-87.
104. Fujii, M., et al., *A Colorectal Tumor Organoid Library Demonstrates Progressive Loss of Niche Factor Requirements during Tumorigenesis*. Cell Stem Cell, 2016.
105. Drost, J., et al., *Sequential cancer mutations in cultured human intestinal stem cells*. Nature, 2015. **521**(7550): p. 43-47.



## Acknowledgments

We apologize to scientists whose primary research we did not cite due to restrictions, and we thank the Kops lab members for useful discussion. Cancer research efforts in the Kops lab are supported by the Dutch Cancer Society (KWF Kankerbestrijding), by the PloidyNet MSCA-ITN network and by Cancer Genomics Netherlands.

2



# Chapter 3

## Sequential cancer mutations in cultured human intestinal stem cells

Jarno Drost<sup>1,2</sup>, Richard H. van Jaarsveld<sup>2,3\*</sup>, Bas Ponsioen<sup>2,3\*</sup>, Cheryl  
Zimmerlin<sup>2,4\*</sup>, Ruben van Boxtel<sup>1,2</sup>, Arjan Buijs<sup>5</sup>,  
Norman Sachs<sup>1,2</sup>, Rene M. Overmeer<sup>2,3</sup>, G. Johan Offerhaus<sup>6</sup>, Harry Begthel<sup>1,2</sup>,  
Jeroen Korving<sup>1,2</sup>, Marc van de Wetering<sup>1,2,7</sup>,  
Gerald Schwank<sup>1,2</sup>, Meike Logtenberg<sup>1,2</sup>, Edwin Cuppen<sup>1,2</sup>, Hugo J. Snippert<sup>2,3</sup>,  
Jan Paul Medema<sup>2,4</sup>, Geert J. P. L. Kops<sup>2,3</sup> & Hans Clevers<sup>1,2</sup>

<sup>1</sup>Hubrecht Institute, Royal Netherlands Academy of Arts and Sciences (KNAW) and UMC  
Utrecht, 3584CT Utrecht, The Netherlands.

<sup>2</sup>Cancer Genomics Netherlands, UMC Utrecht, 3584CG Utrecht, The Netherlands.

<sup>3</sup>Molecular Cancer Research, Centre for Molecular Medicine,  
UMC Utrecht, 3584CG, Utrecht, The Netherlands.

<sup>4</sup>Laboratory of Experimental Oncology and Radiobiology, Centre for  
Experimental Molecular Medicine, AMC, 1105AZ Amsterdam, The Netherlands.

<sup>5</sup>Department of Medical Genetics, UMC Utrecht, 3508AB Utrecht, The Netherlands.

<sup>6</sup>Department of Pathology, UMC Utrecht, 3584CX Utrecht, The Netherlands.

<sup>7</sup>Foundation Hubrecht Organoid Technology (HUB), 3584CT Utrecht, The Netherlands.

\*These authors contributed equally to this work

Nature 521, 43–47 (2015)

## Abstract

Crypt stem cells represent the cells of origin for intestinal neoplasia. Both mouse and human intestinal stem cells can be cultured in medium containing the stem-cell-niche factors WNT, R-spondin, epidermal growth factor (EGF) and noggin over long time periods as epithelial organoids that remain genetically and phenotypically stable. Here we utilize CRISPR/Cas9 technology for targeted gene modification of four of the most commonly mutated colorectal cancer genes (*APC*, *P53* (also known as *TP53*), *KRAS* and *SMAD4*) in cultured human intestinal stem cells. Mutant organoids can be selected by removing individual growth factors from the culture medium. Quadruple mutants grow independently of all stem-cell-niche factors and tolerate the presence of the P53 stabilizer nutlin-3. Upon xenotransplantation into mice, quadruple mutants grow as tumours with features of invasive carcinoma. Finally, combined loss of *APC* and *P53* is sufficient for the appearance of extensive aneuploidy, a hallmark of tumour progression.

## Main

The adenoma–carcinoma sequence proposes that the sequential acquisition of specific genetic alterations underlies the progression of colorectal cancer (CRC) [1]. Activation of the WNT pathway, most commonly through inactivating mutations in *APC*, initiates the formation of benign polyps. Progression is thought to occur through activating mutations in the EGF receptor (EGFR) pathway and inactivating mutations in the P53 and transforming growth factor (TGF)- $\beta$  pathways [2]. Recent sequencing efforts have further explored the genomic landscape underlying CRC [3]. A major hurdle in identifying essential driver mutations is that many CRCs have acquired either microsatellite instability or chromosomal instability (CIN), as tumours typically harbour hundreds to thousands of mutations. Using mouse models, *Lgr5*<sup>+</sup>-intestinal stem cells were identified as cells of origin for intestinal neoplasia and were shown to fuel effective tumour growth [4–6]. A recent study has shown that deregulation (by retroviral expression of short hairpin RNAs (shRNAs) or cDNA) of *APC*, *P53*, *KRAS* and *SMAD4* is sufficient for transformation of cultured mouse colon into tumours with adenocarcinoma-like histology [7]. Of note, the reliance on paracrine growth factors provided by a mesenchymal component in this system does not allow a one-to-one correlation with the individual oncogenic mutations. Comparable human *in vitro* model systems to study tumour initiation and progression have not been developed. We have previously described ‘indefinite’ three-dimensional stem cell culture systems (organoids) derived from several organs including mouse and human small intestine, colon, pancreas and liver that remain genetically stable [11–13].

### Sequential introduction of CRC mutations

We set out to utilize CRISPR/Cas9-mediated genome editing [14–16] to introduce four of the most frequent CRC mutations in human small intestinal organoid stem cell cultures. As the absolute knockout efficiency is low, we made use of functional selection strategies to obtain clonal, mutant organoids. Since loss of *APC* is generally considered to be an early event in CRC [2], we first introduced inactivating mutations in *APC*. As previously described, withdrawal of WNT and R-spondin from the

defined culture medium provides a functional selection for *APC* loss [17] (Figure 1A). Indeed, control-transfected organoids died when seeded in medium lacking WNT and R-spondin (Figure 1B), whereas transfection of plasmids expressing Cas9 and single guide RNAs (sgRNAs) targeting *APC* in its mutation hotspot region allowed cystic clonal organoids to emerge (Figure 1B, Extended Data Figure 1A and Extended Data Table 1a). To obtain clonal cultures, individual organoids were expanded. Genotyping verified the presence of clonal insertions or deletions (indels) at the targeted regions (Extended Data Figure 1B). Quantitative reverse transcription polymerase chain reaction (qRT-PCR) analysis for the WNT target gene *AXIN2* confirmed the constitutive activity of the WNT pathway, as *AXIN2* messenger RNA levels did not decrease upon WNT/R-spondin withdrawal (Figure 1C).

Next, we introduced inactivating mutations in *P53* in *APC* knockout (*APC*<sup>KO</sup>) intestinal organoids. We made use of nutlin-3 [18] to select for organoids with a functionally inactive P53 pathway (Figure 1A). As expected, nutlin-3 stabilized P53 in intestinal organoids and activated transcription of its target gene *P21* (also known as *CDKN1A*) (Figure 1E). Control sgRNA-transfected *APC*<sup>KO</sup> organoids died upon nutlin-3 treatment (Figure 1D), whereas transfection of plasmids expressing Cas9 and sgRNAs targeting *P53* enabled organoid outgrowth (Figure 1D, Extended Data Figure 1A and Extended Data Table 1A). Clonal expansion and genotyping verified the presence of frameshift-inducing indels at the targeted loci (at the start of the DNA-binding domain, thereby yielding an inactive gene product; Extended Data Figure 1C). Loss of P53 protein expression and P53 pathway inactivity were confirmed by western blot (Figure 1E).

The most common *KRAS* mutation in CRC results in the expression of constitutively active *KRAS*(G12D). To introduce this mutation, we designed an oligonucleotide with the oncogenic mutation and two silent mutations to serve as a template for homologous recombination (Figure 2A). *KRAS*<sup>G12D</sup> mutants were selected by withdrawing EGF and adding the EGFR inhibitor gefitinib to the culture medium. Of note, resident Paneth cells produce EGF in organoids [12]. Whereas control-transfected organoids failed to expand in the selection medium, organoids transfected

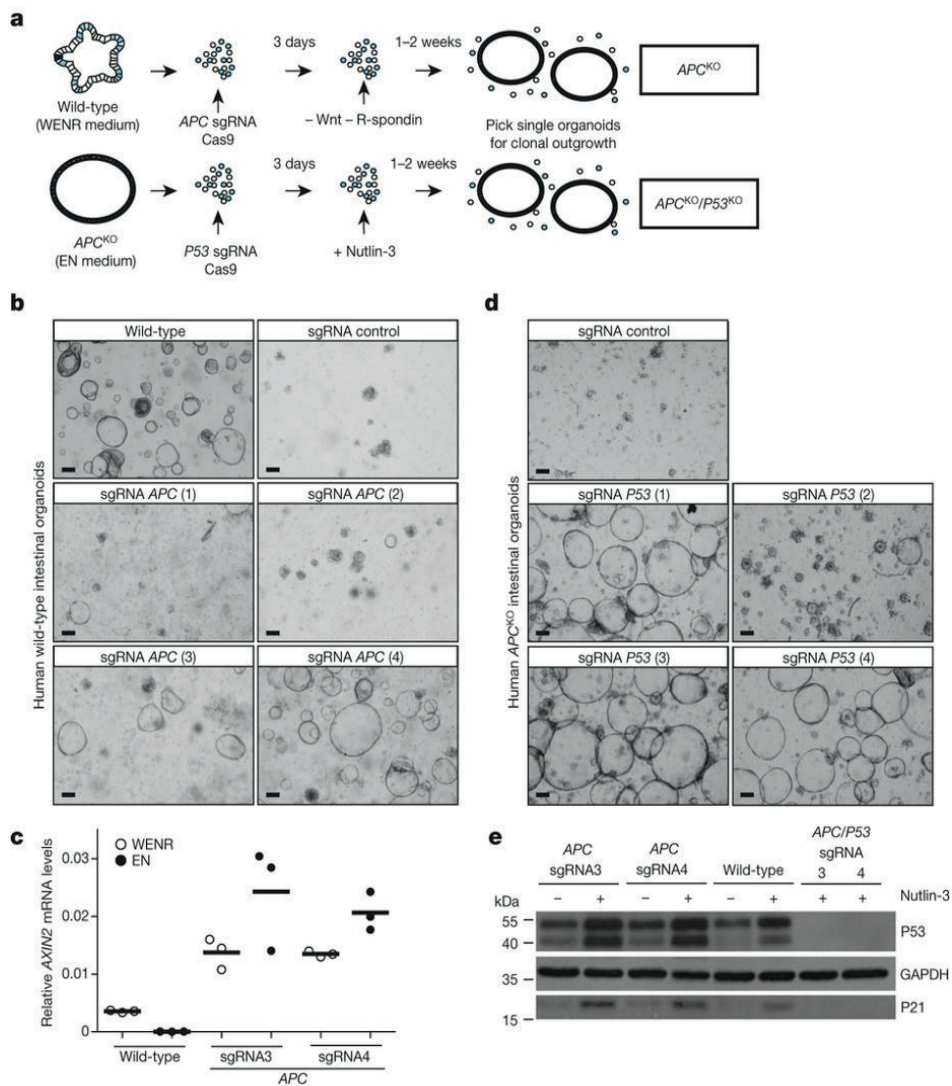
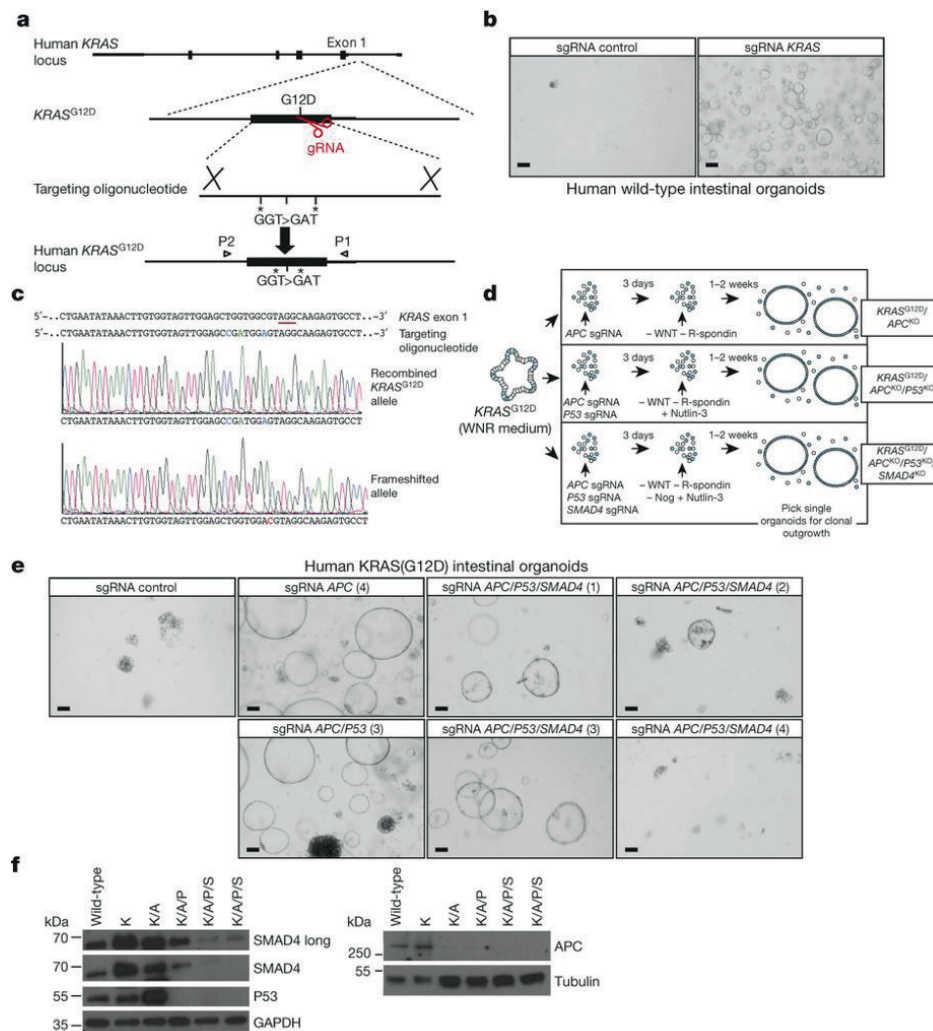


**Figure 1: Inactivation of APC and P53 in human intestinal organoids.** A) Strategy to generate the indicated mutant lines using CRISPR/Cas9. Blue, stem cells. E, EGF; N, noggin; R, R-spondin; W, WNT. B) Wild-type organoids in complete medium (WENR; top left) and transfected with Cas9 and the indicated sgRNAs selected in EN medium (representative pictures from n = 3 independent experiments). C) qRT-PCR for AXIN2 in wild-type and APCKO organoids in the presence or absence of WNT/R-spondin. Expression normalized to GAPDH. Horizontal bars represent mean of n = 3 independent experiments. D) APCKO organoids were transfected with Cas9 and the indicated sgRNAs. P53 mutants were selected in medium with nutlin-3 (representative pictures from n = 3 independent experiments). E) Western blot analysis of P53 and P21 expression in organoids cultured in the presence/absence of nutlin-3 (representative from n = 3 independent experiments). Scale bars, 100  $\mu$ m.

with the oligonucleotide, Cas9 and the *KRAS* sgRNA grew out (Figure 2B and Extended Data Table 1A). Genotyping of clonally expanded organoids confirmed that the resistant clones harboured the *KRAS*<sup>G12D</sup> mutation (Figure 2C). The two silent mutations were also present in the recombined allele, verifying that the mutations were introduced using the provided template. Although the second *KRAS* allele did not recombine, it was often targeted by Cas9 endonuclease, resulting in a frameshift in the second allele.





### Quadruple mutants do not need niche factors

We then set out to introduce combinations of CRC mutations. We used our KRAS(G12D)-expressing organoids to introduce inactivating mutations in *APC*, *P53* and *SMAD4* (Figure 2D). To select for inactivating mutations in *SMAD4*, an essential downstream component of the TGF- $\beta$  and bone morphogenetic protein (BMP) pathways, we made use of the dependence of the intestinal organoids on the presence of the BMP pathway inhibitor noggin in the culture medium [12]. Using the described selection procedures, transfection of Cas9 with either *APC* or both *APC* and *P53* sgRNAs yielded *KRAS*<sup>G12D</sup>/*APC*<sup>KO</sup> and *KRAS*<sup>G12D</sup>/*APC*<sup>KO</sup>/*P53*<sup>KO</sup> organoids, respectively (Figure 2E and F and Extended Data Figure 2A–C). Transfection of Cas9 together with sgRNAs targeting *APC*, *P53* and *SMAD4* yielded organoids growing in medium lacking EGF, WNT, R-spondin and noggin, to which nutlin-3 was added (Figure 2E, Extended Data Figure 2D and Extended Data Table 1A). Clonal expansion and sequencing of the targeted loci in *APC* and *P53* verified frameshift-inducing indels. Sequencing of the targeted exon in *SMAD4* in several different clones revealed a frameshift-inducing deletion in one allele and an in-frame deletion in the other allele (sgRNA 1, P356del; sgRNA 3, V370del) (Extended Data Figure 2C). Western blot confirmed reduced protein expression in *SMAD4*-mutated organoids (Figure 2F). As with all sgRNAs, *SMAD4* sgRNAs target the mutation hotspot region, encoding the MH2 domain required for SMAD4 activity [19, 20]. Recently, in-frame deletions of SMAD4 P356 and V370 were shown to occur in CRC

← **Figure 2: KRAS<sup>G12D</sup>/APC<sup>KO</sup>/P53<sup>KO</sup>/SMAD4<sup>KO</sup> organoids grow in the absence of stem-cell-niche factors in vitro.** A) Strategy to introduce the KRAS<sup>G12D</sup> mutation. Asterisks indicate silent mutations; arrowheads indicate genotype primers. B) Wild-type human intestinal organoids were transfected with Cas9, sgRNA and the oligonucleotide. KRAS<sup>G12D</sup> mutants were selected in medium lacking EGF, with the EGFR inhibitor gefitinib (representative pictures from n = 3 independent experiments). C) Sequence analysis of the targeted KRAS exon. Oncogenic GGT>GAT mutation is indicated in green; silent mutations are in blue; protospacer adjacent motif (PAM) is underlined in red. D) Strategy to generate the indicated mutant lines using CRISPR/Cas9. Blue, stem cells. N, noggin (Nog); R, R-spondin; W, WNT. E) KRAS(G12D)-expressing organoids were transfected with Cas9 and the indicated sgRNAs (representative pictures from n = 3 independent experiments). F) Western blot analysis of SMAD4, P53 and APC expression in the indicated organoid lines (representative from n = 3 independent experiments). K, KRAS<sup>G12D</sup>; A, APC<sup>KO</sup>; P, P53<sup>KO</sup>; S, SMAD4<sup>KO</sup>. Scale bars, 100  $\mu$ m.

[21], indicating that in-frame indels at these locations yield an inactive gene product. Using a candidate off-target prediction tool, we detected no lesions of predicted off-target sites for the sgRNAs used to introduce mutation combinations in our human intestinal organoids (Supplementary Table 1). Although this analysis was limited, in combination with the analysis of multiple independent clonal organoids, the results indicated that the observed effects were not due to off-target effects. In conclusion,  $KRAS^{G12D}/APC^{KO}/P53^{KO}/SMAD4^{KO}$  mutant intestinal organoids can grow in the absence of all stem-cell-niche factors *in vitro* (Extended Data Table 1B).

### Quadruple mutants grow as invasive carcinomas

Next, we investigated whether our engineered organoids were tumorigenic *in vivo*. We subcutaneously injected wild-type and all engineered mutant organoid lines into immunodeficient mice. After 8 weeks, some mice injected with  $KRAS^{G12D}/APC^{KO}/P53^{KO}$  organoids ('triple'; 3 out of 12 injections) and the majority of mice injected with  $KRAS^{G12D}/APC^{KO}/P53^{KO}/SMAD4^{KO}$  organoids ('quadruple'; 13 out of 16 injections) developed visible nodules (Extended Data Figure 4A). Histological analysis confirmed that triple organoids did engraft, but remained small with few proliferating cells and mostly resembled adenomas (Figure 3A and Extended Data Figure 4B and C). Quadruple-derived tumours were larger, highly proliferative and all displayed features of invasive carcinoma, including an irregular multi-layered epithelium consisting of tumour cells with increased nuclear-cytoplasmic ratio, pleiomorphic and hyperchromatic nuclei. Invasion of isolated or small aggregates of tumour cells into the stroma was frequently observed (Figure 3B and Extended Data Figure 4B and D). The tumour origin was verified using a human-specific cytokeratin antibody (hKRT; Figure 3 and Extended Data Figure 4C and D). Thus, introduction of oncogenic mutations in  $KRAS$ ,  $APC$ ,  $P53$  and  $SMAD4$  enables normal human intestinal stem cell organoids to grow as tumours with invasive carcinoma features *in vivo* (Extended Data Table 1B). *In vitro*, both triple- and quadruple-mutant organoids exhibited a high proliferation rate, while only quadruple-mutant organoids frequently appeared as solid tumour masses (Extended Data Figure 5A and C).

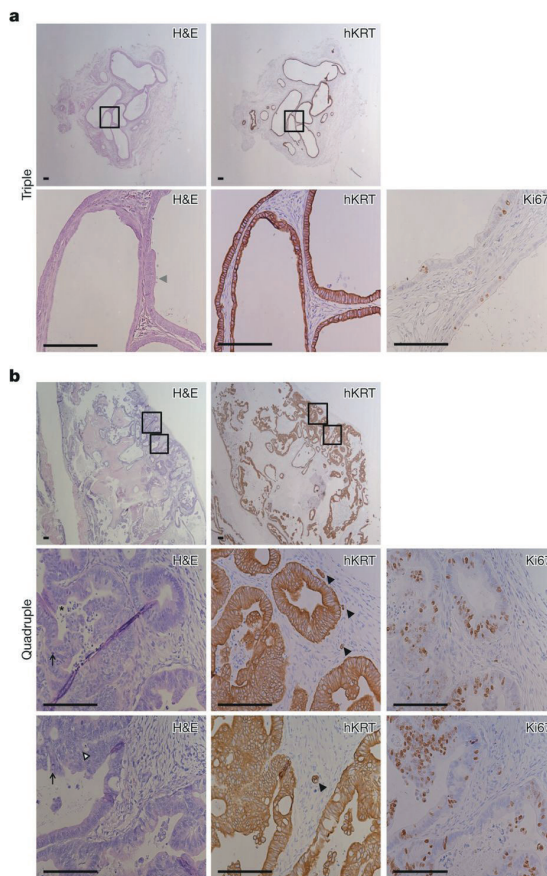


**Figure 3: Quadruple-mutant organoids grow as invasive carcinomas in vivo.**

A) Haematoxylin and eosin (H&E; top left, bottom left), hKRT (top right, bottom middle) and Ki67 (bottom right) immunostainings on nodules isolated from triple-mutant-injected mice. Representative pictures of an adenoma with regular glandular structures lined with a blander epithelium that only focally shows a tendency towards stratification (arrowhead), no invasive growth and low proliferative capacity (Ki67).  $n = 3$  mice. B) As in (A), but for quadruple-mutant-injected mice. Upper and lower boxed regions in top panels correspond to regions imaged in left bottom panels and middle and right bottom panels, respectively. Representative pictures of an invasive carcinoma with irregular glandular architecture, gland in gland formation (white arrowhead) and luminal debris (asterisk). Mitotic figures are encountered (arrows) and there is high proliferative activity (Ki67). Invasion of isolated or small aggregates of cells into the stroma is observed (black arrowheads).  $n = 13$  mice. Scale bars, 100  $\mu\text{m}$ .

### Extensive aneuploidy upon *APC* and *P53* loss

To determine whether our engineered mutant organoids acquired CIN, a hallmark of CRC [22], we transduced all human intestinal organoid lines with a fluorescently tagged histone 2B (H2B)-encoding lentivirus. This enabled us to monitor chromosome segregations using three-dimensional live-cell imaging. Wild-type organoids underwent mitosis without showing any major abnormalities. We did not observe an increase in the percentage of errors in *APC*<sup>KO</sup> organoids (Figure 4A and Supplementary Videos 1 and 2). However, *APC*<sup>KO</sup>/*P53*<sup>KO</sup> organoids showed a progressive increase in the percentage of errors. We mainly observed anaphase bridges, but a few misaligned and lagging chromosomes were also detected (Figure 4A and B and Supplementary Video 3). Importantly, compared to *APC*<sup>KO</sup>/*P53*<sup>KO</sup> organoids, triple and quadruple mutants showed only a minor increase in the percentage of

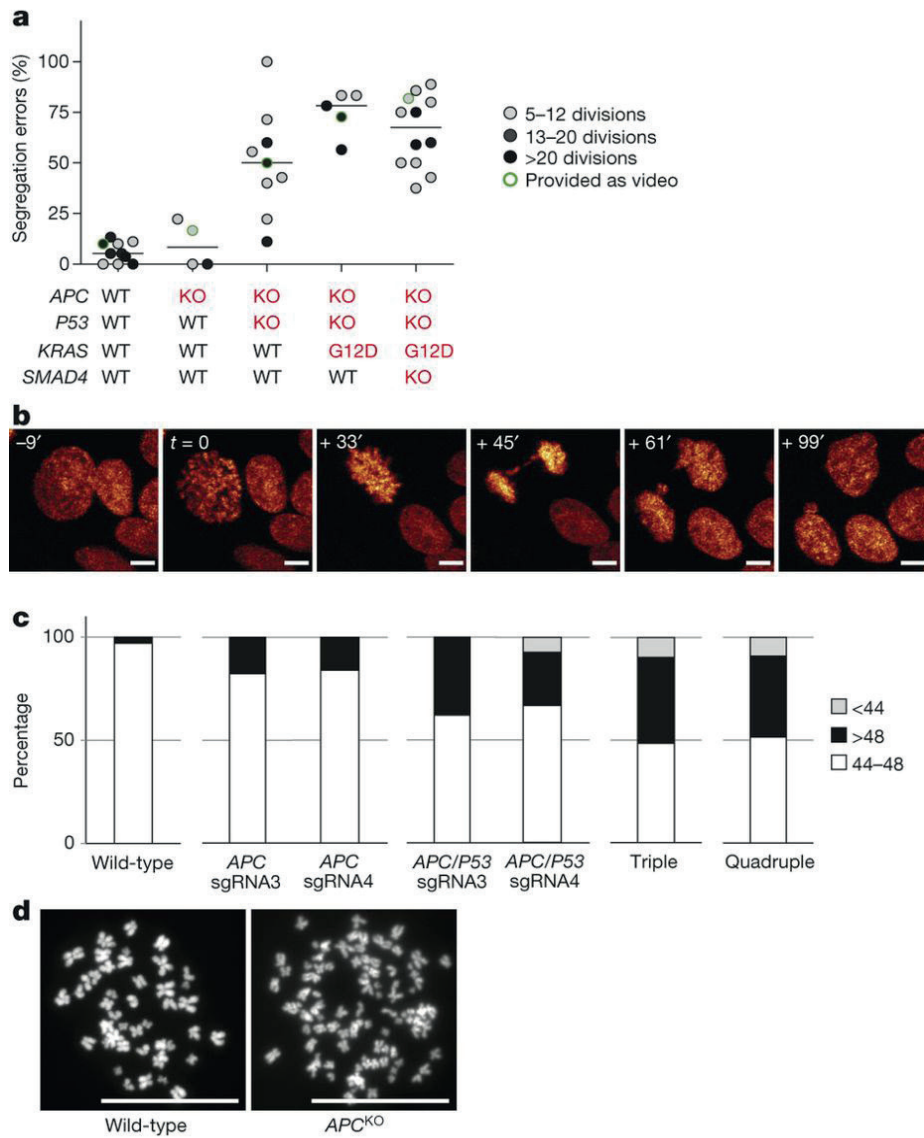


**Figure 4: Progressive CIN and aneuploidy upon introduction of CRC mutations.** A) Live-cell imaging was performed to monitor chromosome segregations. Graph shows the percentage of erroneous mitoses. Each dot represents the percentage of errors in one organoid. Horizontal bars represent median of all dots. Videos are included of organoids depicted as dots with green outline (Supplementary Videos 1, 2, 3, 4, 5). WT, wild-type; KO, knockout. B) Stills of a typical erroneous mitotic event (anaphase bridge) in an APCKO/P53KO organoid. Time points are indicated in minutes relative to prophase onset. Scale bars, 5  $\mu$ m. C) Chromosomes were counted in the indicated organoids. Graphs plot the percentage of cells with chromosome counts <44, 44–48 (normal) and >48 (at least 50 spreads were counted). D) Representative karyotypes of a wild-type culture with  $n = 46$  chromosomal counts (left) and APCKO organoid culture (right) with aberrant chromosome numbers. Scale bars, 25  $\mu$ m.

mitotic errors (Figure 4A and Supplementary Videos 3–5), implying that loss of *APC* and *P53* is sufficient to acquire CIN.

To verify that the observed CIN results in aneuploidy, we next counted chromosome numbers. Unlike wild-type organoids, karyotyping reproducibly revealed numerical aberrations in a low percentage of *APC*<sup>KO</sup> organoids (two independent sgRNAs) (Figure 4C and D). This ranged from a trisomy of chromosome 7 to near-tetraploid metaphases (Extended Data Figure 6A), the latter confirming previous studies in mouse embryonic stem cells [23]. Strikingly, one of the most recurrent chromosomal aberrations in low-grade colorectal adenomas in patients involves copy number gains of chromosome 7 [24–26]. In accordance with the chromosome segregation analyses, *APC*<sup>KO</sup>/*P53*<sup>KO</sup> organoids showed a marked increase in the percentage of aneuploid spreads (Figure 4C and Extended Data Figure 6B). The triple and quadruple mutants also showed extensive aneuploidy (Figure 4C and Extended Data Figure 6C and D).

To confirm these data, *APC*<sup>KO</sup>, *P53*<sup>KO</sup> and *APC*<sup>KO</sup>/*P53*<sup>KO</sup> organoids were engineered in a second human small intestinal line (Extended Data Figure 7A–C). Again, loss of both *APC* and *P53* had the most dramatic effect on CIN and aneuploidy. Although the single loss of *P53* resulted in a substantial increase in the percentage of segregation errors, only a minor increase in the amount of aberrant spreads was observed (Extended Data Figure 7D and F and Supplementary Video 6). Thus, we show that the combined loss of *APC* and *P53* is sufficient for the appearance of extensive aneuploidy. Despite the observed chromosome missegregations, our engineered lines continue proliferating, while maintaining functional DNA damage signaling (Extended Data Figure 7H).

### **CRC mutations in human colon organoids**

Finally, we introduced all the mutation combinations described earlier into a human colon organoid stem cell culture [27], following the same functional selection procedures (Extended Data Figure 3 and Extended Data Table 1B). Importantly, this yielded essentially identical results to those obtained with the small intestinal stem cells, in terms of growth factor independence, *in vitro* appearance, CIN and aneuploidy (Extended Data Figure 5B and 7E and G). Moreover, both triple- and

quadruple-mutant human colon organoids grew with high efficiency as tumours upon xenotransplantation into immunodeficient mice (Extended Data Figure 8A and B). Histological analysis revealed that triple-mutant tumours contained large cysts and locally displayed features of well-differentiated carcinomas with relatively limited invasive growth, whereas the quadruple-mutant-derived invasive carcinomas were faster growing, had a poorly differentiated appearance and displayed very frequent tumour budding at the invasive front, as well as invasion of the underlying muscle tissue (Extended Data Figure 8C-E).

While this manuscript was under final review, a study using a similar strategy appeared [28]. Our CRC progression model selects out functional mutants by changing the culture medium composition and all sgRNAs were designed to target mutation hotspot regions. Therefore, we believe that our model reflects the *in vivo* situation more closely than any other *in vitro* human CRC model so far. Upon oncogenic mutation of *KRAS*, *APC*, *P53* and *SMAD4*, human gut stem cell organoids can grow in the absence of all stem-cell-niche factors and in the presence of the P53 stabilizer nutlin-3 *in vitro* and as tumours with invasive carcinoma features *in vivo*. Moreover, we find that our engineered CRC organoid lines show marked CIN and aneuploidy, both considered to be hallmarks of cancer [22].

## Methods

**Human material for organoid cultures.** Approval for this study was obtained by the ethics committees of the University Medical Centre Utrecht (duodenal biopsies) and The Diaconessen Hospital Utrecht (colonic tissues). Written informed consent was obtained.

**Organoid culture.** Endoscopic duodenal biopsy samples were obtained from two female individuals (patient 1, age 2 years; patient 2, age 8 years). These individuals were admitted for suspected coeliac disease or dyspepsia. Upon immunological and pathophysiological analysis, none of the individuals was diagnosed with coeliac disease, whereas patient 1 presented with signs of gastric metaplasia. All duodenal biopsies that were used in this study were found to be healthy on the basis of histological examination. Normal human colon tissue was isolated from a resected



colon segment derived from a patient (female, age 60 years) diagnosed with CRC (sigmoid). Culture establishment was described previously [17, 27]. Culture medium contains advanced DMEM/F12 medium (Invitrogen) including B27 (Invitrogen), nicotinamide (Sigma-Aldrich), *N*-acetylcysteine (Sigma-Aldrich), noggin (Peprotech), R-spondin 1 [29], EGF (Peprotech), WNT conditioned media (50%, produced using stably transfected L cells), TGF- $\beta$  type I receptor inhibitor A83-01 (Tocris) and P38 inhibitor SB202190 (Sigma-Aldrich). For selection of *KRAS*<sup>G12D</sup> mutants, organoids were grown in culture medium lacking EGF and containing 0.5–1.0  $\mu$ M of gefitinib (Selleck Chemicals). For mutant *P53* selection, organoids were cultured in the presence of 5–10  $\mu$ M nutlin-3 (Cayman Chemical). Organoids were repeatedly tested for mycoplasma contamination and resulted negative.

**Organoid transfection and genotyping.** The organoid lipofection protocol was previously described in detail [17]. In short, human organoids were grown in the media described earlier, and trypsinized for 10 min at 37 °C. After trypsinization, cells were resuspended in 450  $\mu$ l growth medium (containing the Rho kinase inhibitor Y-27632) and plated in 48-well plates at high density (80–90% confluent). Nucleic acid–Lipofectamine 2000 complexes were prepared according to the standard Lipofectamine 2000 protocol (Invitrogen). Four microlitres of Lipofectamine 2000 reagent in 50  $\mu$ l Opti-MEM medium (Gibco), and a total of 1.5  $\mu$ g of DNA (sgRNA, Cas9, with/without oligonucleotide in 50  $\mu$ l Opti-MEM medium) were mixed together, incubated for 5 min, and added to the cells (50  $\mu$ l per well). The plate was centrifuged at 600g at 32 °C for 1 h, and incubated for 4 h at 37 °C before single cells were plated in Basement Membrane Extract (BME; Amsbio) or Matrigel (BD Biosciences). Growth medium plus Y-27632 was exchanged with selection medium 3 days after transfection. For clonal expansion single organoids were picked. On average, the efficiency of introduction of frameshift-inducing mutations was approximately 1%. sgRNA transfections and subsequent selections were performed at least three times in both human small intestine and colon lines.

For genotyping, genomic DNA was isolated using Viagen Direct PCR (Viagen). Primers for the PCR amplification using GoTaq Flexi DNA polymerase (Promega)

were as follows: *APC\_for*, 5'-TGTAATCAGACGACACAGGAAGCAGA-3', *APC\_rev*, 5'-TGGACCCTCTGAACTGCAGCAT-3'; *P53\_for*, 5'-CAGGAAGCCAAAGGGTGAAGA-3', *P53\_rev*, 5'-CCCATCTACAGTCCCCCTTG-3'; *KRAS\_for*, 5'-TGGACCCTGACATACTCCCA-3', *KRAS\_rev*, 5'-AAGCGTCGATGGAGGAGTTT-3'; *SMAD4\_for*, 5'-TGGAGTGCAAGTGAAAGCCT-3', *SMAD4\_rev*, 5'-ACCGACAATTAAGATGGAGTGCT-3'. Products were cloned into pGEM-T Easy vector system I (Promega) and subsequently sequenced using T7 sequencing primer.

**Vector construction.** The human codon-optimized Cas9 expression plasmid was obtained from Addgene (41815). The sgRNA-GFP plasmid was obtained from Addgene (41819) and used as a template for generating target-specific sgRNAs. The GFP targeting sequence was exchanged by inverse PCR followed by DpnI digestion and T4 ligation as described previously [17]. *APC*, *P53* and *SMAD4* sgRNA sequences are included in Extended Data Figure 1A and 2D. *KRAS* target sequences: number 1, 5'-GAATATAAACTTGTGGTAGTTGG-3'; number 2, 5'-GTAGTTGGAGCTGGTGGCGTAGG-3'.

**RNA isolation, cDNA preparation and qRT-PCR.** Organoids were harvested in RLT lysis buffer and RNA was isolated using the Qiagen RNeasy kit (Qiagen) according to the manufacturer's instructions. Extracted RNA was used as a template for cDNA production using GoScript reverse transcriptase (Promega) according to the manufacturer's protocol. qRT-PCR was performed using IQ SYBR green mix (Bio-Rad) according to the manufacturer's protocol. Results were calculated by using the  $\Delta\Delta C_t$  method. Organoid treatments: WNT/R-spondin withdrawal, 48 h; nutlin-3 10  $\mu$ M, 24 h. Primer sequences: *AXIN2\_for*, 5'-AGCTTACATGAGTAATGGGG-3', *AXIN2\_rev*, 5'-AATCCATCTACACTGCTGTC-3'; *P21\_for*, 5'-TACCCTTGTGCCTCGCTCAG-3', *P21\_rev*, 5'-GAGAAGATCAGCCGGCGTTT-3'; *GAPDH\_for*,



5'-TGCACCACCAACTGCTTAGC-3', *GAPDH\_rev*,  
5'-GGCATGGACTGTGGTCATGAG-3'.

**Western blot.** Samples were lysed using RIPA buffer (50 mM Tris-HCl pH 8.0, 150 mM NaCl, 0.1% SDS, 0.5% Na-Deoxycholate, 1% NP-40) containing Complete protease inhibitors (Roche). Protein content was quantified using standard Bradford assay (BioRad) and equal amounts of protein were run on SDS-PAGE gels and transferred to PVDF membranes (Millipore). For APC western blotting, protein lysates were loaded on gradient polyacrylamide gels (4–15%; BioRad) and subsequently transferred. Membranes were blocked and probed with antibodies directed against P53 (DO-1, Santa Cruz Biotechnology), P21 (F-5, Santa Cruz Biotechnology), APC (FE9, Calbiochem), SMAD4 (B8, Santa Cruz Biotechnology), phospho-Chk1 Ser 345 (Bioke) and GAPDH (ab-9485, Abcam). Organoid treatments: nutlin-3 10  $\mu$ M, 24 h; doxorubicin 10  $\mu$ M, overnight. Uncropped versions of the most relevant images are provided in Supplementary Figure 1.

**In vivo transplantation assays.** Approval for this study was obtained by the Animal Experimentation Committee at the Academic Medical Centre in Amsterdam (DEC102581). Human organoid lines were expanded in their corresponding selection media and trypsinized for 10 min at 37 °C. After trypsinization, 200,000 cells were resuspended in 50  $\mu$ l of medium containing 2 $\times$  required growth factors, mixed with Matrigel (BD Biosciences) at a 1:1 ratio and injected subcutaneously into NOD scid gamma (NSG; NOD.Cg-Prkdc<sup>scid</sup> Il2rg<sup>tm1Wjl</sup>/SzJ) mice ( $\geq 6$  injections per organoid line). After 7 (colon) or 8 (small intestine) weeks, mice were killed and nodules were processed for analysis. Both males and females (aged 8–10 weeks at the start of the experiment; weights, ~30 g for males and ~25 g for females) were used. This was randomly distributed and does not affect outgrowth. All animals were included in the analysis. Ear clipping was used for animal recognition. Number of injections was chosen following previous experience in the assessment of experimental variability. Animals were caged together and treated in the same way.

**Immunohistochemistry.** Tissues were fixed in 4% paraformaldehyde, dehydrated and embedded in paraffin. Sections were subjected to H&E as well as

immunohistochemical staining. The following primary antibodies were used for immunohistochemical staining: anti-cytokeratin clone Cam5.2 (BD Biosciences), anti-Ki67 clone MM1 (Sanbio) and E-cadherin clone 36 (BD Biosciences).

**Live-cell imaging and karyotyping.** To visualize mitoses, organoids were infected with lentivirus encoding mNeon-tagged histone 2B and a puromycin-resistance cassette (pLV-H2B-mNeon-ires-Puro) [30]. After two passages, these were plated in BME in glass-bottom 96-well plates and mounted on an inverted confocal laser scanning microscope (Leica SP8X), which was continuously held at 37 °C and equipped with a culture chamber for overflow of 6.0% CO<sub>2</sub>. Over 16–20 h, ~10 H2B-mNeon-expressing organoids were imaged simultaneously in XYZT-mode using a ×40 objective (N.A. 1.1), using minimal amounts of 506 nm laser excitation light from a tuneable white light laser. Time interval was approximately 3 min (2:30–3:20 min). For post-acquisition analyses of mitotic behaviour, data sets were converted into manageable and maximally informative videos, combining z-projection, depth colour-coding and merging with transmitted light images (Supplementary Videos 1–6). Mitoses were scored, judged and counted manually.

For karyotyping, organoids were treated with 0.1 µg ml<sup>-1</sup> colcemid (Gibco) for 16 h. Cultures were washed and dissociated into single cells using TrypLE (Gibco) and processed as described [8]. Slides were mounted with DAPI-containing vectashield and analysed on a DM6000 Leica microscope (at least 50 spreads were analysed, n = 3).

**Off-target effect analysis.** To assess off-target mutational effects, we computationally identified candidate off-target sites for each sgRNA using COD software (<http://cas9.wicp.net/>). The software calculates an off-target score depending on sequence similarity: if the sequence perfectly matches the tested sgRNA (the target site) the score is 1 and decreases with increasing sequence differences. For the sgRNA targeting P53 and SMAD4 we identified 2 and 11 candidate off-target sites (Supplementary Table 1). For the sgRNA targeting APC and KRAS we only considered sites with an off-target scores of at least 0.15 or higher, resulting in 74 and 15 candidate off-target sites, respectively. We evaluated off-target mutational effects by amplicon-based NGS

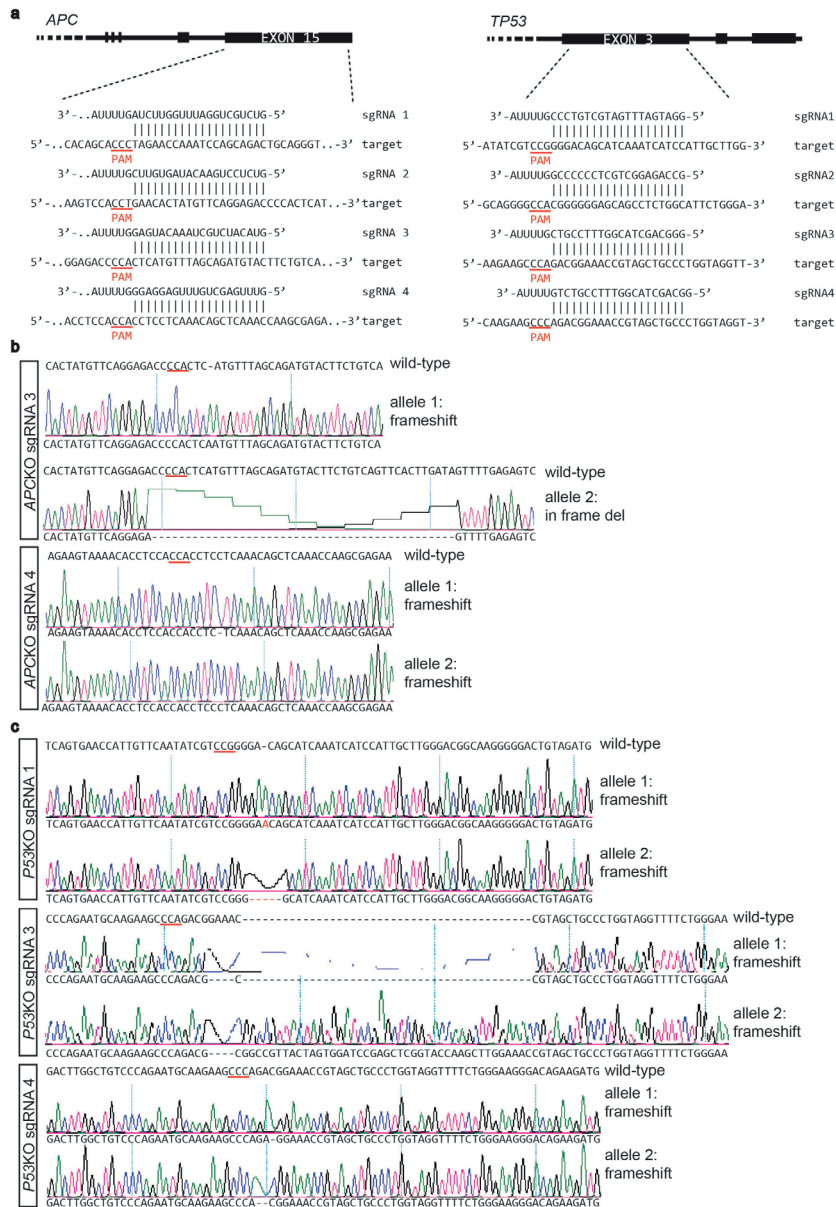
sequencing 93 candidate off-target sites and included the target sites for P53, KRAS and SMAD4 as positive controls (Supplementary Table 1). To this end, primers were designed ~350 nucleotides 5' and ~150 nucleotides 3' from the candidate site to obtain amplicons of ~500 bp (primer sequences available upon request). These regions were PCR amplified for each of the cultures using 5 ng genomic DNA, 1× GoTaq PCR Buffer (Promega), 1.5 mM MgCl<sub>2</sub>, 0.2 mM of each dNTP, 0.2 mM of each primer of a primer pair and 0.25 units of GoTaq polymerase (Promega) in a final volume of 10 ml at 94 °C for 60 s; 15 cycles at 92 °C for 30 s, 65 °C for 30 s with a decrement of 0.2 °C per cycle and 72 °C for 60 s; followed by 30 cycles at 92 °C for 30 s, 58 °C for 30 s and 72 °C for 60 s; and a final extension at 72 °C for 180 s. Per culture the PCR products were pooled and barcoded. Illumina sequence libraries were generated using the TruSeq DNA Sample Preparation Kit (Illumina) according to the manufacturer's protocol. Subsequently, the libraries were pooled and sequenced using the MiSeq sequencer (2 × 250 bp) to a depth of >10,000× base coverage. Sequence reads were mapped to the human reference genome (GRCh37/hg19), using the Burrows–Wheeler Aligner (BWA) Maximal Exact Matches (MEM) v.0.7.5a mapping tool [31] with settings '-c 100 -m'. Small indel calling was performed using the Genome Analysis Toolkit (GATK) [32] haplotype caller v.3.2-2 with 'best practices' settings. We only considered indels with a variant allele frequency (VAF) of at least 0.15 or higher (Supplementary Table 1).

## References

1. Fearon, E.R. and B. Vogelstein, *A genetic model for colorectal tumorigenesis*. Cell, 1990. **61**(5): p. 759–767.
2. Fearon, E.R., *Molecular genetics of colorectal cancer*. Annu Rev Pathol, 2011. **6**: p. 479–507.
3. Cancer Genome Atlas, N., *Comprehensive molecular characterization of human colon and rectal cancer*. Nature, 2012. **487**(7407): p. 330–337.
4. Barker, N., et al., *Crypt stem cells as the cells-of-origin of intestinal cancer*. Nature, 2009. **457**(7229): p. 608–611.
5. Schepers, A.G., et al., *Lineage tracing reveals Lgr5+ stem cell activity in mouse intestinal adenomas*. Science, 2012. **337**(6095): p. 730–5.
6. Zhu, L., et al., *Prominin 1 marks intestinal stem cells that are susceptible to neoplastic transformation*. Nature, 2009. **457**(7229): p. 603–7.
7. Li, X., et al., *Oncogenic transformation of diverse gastrointestinal tissues in primary organoid culture*. Nature Medicine, 2014. **20**: p. 769.
8. Huch, M., et al., *In vitro expansion of single Lgr5+ liver stem cells induced by Wnt-driven regeneration*. Nature, 2013. **494**(7436): p. 247–50.
9. Jung, P., et al., *Isolation and in vitro expansion of human colonic stem cells*. Nature Medicine, 2011. **17**:

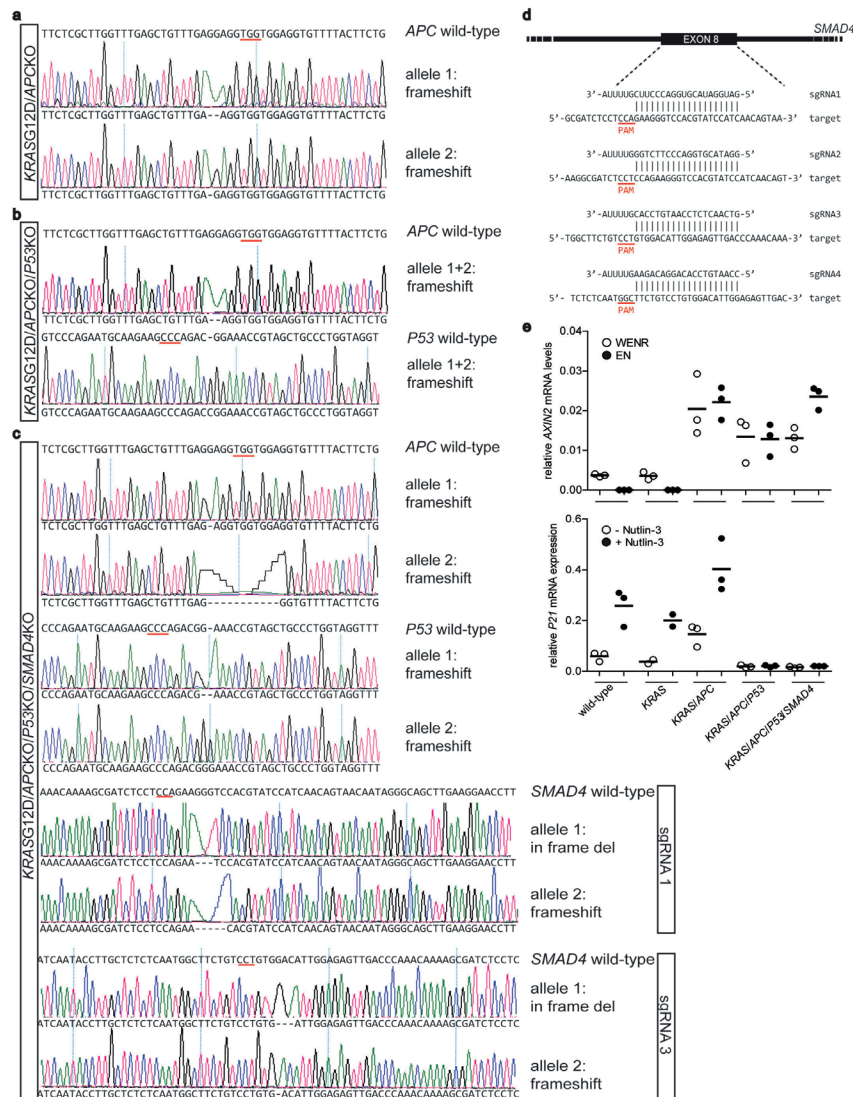
- p. 1225.
10. Huch, M., et al., *Unlimited in vitro expansion of adult bi-potent pancreas progenitors through the Lgr5/R-spondin axis*. The EMBO Journal, 2013. **32**(20): p. 2708–2721.
  11. Sato, T., et al., *Single Lgr5 stem cells build crypt-villus structures in vitro without a mesenchymal niche*. Nature, 2009. **459**(7244): p. 262–265.
  12. Sato, T., et al., *Long-term Expansion of Epithelial Organoids From Human Colon, Adenoma, Adenocarcinoma, and Barrett's Epithelium*. Gastroenterology, 2011. **141**(5): p. 1762–1772.
  13. Sato, T. and H. Clevers, *Primary mouse small intestinal epithelial cell cultures*. Methods Mol Biol, 2013. **945**: p. 319–28.
  14. Mali, P., et al., *RNA-guided human genome engineering via Cas9*. Science, 2013. **339**(6121): p. 823–6.
  15. Cho, S.W., et al., *Targeted genome engineering in human cells with the Cas9 RNA-guided endonuclease*. Nature Biotechnology, 2013. **31**: p. 230.
  16. Cong, L., et al., *Multiplex genome engineering using CRISPR/Cas systems*. Science, 2013. **339**(6121): p. 819–23.
  17. Schwank, G., et al., *Functional Repair of CFTR by CRISPR/Cas9 in Intestinal Stem Cell Organoids of Cystic Fibrosis Patients*. Stem Cell, 2013. **13**(6): p. 653–658.
  18. Vassilev, L.T., et al., *In vivo activation of the p53 pathway by small-molecule antagonists of MDM2*. Science, 2004. **303**(5659): p. 844–8.
  19. Shi, Y., et al., *A structural basis for mutational inactivation of the tumour suppressor Smad4*. Nature, 1997. **388**(6637): p. 87–93.
  20. Chacko, B.M., et al., *Structural basis of heteromeric smad protein assembly in TGF-beta signaling*. Mol Cell, 2004. **15**(5): p. 813–23.
  21. Fleming, N.I., et al., *SMAD2, SMAD3 and SMAD4 mutations in colorectal cancer*. Cancer Res, 2013. **73**(2): p. 725–35.
  22. Rajagopalan, H., et al., *The significance of unstable chromosomes in colorectal cancer*. Nature reviews. Cancer, 2003. **3**(9): p. 695–701.
  23. Fodde, R., et al., *Mutations in the APC tumour suppressor gene cause chromosomal instability*. Nature cell biology, 2001. **3**(4): p. 433–438.
  24. Bomme, L., et al., *Clonal karyotypic abnormalities in colorectal adenomas: clues to the early genetic events in the adenoma-carcinoma sequence*. Genes Chromosomes Cancer, 1994. **10**(3): p. 190–6.
  25. Herbergs, J., et al., *Chromosome aberrations in adenomas of the colon. Proof of trisomy 7 in tumor cells by combined interphase cytogenetics and immunocytochemistry*. Int J Cancer, 1994. **57**(6): p. 781–5.
  26. Ried, T., et al., *Comparative genomic hybridization reveals a specific pattern of chromosomal gains and losses during the genesis of colorectal tumors*. Genes Chromosomes Cancer, 1996. **15**(4): p. 234–45.
  27. van de Wetering, M., et al., *Prospective derivation of a living organoid biobank of colorectal cancer patients*. Cell, 2015. **161**(4): p. 933–945.
  28. Matano, M., et al., *Modeling colorectal cancer using CRISPR-Cas9-mediated engineering of human intestinal organoids*. Nature Medicine, 2015. **21**(3): p. 256–262.
  29. Kim, K.A., et al., *Mitogenic influence of human R-spondin1 on the intestinal epithelium*. Science, 2005. **309**(5738): p. 1256–9.
  30. Shaner, N.C., et al., *A bright monomeric green fluorescent protein derived from Branchiostoma lanceolatum*. Nature Methods, 2013. **10**(5): p. 407–409.
  31. Li, H. and R. Durbin, *Fast and accurate short read alignment with Burrows-Wheeler transform*. Bioinformatics, 2009. **25**(14): p. 1754–60.
  32. DePristo, M.A., et al., *A framework for variation discovery and genotyping using next-generation DNA sequencing data*. Nature Genetics, 2011. **43**: p. 491.

## Exetended Data



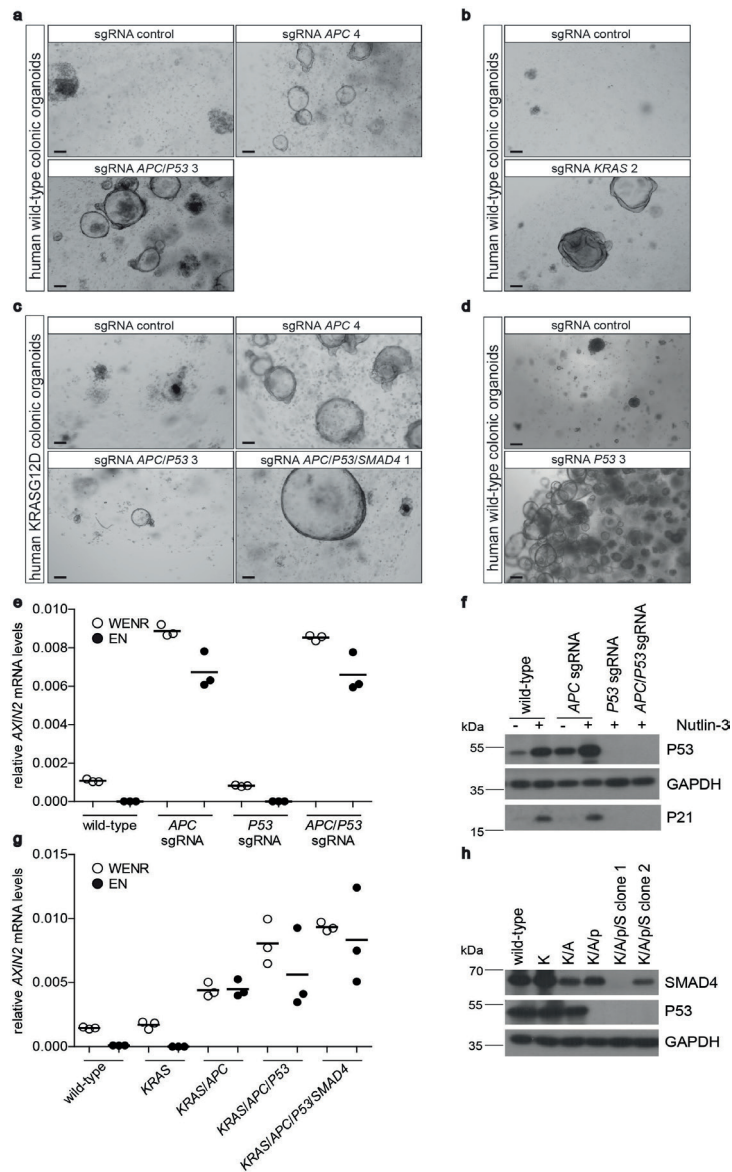
3

**Extended Data Figure 1: Introducing inactivating mutations in the APC and P53 genes in human intestinal organoids using CRISPR/Cas9.** A) Schematic representation of the targeted exon of the human APC (left) and P53 (right) loci and sequences of the designed sgRNAs. B,C) PCR amplification products of the mutated alleles of APC (B) and P53 (C) were obtained using primers flanking the targeted exon. Subsequent sequencing revealed indels at the expected locations. PAM sequences are underlined in red in wild-type sequences. Of note, the curved lines bridging the gaps in deleted alleles are drawn by the alignment software.



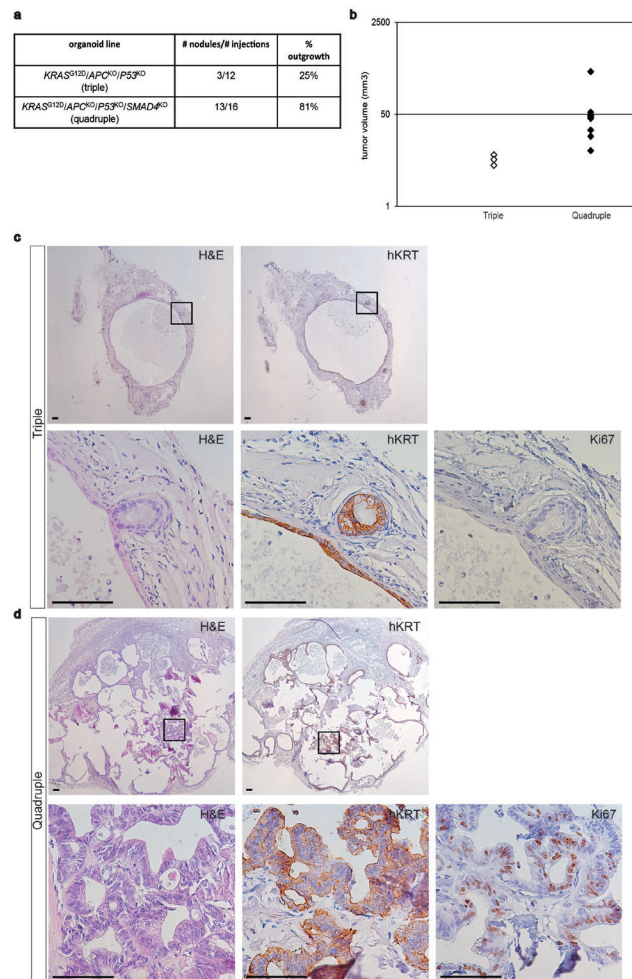
Extended Data Figure 2: KRASG12D, APCKO, P53KO and SMAD4KO mutation combinations in human intestinal organoids. A–C), PCR amplification products of the indicated genes of KRASG12D/APCKO (A), KRASG12D/APCKO/P53KO (B) and KRASG12D/APCKO/P53KO/SMAD4KO (C) organoids were obtained using primers flanking the targeted exon. Subsequent sequencing revealed indels at the expected locations. PAM sequences are underlined in red. Of note, the curved lines bridging the gaps in deleted alleles are drawn by the alignment software. D) Schematic representation of the targeted exon of the human SMAD4 locus and sequences of the designed sgRNAs. E) qRT–PCR for AXIN2 (top) and P21 (bottom) in the indicated organoid cultures. Top, the indicated organoid lines were cultured in the presence (WENR) or absence (EN) of WNT/R-spondin. Bottom, the indicated organoid lines were cultured in the presence or absence of nutlin-3 for 24 h. Expression was normalized to GAPDH. Horizontal bars represent mean of n = 3 independent experiments.





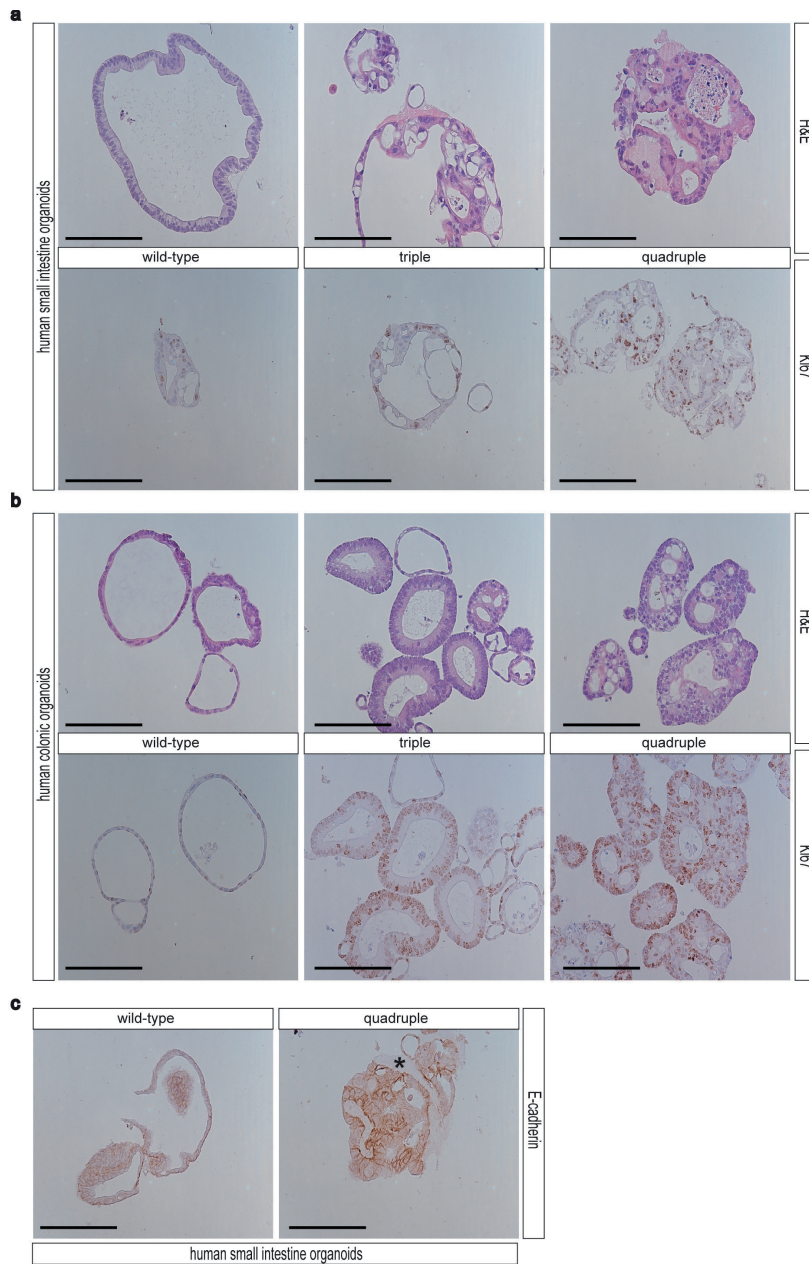
**Extended Data Figure 3: Using CRISPR/Cas9-mediated genome editing to introduce APC, P53, KRASG12D and SMAD4 mutations in human colonic organoids.** A–D) Using the strategies depicted in Figs 1a and 2a, d, APCKO, APCKO/P53KO (A), KRASG12D (B), KRASG12D/APCKO, KRASG12D/APCKO/P53KO, KRASG12D/APCKO/P53KO/SMAD4KO (C) and P53KO (D) mutant human colon organoids were generated. Experiment was performed at least three independent times for each mutation. E) qRT–PCR for AXIN2 in the indicated organoid lines cultured in the presence (WENR) or absence (EN) of WNT/R-spondin. Expression was normalized to GAPDH. Horizontal bars represent mean of  $n = 3$  independent experiments. F) Western blot analysis of P53 and P21 expression in the indicated human colon organoid lines cultured in the presence or absence of nutlin-3. GAPDH, loading control. G) qRT–PCR for AXIN2 in the indicated organoid lines cultured in the presence (*continues on next page*)

(WENR) or absence (EN) of WNT/R-spondin. Expression was normalized to GAPDH. Horizontal bars represent mean of  $n = 3$  independent experiments. H) Western blot analysis of SMAD4 and P53 expression in the indicated human colon organoid lines. Please note that quadruple-mutant clone 1 contains SMAD4 frameshift-inducing indels in both alleles whereas clone 2 contains a frameshift-inducing indel in one and an in-frame deletion in the other allele (reduced SMAD4 expression). GAPDH, loading control. Scale bars, 100  $\mu\text{m}$ .

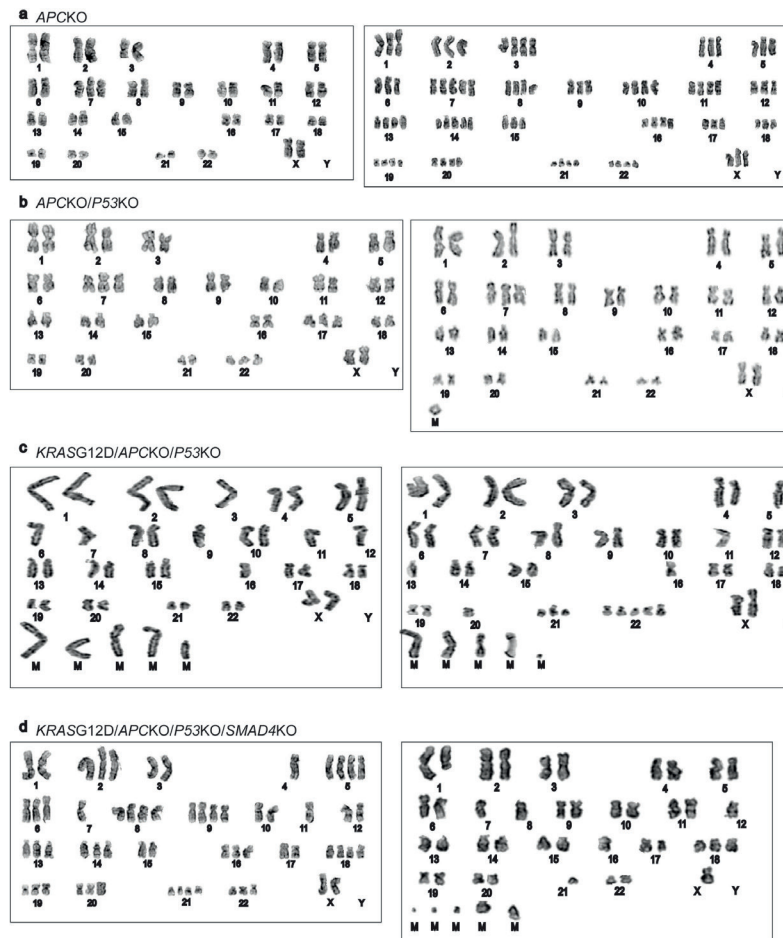


**Extended Data Figure 4: Quadruple-mutant human intestinal organoids grow as tumours with features of invasive carcinoma in vivo.** A) Wild-type and all engineered human intestinal organoid lines were injected subcutaneously in immunodeficient mice. Mice injected with *KRAS*<sup>G12D</sup>/*APCKO*/*P53*<sup>KO</sup> (triple) and *KRAS*<sup>G12D</sup>/*APCKO*/*P53*<sup>KO</sup>/*SMAD4*<sup>KO</sup> (quadruple) organoids developed visible nodules. B) Tumour sizes were examined 8 weeks after transplantation. C-D) H&E (top left, bottom left), hKRT (top right, bottom middle) and Ki67 (bottom right) immunostainings on nodules isolated from triple- (C) and quadruple-mutant (D) injected mice. Triple-mutant organoids did engraft but remained small, showed only weak proliferation and had adenoma features ( $n = 3$  mice). Quadruple-mutant-derived tumours were highly proliferative with features of invasive carcinoma ( $n = 13$  mice). See Fig. 3 for more details. Scale bars, 100  $\mu\text{m}$ .



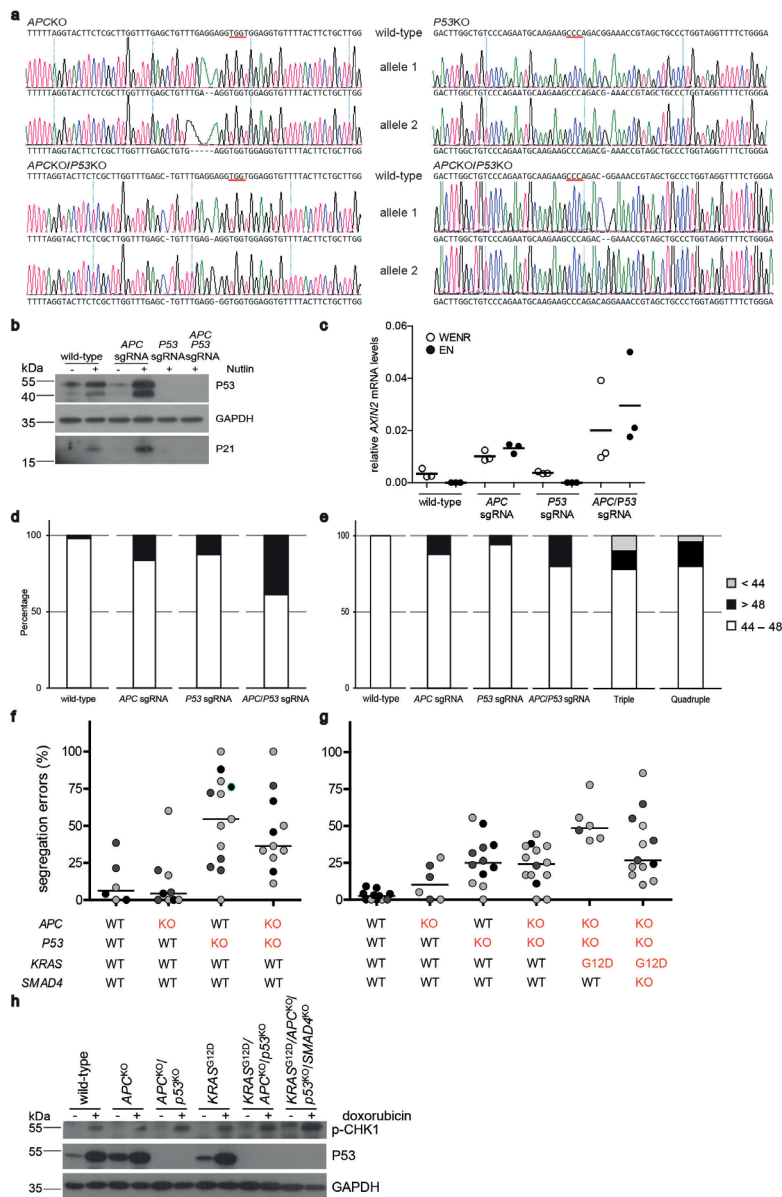


**Extended Data Figure 5: Histological analysis of triple- and quadruple-mutant organoids reveals morphological changes *in vitro*.** A) Representative H&E and Ki67 immunostainings on the indicated human small intestinal organoid lines (n = 4 independent experiments). B) Representative H&E and Ki67 immunostainings on the indicated human colon organoid lines (n = 3 independent experiments). C) Representative E-cadherin immunostainings on wild-type and quadruple-mutant human small intestinal organoids (n = 4 independent experiments). Asterisk indicates residual Matrigel. Scale bars, 100  $\mu$ m.

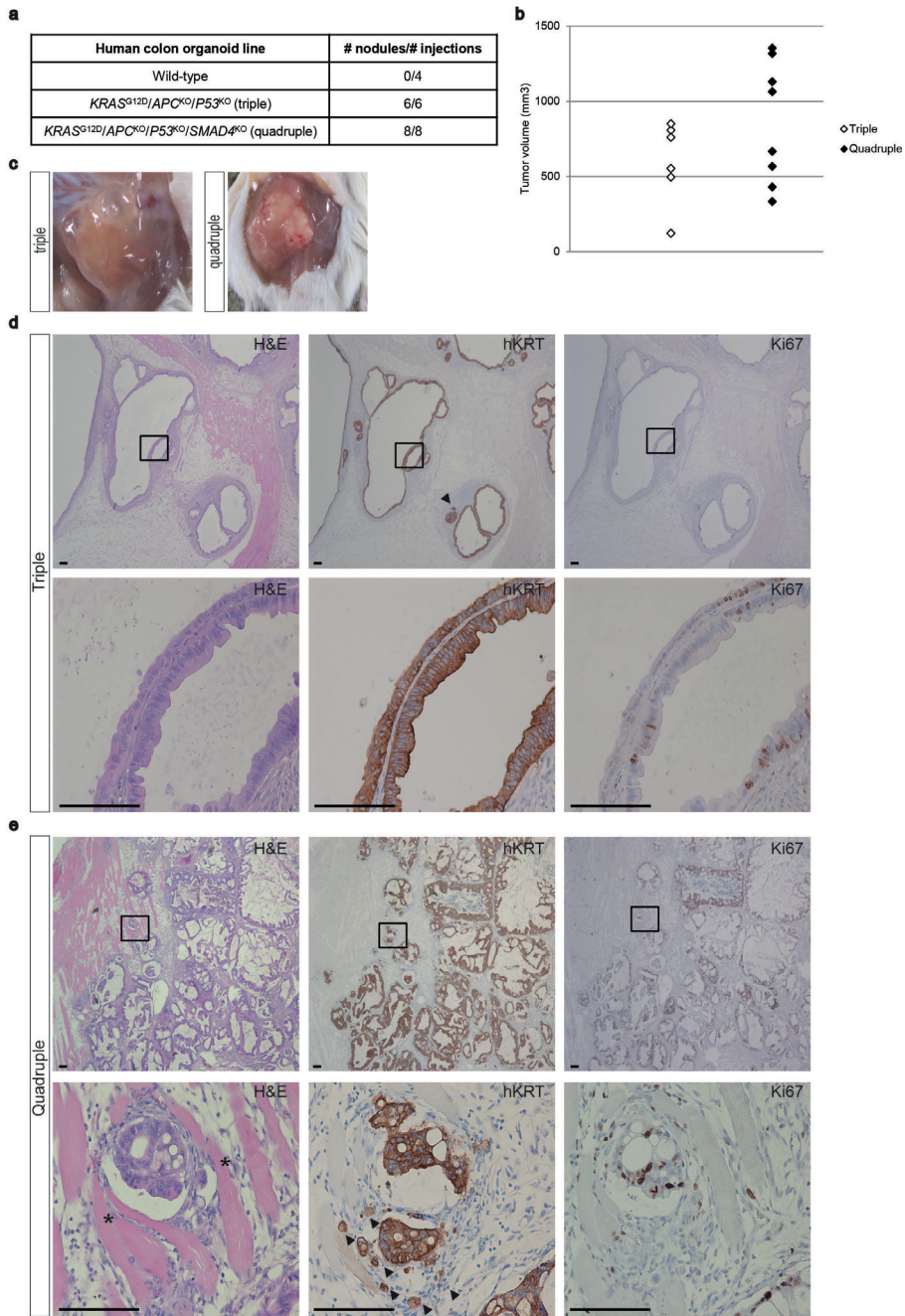


**Extended Data Figure 6: Progressive aneuploidy upon introduction of CRC mutations.** A–D) Karyograms of APCKO (A), APCKO/P53KO (B), KRASG12D/APCKO/P53KO (C) and KRASG12D/APCKO/P53KO/SMAD4KO (D) organoids, showing extensive aneuploidy in organoids harbouring CRC mutations (20 spreads were analysed per line). Note the occurrence of trisomy 7 in APCKO and APCKO/P53KO (independent clones) organoids. M, marker chromosomes.

→ **Extended Data Figure 7: Loss of both APC and P53 results in extensive CIN and aneuploidy.** A) APCKO, P53KO and APCKO/P53KO mutations were introduced in a second independent human intestinal organoid line. PCR amplification products of the mutated alleles of APC and P53 were obtained using primers flanking the targeted exon. Subsequent sequencing revealed frameshift-inducing indels at the expected locations. Left, APC genotyping; right, P53 genotyping. PAM sequences are underlined in red. Of note, the curved lines bridging the gaps in deleted alleles are drawn by the alignment software. B) Western blot analysis for P53 and P21 expression in the second human intestinal organoid line cultured in the presence or absence of nutlin-3. GAPDH, loading control. C) qRT-PCR for AXIN2 in the second human intestinal organoid line cultured in the presence (WENR) or absence (EN) of WNT/R-spondin. Expression was normalized to GAPDH. Horizontal bar represents mean of  $n = 3$  independent experiments. D) Chromosome numbers were counted in the second human (*continues on next page*)



intestinal organoid lines. Graphs plot the percentage of cells with chromosome counts <44, 44–48 (normal) and >48 (at least 50 spreads were counted). E) As in (D) but for indicated human colon organoid lines. F) Live-cell imaging was performed to monitor chromosome segregations in the indicated human small intestinal organoid lines. Graph shows the percentage of erroneous mitoses. Each dot represents the percentage of errors in one organoid. Horizontal bars represent median of all dots. A video is included of organoids depicted as dots with green outline (Supplementary Video 6). WT, wild type; KO, knockout. G) As in (F) but for indicated human colon organoid lines. H) Western blot analysis of phospho-CHK1 and P53 expression in the indicated organoid lines treated with the DNA-damaging drug doxorubicin, or left untreated. GAPDH, loading control.





← **Extended Data Figure 8: Engineered mutant human colon organoids grow as invasive carcinomas in vivo.** A) Wild-type, triple- and quadruple-mutant human colon organoids were injected subcutaneously in immunodeficient mice. Nodules were counted 7 weeks after transplantation. B) Tumour sizes were examined 7 weeks after transplantation. C) Representative pictures of a 'cystic' triple-mutant (left) and 'solid' quadruple-mutant (right) tumour in immunodeficient mice. D) H&E (top left, bottom left), hKRT (top middle, bottom middle) and Ki67 (top right, bottom right) immunostainings on nodules isolated from triple-mutant-injected mice. Representative pictures of a well-differentiated carcinoma with limited invasive growth. The invasive growth has an expansive growth pattern with little tumour budding. n = 6 mice. E) As in (D) but for quadruple-mutant-derived tumours. Representative pictures of a poorly differentiated invasive carcinoma with frequent tumour budding at the invasive front (invasion of isolated or small aggregates of cells into the stroma is frequently observed (black arrowheads)). Invasive character is confirmed by the invasive growth into the underlying muscle tissue (asterisk, muscle tissue). n = 8 mice. Scale bars, 100  $\mu$ m.

Extended Data Table 1: Introducing oncogenic mutations in human intestinal organoids using CRISPR/Cas9

**a**

Gene targeted	Selection procedure	# of functional sgRNAs
<i>APC</i>	- Wnt - R-spondin	2 out of 4
<i>P53</i>	+ Nutlin-3	3 out of 4
<i>KRAS</i>	- EGF (+ gefitinib)	2 out of 2
<i>SMAD4</i>	- Noggin	2 out of 4

**b**

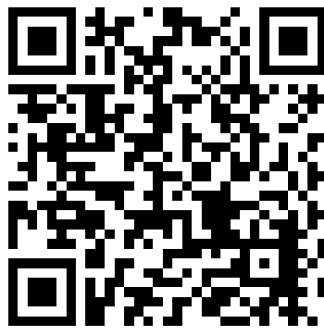
Organ	Organoid line	Mutation order	Genotype	<i>In vitro</i> phenotype	<i>In vivo</i> tumorigenicity
Small intestine	Wild-type		-	-; stable genome	No
Small intestine	<i>APC</i> <sup>KO</sup> (sgRNA 4)	<i>APC</i>	<i>APC</i> FS_pro1443/FS_pro1443	- Wnt - R-spondin; mild aneuploidy	No
Small intestine	<i>APC</i> <sup>KO</sup> / <i>P53</i> <sup>KO</sup> (sgRNA 4/3)	<i>APC</i> > <i>P53</i>	<i>APC</i> FS_pro1443/FS_pro1443 <i>P53</i> FS_phe109/FS_phe109	- Wnt - R-spondin + Nut-3; extensive aneuploidy	No
Small intestine	<i>KRAS</i> <sup>G12D</sup> (sgRNA 2)	<i>KRAS</i>	<i>KRAS</i> c.35G>A/FS_gly13	- EGF + gefitinib; N.D.	No
Small intestine	<i>KRAS</i> <sup>G12D</sup> / <i>APC</i> <sup>KO</sup> (sgRNA 2/4)	<i>KRAS</i> > <i>APC</i>	<i>KRAS</i> c.35G>A/FS_gly13 <i>APC</i> FS_pro1443/FS_pro1443	- EGF - Wnt - R-spondin; N.D.	No
Small intestine	<i>KRAS</i> <sup>G12D</sup> / <i>APC</i> <sup>KO</sup> / <i>P53</i> <sup>KO</sup> (sgRNA 2/4/3)	<i>KRAS</i> > <i>APC</i> , <i>P53</i>	<i>KRAS</i> c.35G>A/FS_gly13 <i>APC</i> FS_pro1443/FS_pro1443 <i>P53</i> FS_phe109/FS_phe109	- EGF - Wnt - R-spondin + Nut-3; extensive aneuploidy	Adenoma
Small intestine	<i>KRAS</i> <sup>G12D</sup> / <i>APC</i> <sup>KO</sup> / <i>P53</i> <sup>KO</sup> / <i>SMAD4</i> <sup>KO</sup> (sgRNA 2/4/3/1)	<i>KRAS</i> > <i>APC</i> , <i>P53</i> , <i>SMAD4</i>	<i>KRAS</i> c.35G>A/FS_gly13 <i>APC</i> FS_pro1443/FS_pro1443 <i>P53</i> FS_phe109/FS_phe109 <i>SMAD4</i> DEL_pro356/FS_pro356	- EGF - Wnt - R-spondin - Noggin + Nut-3; extensive aneuploidy; grow as solid tumour masses	Invasive carcinoma
Colon	Wild-type		-	-; stable genome	No
Colon	<i>APC</i> <sup>KO</sup> (sgRNA 4)	<i>APC</i>	<i>APC</i> FS_pro1443/FS_pro1443	- Wnt - R-spondin; mild aneuploidy	N.D.
Colon	<i>P53</i> <sup>KO</sup> (sgRNA 3)	<i>P53</i>	<i>P53</i> FS_phe109/FS_phe109	+ Nut-3; mild aneuploidy	N.D.
Colon	<i>APC</i> <sup>KO</sup> / <i>P53</i> <sup>KO</sup> (sgRNA 4/3)	<i>APC</i> > <i>P53</i>	<i>APC</i> FS_pro1443/FS_pro1443 <i>P53</i> FS_gly108/FS_gly108	- Wnt - R-spondin + Nut-3; extensive aneuploidy	N.D.
Colon	<i>KRAS</i> <sup>G12D</sup> (sgRNA 2)	<i>KRAS</i>	<i>KRAS</i> c.35G>A/c.35G>A	- EGF + gefitinib; N.D.	N.D.
Colon	<i>KRAS</i> <sup>G12D</sup> / <i>APC</i> <sup>KO</sup> (sgRNA 2/4)	<i>KRAS</i> > <i>APC</i>	<i>KRAS</i> c.35G>A/c.35G>A <i>APC</i> FS_pro1443/FS_pro1441	- EGF - Wnt - R-spondin; N.D.	N.D.
Colon	<i>KRAS</i> <sup>G12D</sup> / <i>APC</i> <sup>KO</sup> / <i>P53</i> <sup>KO</sup> (sgRNA 2/4/3)	<i>KRAS</i> > <i>APC</i> , <i>P53</i>	<i>KRAS</i> c.35G>A/c.35G>A <i>APC</i> FS_pro1443/FS_pro1443 <i>P53</i> FS_phe109/FS_phe109	- EGF - Wnt - R-spondin + Nut-3; extensive aneuploidy	Well differentiated carcinoma with limited invasive growth
Colon	<i>KRAS</i> <sup>G12D</sup> / <i>APC</i> <sup>KO</sup> / <i>P53</i> <sup>KO</sup> / <i>SMAD4</i> <sup>KO</sup> (sgRNA 2/4/3/1)	<i>KRAS</i> > <i>APC</i> , <i>P53</i> , <i>SMAD4</i>	<i>KRAS</i> c.35G>A/c.35G>A <i>APC</i> FS_pro1443/FS_pro1443 <i>P53</i> FS_gly105/FS_gly105 <i>SMAD4</i> DEL_pro356/FS_pro356	- EGF - Wnt - R-spondin - Noggin + Nut-3; extensive aneuploidy; grow as solid tumour masses	Poorly differentiated carcinoma with frequent invasive growth

a. Overview of the number of functional sgRNAs and the selection strategy used. b. Overview of the engineered lines. N.D., not determined.

## Supplementary Videos

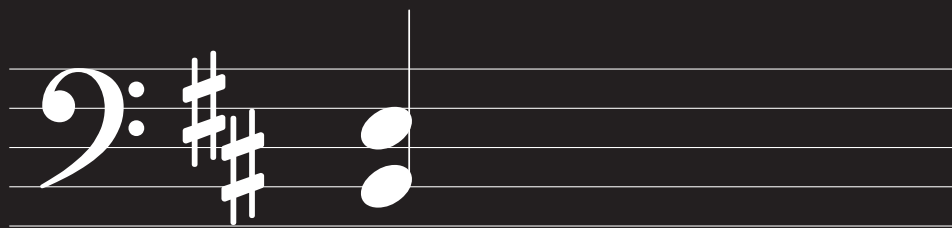
All supplementary videos are available via:

<https://www.youtube.com/channel/UC4e49VyC2RWUCgAD-HB0aPQ?>



3

Representative live cell imaging experiments of wild-type (1), APCKO (2), APCKO/P53KO (3), KRASG12D/APCKO/P53KO (4) and RASG12D/APCKO/P53KO/SMAD4KO (5) organoids and P53KO in the second human intestinal organoid line (6). Organoids were subjected to confocal imaging for 16 – 20 hours. Shown are representative parts of this time window and organoids presented are depicted as green-lined dots in quantification plot Figure 4a. Upper right quadrant shows H2B-mNeon fluorescence after maximum-projection of 3D z-stacks; upper left represents same data, color-coded for depth (z), facilitating tracking of individual events; lower quadrants include transmitted light images with and without merged H2B-mNeon (green). Scale bars as indicated in video.





# Chapter 4

## **p38 restrains chromosomal instability upon p53 loss in human colon organoid cultures**

**R.H. van Jaarsveld<sup>1</sup>, B. Ponsioen<sup>2</sup>, N. van den Tempel<sup>3</sup>, C. Rebel<sup>1</sup>,  
T. Kuijt<sup>1</sup>, A. Teixeira<sup>1</sup>, E. Fessler<sup>4</sup>, J.P. Medema<sup>4</sup>, M.A.T.M. van  
Vught<sup>3</sup>, H.J. Snippert<sup>2</sup>, J. Drost<sup>5</sup>, G.J.P.L. Kops<sup>1</sup>**

<sup>1</sup> Oncode Institute, Hubrecht Institute – KNAW and University Medical Centre Utrecht, Utrecht, the Netherlands

<sup>2</sup> Molecular Cancer Research, Center for Molecular Medicine, University Medical Center Utrecht, Utrecht University, Universiteitsweg 100, 3584 CG Utrecht, The Netherlands

<sup>3</sup> Department of Medical Oncology, University Medical Center Groningen, University of Groningen, Groningen, The Netherlands

<sup>4</sup> Oncode Institute, LEXOR, Center of Exp Mol Medicine, Cancer Center Amsterdam, Amsterdam UMC, Meibergdreef 9, 1105AZ Amsterdam, The Netherlands

<sup>5</sup> Princess Máxima Center for Pediatric Oncology, Utrecht, The Netherlands

Manuscript submitted

## Abstract

Chromosomal instability (CIN) drives tumor evolution and is a hallmark of colorectal cancer. How and when CIN arises during colorectal cancer progression is unknown. We have previously shown that the appearance of CIN coincides with loss of p53 in a human intestinal organoid model that mimics the adenoma-to-carcinoma sequence of colorectal cancer. We now show that loss of p53 causes the formation of bulky anaphase bridges within one cell cycle and identify inhibition of the p38 stress kinase as a key prerequisite for this phenotype. Combined loss of p53 and p38 generates bulky anaphase bridges characterized by unresolved DNA damage of which replication stress is unlikely to be the dominant cause. Strikingly, mitotic fidelity was restored when the DNA damage response was inhibited in the preceding G2. Anaphase bridge formation in p53-deficient tumor organoids from colorectal cancer patients increased when p38 was inhibited. We thus conclude that p38 activity restrains excessive CIN upon p53 loss in colon cancer, which may present therapeutic opportunities for p53-deficient colorectal cancers.

## Introduction

The genetic landscape of the majority of human colorectal cancers (CRCs) is characterized by aneuploidy [1]. Aneuploidy is caused by the missegregation of chromosomes during mitosis. Cell populations with frequent mitotic infidelities are referred to as having a chromosomal instability (CIN) phenotype [2]. CIN is thought to promote tumor development, tumor evolution, and metastases, and the resulting aneuploid karyotypes are associated with immune evasion and poor patient prognosis [3-9]. Despite its important role in shaping tumor genotypes, the mechanisms and underlying (epi)genetic defects that lead to CIN in CRC are still unclear. It is also unknown when during CRC development CIN arises.

The development of CRC is thought to follow an adenoma-to-carcinoma sequence, in which specific successive mutations cause progression of the tumor from a premalignant lesion (adenoma) to a malignant and invasive one (carcinoma) [10]. According to this model, the sequence is initiated by activation of the Wnt-pathway, followed by activation of the EGF-receptor (EGFR) and inactivation of the p53 and TGF- $\beta$  pathways. We previously developed a human intestinal, stem cell-based, 3D ('organoid') culture model that mimics this progression, by introducing the most common mutations in CRC in a step-wise manner (loss of *APC*, gain of *KRAS*<sup>G12D</sup>, and losses of *TP53* and *SMAD4*, respectively) [11]. Live-cell imaging of chromosome segregation in this organoid panel showed that CIN arose once *TP53* was lost [11]. Importantly, *TP53* mutation alone, in the absence of any other oncogenic event, was sufficient for causing CIN.

After *APC*, *TP53* is the most commonly mutated gene in non-hypermethylated CRC, the predominant form of CRC, which is characterized by extensive karyotype abnormalities [1, 12]. *TP53* is central to cell fate decisions under several stress conditions, most prominently DNA-damage [13-16]. These cellular stresses activate p53 which then initiates a transcriptional program to induce cell cycle arrest or cell death [16]. Loss of p53 function thus allows continued cell proliferation despite the presence of DNA-damage, thereby promoting the accumulation of (oncogenic)

#### 4

mutations. p53 mutations are additionally associated with the accumulation of gross copy number alterations (CNAs) [17, 18], which is in line with recent observations that p53 loss allows proliferation of cells that have acquired gross structural chromosome abnormalities as a result of chromosome breakage following mitotic errors [19]. p53 loss is furthermore associated with generation and propagation of polyploid cells [20–22], with genomic rearrangements such as chromothripsis [23] and with replication stress [24, 25]. *TP53*<sup>-/-</sup> mouse embryonic fibroblasts display centrosome amplification, leading to chromosome segregation errors [26], implying p53 may also have more direct roles in protecting from mitotic infidelities.

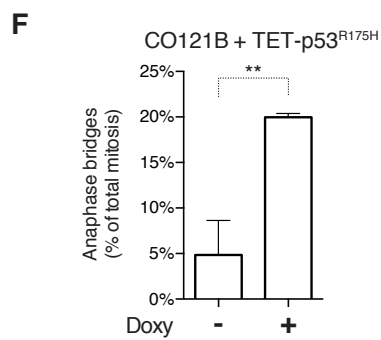
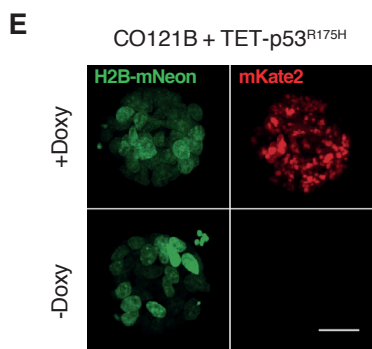
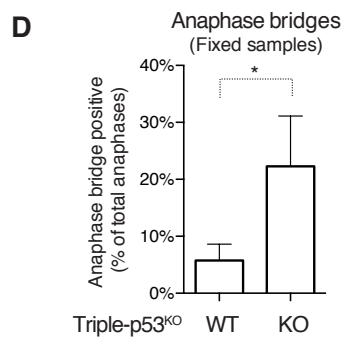
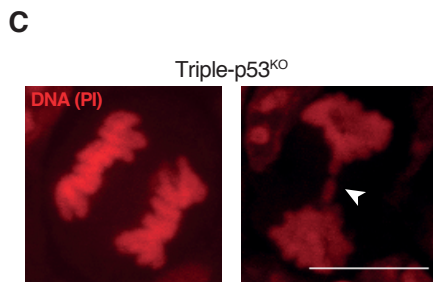
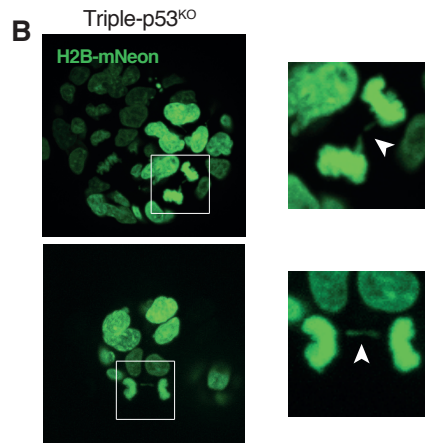
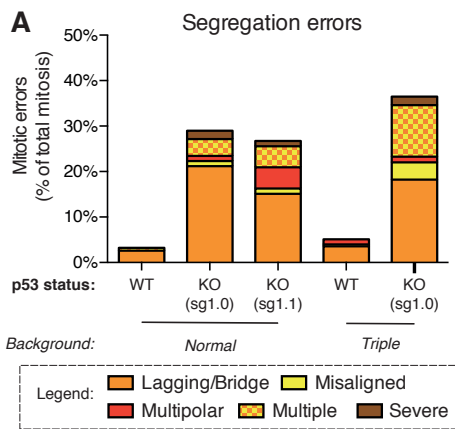
The large body of studies showing that p53 loss is important for tolerating continued proliferation of damaged cells led us to further examine the causes of chromosomal instability in *TP53*-knockout human intestinal organoids. We here show that loss of p53 function leads to bulky anaphase bridges within one cell cycle. These bridges are associated with DNA-damage and depend on an active DNA-damage response in the G2 phase preceding the faulty mitosis. Importantly, we identify inhibition of the p38 stress kinase as a key prerequisite in the appearance of anaphase bridges following p53 loss and show that inhibition of p38 increases bridges in p53 deficient tumor-derived organoids.

## Results

### Loss of p53 leads to the formation of anaphase bridges during mitosis

Our previous work using a panel of human colon organoids mimicking the adenoma-to-carcinoma transition in CRC showed that the loss of p53 function by CRISPR/Cas9 knockout was associated with the onset of CIN in the absence of any other oncogenic mutation [11]. To further examine this, we first wished to confirm our findings. Two independent gRNAs that targeting *TP53* induced similar levels of chromosome missegregation as judged from live-cell imaging of organoids expressing a fluorescently tagged Histone 2B (H2B-mNeon) (Figure 1A, Supplemental movie 1). Furthermore, the missegregation rates in organoid lines carrying CRISPR/Cas9-mediated mutations in three other genes commonly involved in CRC (*APC*, *KRAS* and *SMAD4*; hereafter referred to as Triple-p53<sup>WT</sup>) was elevated by additional knockout of *TP53* (hereafter referred to as Triple-p53<sup>KO</sup>), to levels similar to cultures with only *TP53* mutated (Figure 1A). We therefore conclude that loss of p53 function induces CIN in human colon organoid cultures. From here on, we mostly use the comparison of Triple-p53<sup>WT</sup> to Triple-p53<sup>KO</sup> to study the role of p53 in CIN, because wild-type organoid cultures and those mutated only for *TP53* were difficult to maintain in culture.

To further investigate the role of p53 in protecting from mitotic infidelities, we quantified which types of errors occurred most frequently. Although we occasionally observed misaligned chromosomes, lagging chromosomes and multipolar divisions, the predominant form of mitotic error upon p53 knockout was an anaphase bridge (Figure 1A and B). This was observed in both p53<sup>KO</sup> single mutant organoids and Triple-p53<sup>KO</sup> organoids. The anaphase bridges were not caused by H2B-mNeon-expression procedures or imaging-induced phototoxicity, as similar levels of CIN and anaphase bridges were seen when unmodified organoid cultures were fixed and stained with propidium iodide (PI) to visualize DNA (Fig. 1C and D). Interestingly, since both H2B-mNeon and PI were able to stain the anaphase bridges, they were distinct from the most commonly described type of anaphase bridges, ultra-fine bridges (UFBs) [27, 28]. We therefore refer to the *TP53*<sup>KO</sup>-induced bridges as bulky anaphase bridges (BABs).



← **Figure 1: Loss of p53 leads to the formation of anaphase bridges during mitosis.** A) Quantifications of chromosome segregation errors and types in living human colon organoids infected with H2B-mNeon and either wild-type (WT) or knockout (KO) for TP53. Sg1.0 and 1.1 indicate two independent sgRNAs for p53 KO. *TP53* was mutated in either healthy colon-derived organoids without any further perturbations (Normal) or mutated for the most common CRC mutations (Triple). B) Stills from movies showing bulky anaphase bridges in Triple-p53<sup>KO</sup> organoids, indicated by white arrowheads in blow-out pictures. C) Example of a correct mitosis (left panel) and a propidium iodide (PI) positive anaphase bridge (indicated with white arrowhead, right panel) in fixed, non-H2BmNeon transduced Triple-p53<sup>KO</sup> organoids. Scale bar: 10µm D) Quantifications of the number of bulky anaphase bridges in fixed samples. Anaphases showing multipolar divisions and severe missegregations were excluded from analysis. Error bars show S.D. of three independent experiments. Statistical testing by two-tailed, unpaired t-test as performed by Prism Graphpad software. \*p<0.05. E) Example images indicating doxycycline mediated induction of expression of TET-p53<sup>R175H</sup> in FAP patient adenoma-derived organoids (CO121B) expressing H2B-mNeon. F) Quantifications of the number of bulky anaphase bridges in CO121B + TET-p53<sup>R175H</sup> organoids. Statistics as in (D). \*\*p<0.005.

### **Acute loss of *TP53* function causes chromosomal instability within one cell cycle.**

*TP53* has a well-described role in DNA damage responses [15, 16]. We next wondered whether the formation of BABs upon loss of p53 may be an indirect effect of DNA damage accumulated over several generations following CRISPR/Cas9-mediated *TP53* knockout and subsequent selection procedures. To address this, we used a strategy for relatively acute p53 inactivation by means of doxycycline-inducible overexpression of a dominant-negative p53 mutant (p53<sup>R175H</sup>) [29, 30]. Of note: R175 is the most commonly mutated p53 residue in large intestinal tumors according to the COSMIC database [31]. Co-expression of mKate2 was used to ensure that imaged cells indeed expressed the mutant p53 (construct referred to as TET-p53<sup>R175H</sup>). We were unable to establish wild-type or Triple-p53<sup>KO</sup> organoids carrying both H2B-mNeon and TET-p53<sup>R175H</sup> expression systems for unknown reasons but managed to obtain a FAP patient adenoma organoid line with correct expressions [32]. This organoid line has normal p53 function as judged from p53 stabilization after DNA-damage and sensitivity to the p53-activating drug Nutlin3a (Supplemental Figure S1A and B). As expected, doxycycline-mediated overexpression of p53<sup>R175H</sup> (Supplemental Figure S1C) rendered the organoids resistant to Nutlin3a, confirming its dominant-negative properties (Supplemental Figure S1B). Importantly, organoids with high p53<sup>R175H</sup> expression (based on mKate2 levels, Figure 1E) had a marked

increase in BABs (Figure 1F). This increase was observed between 8 and 24 hours post induction of the mutant, strongly arguing for a relatively direct involvement of p53 in preventing BABs, and against a role for DNA damage accumulated over several generations. These data support the hypothesis that p53 function is required to maintain mitotic fidelity during normal cell cycles.

### **The p38 stress kinase prevents chromosomal instability upon p53 loss**

*TP53* has a well-established role in protecting genome stability when genome integrity is compromised by various means, including during early stages of tumor initiation. However, an active role for p53 in maintaining chromosomal stability is not commonly observed in monolayer cell cultures [33–35], and we confirmed this using wild-type or mutant p53 variants of the human CRC cell line HCT116 [33] (Supplemental Figure S2A and B). We next wondered how this role for p53 could have become apparent in 3D human stem cell cultures. To test whether components specific to organoid culture media could account for the difference, we examined chromosome segregation fidelity in HCT116 cells cultured in media supplemented with organoid-media components for seven days. Strikingly, addition of the p38 inhibitor SB202190 (p38i) markedly increased CIN as seen by the appearance of BABs in HCT116 cells (Supplemental Figure S2B). In contrast to the colon organoid cultures, however, this increase was independent of *TP53* status, as recently also observed in monolayer embryonic fibroblasts from p38<sup>KO</sup> mice [36]. Removal of p38i from our Triple-p53<sup>KO</sup> organoid cultures for two weeks or longer restored mitotic fidelity, and high levels of BABs returned upon re-exposure to p38i for one week but no significant difference was found after 24h exposure (Figure 2A and B, Supplemental movies 2 and 3). No effects of p38i removal on the low CIN levels of Triple-p53<sup>WT</sup> organoids were observed (Figure 2C). The induction of BABs by p38i in the background of p53 inactivation was an on-target effect of SB202190, since inducible depletion of p38 by doxycycline-controlled expression of p38 shRNA [37] phenocopied p38i in Triple-p53<sup>KO</sup> (Figure 2D, Supplemental movies 4 and 5). Our results therefore show that p53 and p38 co-operate to prevent CIN in human colon organoids.



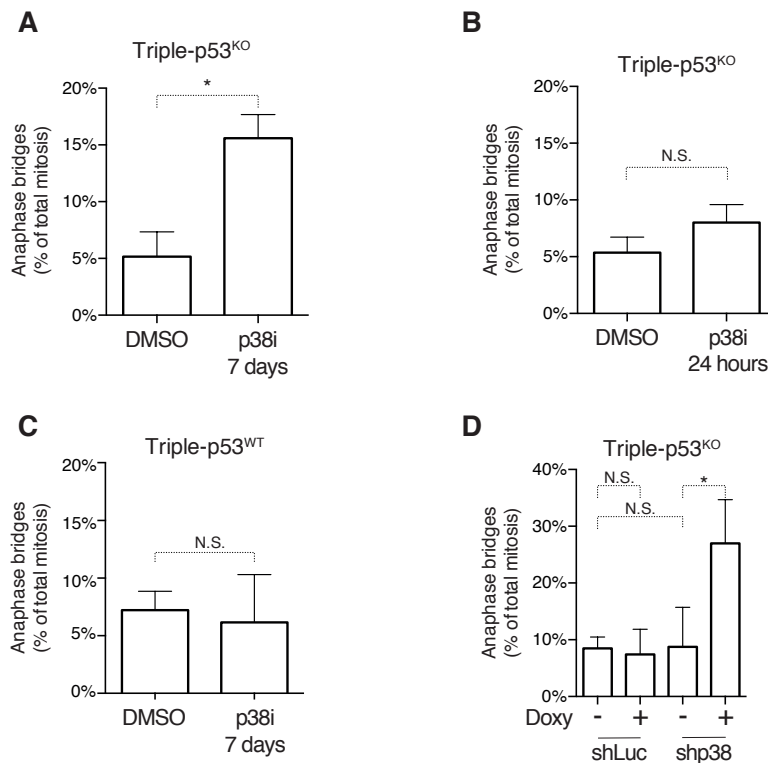


**Figure 2: The p38 stress kinase prevents chromosomal instability upon p53 loss.** A-B) Quantification of anaphase bridges in movies of Triple-p53<sup>KO</sup> organoids expressing H2B-mNeon and cultured for >2 weeks in the absence of p38i and re-exposed for seven days (A) or 24h (B) to p38i or control conditions (DMSO). Statistics as in Figure 1D. \*p<0.05. N.S.: not significant (p>0.05). C) Quantifications of anaphase bridges in movies of Triple-p53<sup>WT</sup> organoids. Statistics as in Figure 1D. N.S.: not significant (p>0.05). D) Quantifications of anaphase bridges in movies of Triple-p53<sup>KO</sup> organoids after doxycycline-induced expression of shLuciferase (shLuc) or shp38. Error bars depict S.D. of two independent experiments.

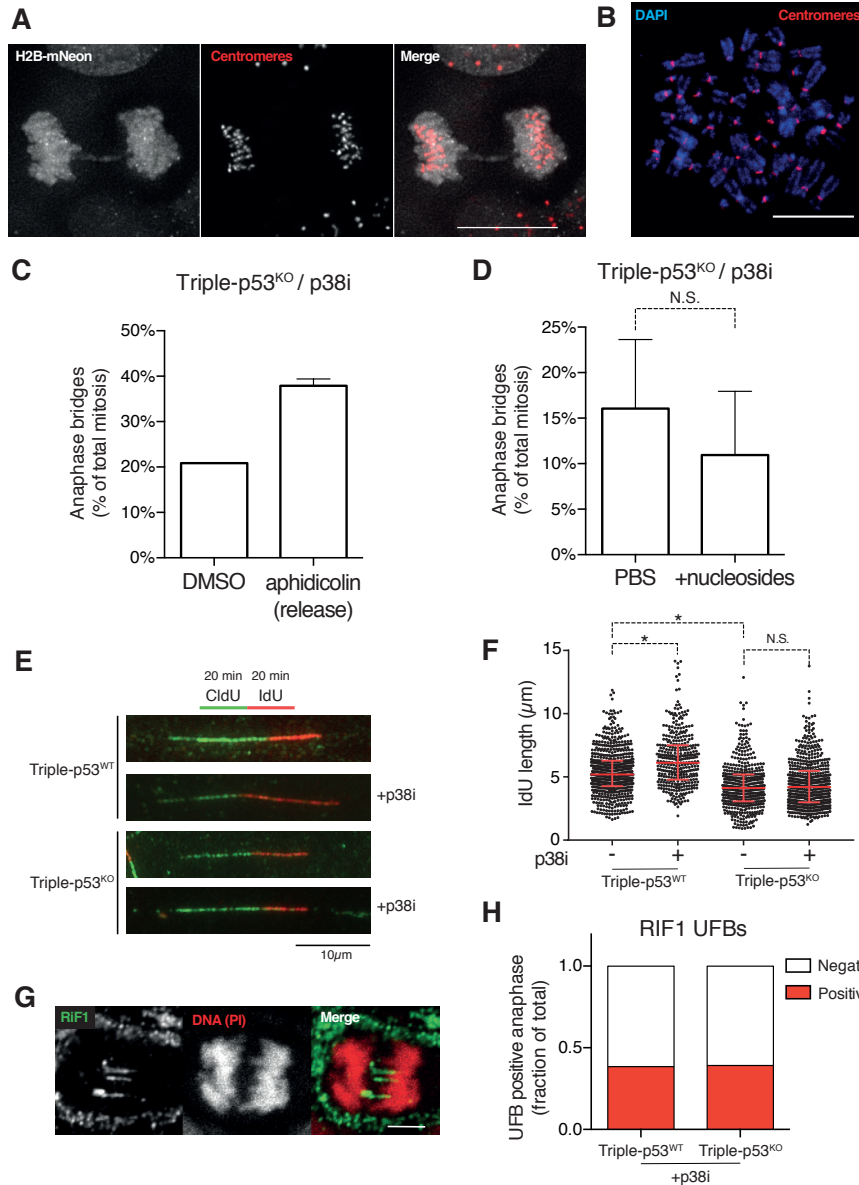
### Bulky anaphase bridge formation after combined p53 and p38 loss depends on active DNA-damage signaling

To explain the appearance of BABs upon loss of p53 and p38 functions, we considered two hypotheses: First, BABs can arise from breakage-fusion-bridge cycles that create dicentric chromosomes, either from telomere fusions or other chromosomal translocations [38]. Dicentrics can cause BABs by virtue of attachment of each centromere to opposite sides of the mitotic spindle. Dicentric chromosomes did not appear to underlie the BABs in Triple-p53<sup>KO</sup> organoids grown in p38i (hereafter Triple-p53<sup>KO</sup>/p38i), since we were unable to identify them in >30 metaphase spreads and BABs did not contain centromeric regions (Figure 3A and B). Second, BABs

→ **Figure 3: Dicentric chromosomes and replication deficiencies are an unlikely cause for bulky anaphase bridges upon loss of p53 and p38.** A) Example image showing a BAB negative for centromeric FISH signals in Triple-p53<sup>KO</sup>/p38i cells. Scale bar: 10µm. B) Example image of a metaphase spreads of Triple-p53<sup>KO</sup>/p38i cells showing no evidence for dicentric chromosomes. C) Quantifications of anaphase bridges in movies of Triple-p53<sup>KO</sup>/p38i organoids arrested by and released from an aphidicolin-induced S-phase block. Error bars depict S.D. of two independent experiments. D) Quantifications of anaphase bridges in movies of Triple-p53<sup>KO</sup>/p38i organoids cultured in the presence of additional nucleosides for seven days. Statistics as in Figure 1D. N.S.: not significant (p>0.05). E) Examples of replication fibers. PBS: phosphate buffered saline. F) Quantifications of replication fibers in Triple-p53<sup>KO</sup> and Triple-p53<sup>WT</sup> organoids cultured in the presence or absence of p38i for 24 hours. \*p<0.0001. G) Example images of RIF1-positive ultra-fine bridges (UFBs) in Triple-p53<sup>KO</sup>/p38i cells. Scale bar: 10µm. H) Quantifications of the number of anaphases showing RIF1-positive UFBs in Triple-p53<sup>WT</sup>/p38i and Triple-p53<sup>KO</sup>/p38i organoids.

may result from similar mechanisms that spawn UFBs [27, 39]. These include persistent catenates, recombination intermediates and incomplete replication (including stalled replication forks) [27, 28, 40-44]. To examine if replication issues could underlie BABs, we first examined if artificially stalling replication could lead to BAB formation. Imaging Triple-p53<sup>KO</sup>/p38i organoids after aphidicolin treatment indeed showed an increase in BABs (Figure 3C). Nevertheless, we did not observe enrichment of FANCD2 on the extremities of BABs (not shown) and observed only minor reductions in BAB formation upon culture of the organoids for five days in media supplemented with high concentrations of nucleosides (Figure 3D), an approach previously shown to rescue replication stress [45]. Finally, DNA-fiber analyses showed a reduction in replication speeds in Triple-p53<sup>KO</sup> organoids, but this was independent of p38 activity and did not result in an increase in UFBs in mitosis, as would be expected from increased replication stress (Figure 3E-G). Taken together, these results argue that replication deficiencies are an unlikely cause for the BABs upon loss of p53 and p38.

We next wondered what structures might underlie the formation of BABs upon loss of p53 and p38. Given that both genes are known to be involved in DNA-damage responses and since we observed an increase of BABs after aphidicolin treatment (which increases DNA-damage foci), we hypothesized that BABs are associated with DNA-damage. Therefore, we next analyzed 53BP1 recruitment to chromatin and phosphorylation of H2AX (γH2AX), markers of DNA double

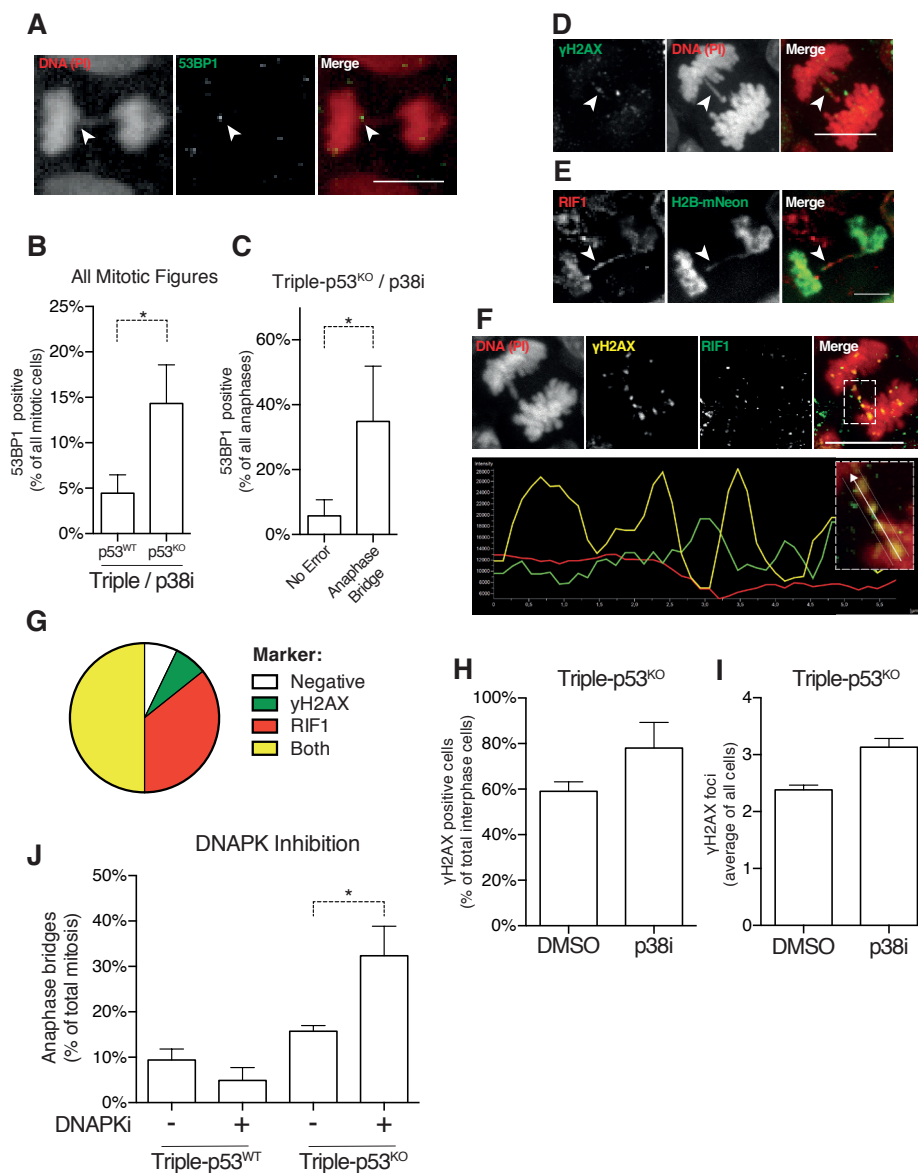


strand breaks, in asynchronous Triple-p53<sup>WT</sup>/p38i and Triple-p53<sup>KO</sup>/p38i organoids. We found more 53BP1-positive foci in mitotic figures of Triple-p53<sup>KO</sup>/p38i cells as compared to Triple-p53<sup>WT</sup>/p38i cells, and the foci were observed predominantly on BAB-positive anaphases (Figure 4A-C). Whereas 53BP1 was not found localized on the BABs, the majority of BABs did stain positive for  $\gamma$ H2AX, for the UFB marker and 53BP1 effector protein RIF1, or for both (Figure 4D-G). RIF1 and  $\gamma$ H2AX showed a

→ **Figure 4: Bulky anaphase bridges are associated with DNA-damage and positive for DNA-damage markers.** A) Example images of 53BP1 signals in a Triple-p53<sup>KO</sup>/p38i cell with a bulky anaphase bridge. Arrowheads point to location of 53BP1 foci. B) Quantification of 53BP1 foci in mitotic figures (prophase to telophase) in asynchronous Triple-p53<sup>WT</sup>/p38i and Triple-p53<sup>KO</sup>/p38i organoids. Statistics as in Figure 1D. \*p<0.05. C) Quantifications of 53BP1 foci in anaphases of Triple-p53<sup>KO</sup>/p38i divided in BAB positive and negative anaphase figures. Statistics as in Figure 1D. \*p<0.05. D-E) Example images of BABs in Triple-p53<sup>KO</sup>/p38i organoids showing regions positive for  $\gamma$ H2AX (D) and RIF1 (E). Arrowheads point to  $\gamma$ H2AX and RIF1 foci on the bridge, respectively. F) Top panel: example of a  $\gamma$ H2AX and RIF1 double-positive BAB. Bottom: Line-plot indicating average intensities (A.U.) of PI (red),  $\gamma$ H2AX (yellow) and RIF1 (green) over the length of the BAB. Scale bars D-F: 10 $\mu$ m. G) Pie chart depicting fractions of BABs positive for  $\gamma$ H2AX, RIF1 or both. H,I) Quantifications of  $\gamma$ H2AX positive interphase cells (H) and the average number of foci per nucleus (I). Error bars depict S.D. of two independent experiments. J) Quantifications of anaphase bridges of Triple-p53<sup>WT</sup>/p38i and Triple-p53<sup>KO</sup>/p38i organoids cultured in the presence of an inhibitor for DNAPK (DNAPKi, NU7441) or control conditions (DMSO). Triple-p53<sup>WT</sup>: N=2, Triple-p53<sup>KO</sup>: N=3. \*p<0.05. A.U.: Arbitrary Units. PI: Propidium Iodide.

mutually exclusive pattern and RIF1 was especially localized on regions where PI or H2B-mNeon signals were low (Figure 4F). These data thus indicate that the BABs in Triple-p53<sup>KO</sup>/p38i organoids coincided with damaged DNA that persisted in mitosis. It is unclear how the DNA damage originated, but as shown earlier it is unlikely to come from replication issues. Instead, we favor the hypothesis that p53 and p38 loss results in endogenous damages that are left poorly detected and unrepaired. In support of this hypothesis, inhibition of p38 increased the number of cells with DNA-damage foci and the average number of foci per cell (Figure 4H and I). BAB-causing DNA damage can originate even in G1, as treating p53<sup>KO</sup>/p38i organoids with an inhibitor of DNAPK (DNAPKi, NU7441) [46], the main regulator of DNA-damage repair in G1, increased the number of BABs (Figure 4J). DNAPKi did not increase BABs in Triple-p53<sup>WT</sup>/p38i organoids, suggesting that loss of p53 allows mitotic entry in the presence of DNA-damage.

Our data thus far support the hypothesis that the BABs upon loss of p53 and p38 function are caused by mitotic entry with unrepaired DNA damage. The presence of RIF1 in a punctuated pattern on BABs furthermore suggested that BABs are similar but not identical to UFBs, and we showed they were not caused by chromosome fusions as a result of breakage-fusion-bridge cycles or unresolved recombination intermediates. We thus considered it most likely that BABs were caused by persistent catenates, for



example from persistent DNA-damage foci formed before cells enter mitosis. Strikingly, inhibition of the DNA damage response effector kinases ATM (with KU55933) [47] or CHK2 (with PV1019) [48] for only a few hours rescued BAB formation in Triple-p53<sup>KO</sup>/p38i (Figure 5A and B). Combined with the observation that BABs were positive for yH2AX, this suggests that the inactivation of p53 and p38 caused CIN as a result of the maintenance of DNA damage foci by the DNA damage response pathway.

## p38 restrains anaphase bridge formation in human colorectal cancer

We wondered if human tumors that have lost a functional p53 pathway indeed depend on p38 to prevent BABs. To this end we selected two CRC patient-derived organoid lines that were resistant to Nutlin3a, suggesting these tumors had lost functional p53 (Figure 6A). We treated the lines with p38i for seven days and measured CIN by live-cell imaging. Both tumor-derived organoid lines show increased BABs when treated with p38i (Figure 6B). These results argue that in human CRC, p38 functions to restrain anaphase bridge formation when p53 function is lost.

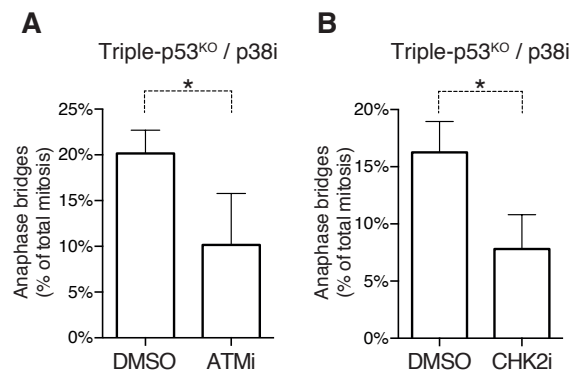
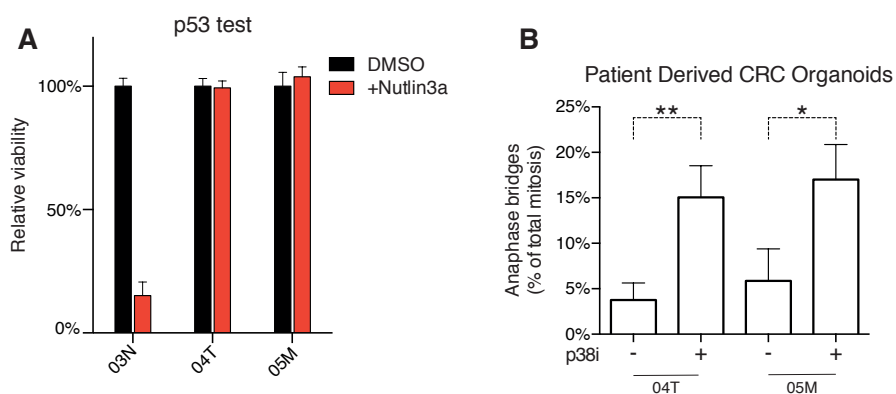


Figure 5: Loss of p53 and p38 cause bulky anaphase bridge formation via a persistent DNA damage response. A-B) Quantifications of anaphase bridges from movies of Triple-p53<sup>KO</sup>/p38i organoids treated with an inhibitor for ATM (ATMi; KU55933) (A) or for CHK2 (CHK2i; PV1019) (B). Statistics as in Figure 1C. \*p<0.05.



## Discussion

We here establish that loss of p53 in human colon organoid cultures induces the appearance of bulky anaphase bridges (BABs) during mitosis in a manner dependent on inactivation of p38. These BABs are characterized by the presence of DNA damage and rely on active DDR signaling in G2. We thus propose that loss of p53 renders cells dependent on p38 to prevent DNA-damage related chromosome missegregation in mitosis.

Our findings expand the reported functional interactions between p53 and p38. p38 can directly activate p53, for example after UV radiation [49, 50], or following mitotic errors by loss of centrosome integrity [51]. p38 furthermore stabilizes p53 following chromosome missegregations and limits survival of aneuploid cells [34]. On the other hand, p38 promotes survival of p53-deficient cells exposed to DNA damaging agents [52], and is required for adequate DDR signaling [36]. These observations combined with our findings suggest that p38 inhibition causes accumulation of endogenous DNA damage that goes unnoticed in G2 due to p53 inactivation, leading to BAB formation in mitosis. This is in agreement with our observation that BABs became apparent only when Triple-p53<sup>KO</sup> organoids were cultured in p38i for prolonged periods (>7 days). Combined loss of p53 and p38 might thus result in a vicious cycle where DNA-damage induces the formation of BABs, which subsequently results in additional DNA-damage resulting from the missegregation [53, 54].

Loss of p53 allows cells to proliferate in the presence of DNA-damage and so sets the stage for the accumulation of potentially oncogenic mutations [15, 16]. The role for p53 in preventing BABs shows that p53 protects from additional mutations

← **Figure 6: Activity of p38 restrains anaphase bridge formation in human colorectal cancer organoids.** A) Relative viability of two human colorectal cancer (CRC) derived organoid lines (04T and 05M) and an independent line derived from healthy tissue (03N) treated with Nutlin3a (10 $\mu$ M) for 7 days to assess p53 pathway functionality. Viability according to Cell TiterGlo assay, values normalized to control (DMSO) conditions. Data modified from Chapter 5, Figure 2 of this thesis. B) Quantifications of anaphase bridges in movies of two human CRC derived organoid lines cultured in the presence of p38i for >7 days or control conditions (DMSO). Statistics as in Figure 1D.

also more directly. Loss of p53 therefore acts as a double-edged sword in acquiring genetic instability: It not only permits continued proliferation of damaged cells but also exposes them to chromosomal breakage in mitosis, which can lead to extensive damage and chromosomal rearrangements [19, 55]. Our study revealed an interesting dependency on p38 to limit such excessive instability in the context of p53 loss in CRC. Cancer cells maintain mutation rates to enable sufficiently swift tumor evolution but these are limited so as to prevent lethality [56, 57]. If loss of p38 in a p53 mutated background results in exceeding the optimal level of genetic instability, this might explain the relatively low number of p38 mutations found in large intestinal tumors (0.24%; according to the COSMIC database) [31]. Because exacerbating CIN presents possible therapeutic opportunities [9], inhibition of p38 might be a therapeutic strategy for tumors that harbor mutations in p53. In combination with mitotic drugs, this strategy was shown to be effective in PDX models of human breast tumors [36].





## Materials and Methods

**Cell culture and treatment.** HCT116 p53<sup>WT</sup> and p53<sup>-/-</sup> cells were a gift from the R. Medema lab and cultured in DMEM high glucose (Sigma) supplemented with 8% FBS (Sigma) and penicillin/streptomycin (Sigma). The healthy organoid line and all CRISPR/Cas9 mutated derivatives were published previously [11, 58], with the exception of p53-single mutant (sg1.1). This line was generated and validated with identical methods. Human FAP adenoma-derived line CO121B was published previously [32]. Lines 03N, 04T and 05M were obtained from the HUB Biobank. HUB organoids were established from resected tissue and expanded to generate master (MCB) and working cell banks (WCB) following internal HUB SOP's and LM under stringent QC standards, including the fingerprinting confirmation of organoid origin. WCB vials were provided for the execution of the experiments described here. Human organoid cultures were maintained in Matrigel (Corning) in advanced DMEM/F12 (Gibco) supplemented with HEPES (Sigma), Ala-Glu (Sigma), penicillin/streptomycin (Sigma), Noggin conditioned medium, B27 (Gibco), *N*-Acetyl-L-cysteine (Sigma), EGF (Peprotech), nicotinamide (Sigma) and A-83-01 (Tocris). Medium for 04T and 05M contained additional RSPO conditioned medium. For 03N, normal and p53 single mutant lines the medium was additionally supplemented with RSPO and WNT conditioned medium and these lines were seeded in the presence of Y-27632 for 16-24 hours. Lines mutant for *KRAS* were cultured without EGF and lines mutant for *SMAD4* without NOGGIN. All conditioned media were kindly provided by the H. Clevers lab.

Chemical inhibitors and concentrations (unless indicated otherwise): Nutlin3a (10 $\mu$ M, Cayman Chemical), ATMi (KU55933, 25 $\mu$ M, Selleck), CHK2i (PV1019, 10  $\mu$ M, Millipore), DNAPKi (NU7441, 500 nM, Selleck), p38i (12 $\mu$ M, SB202190, Selleck), doxycycline (1 $\mu$ g/ml, Sigma), nocodazole (2 $\mu$ g/ml, Sigma), aphidicolin (5  $\mu$ g/ml, Sigma), nucleosides (30 $\mu$ M, Sigma).

**Genetic modification and lentiviral transduction.** p53 single mutant mediated by sg1.1 (target sequence CCAGAGGCTGCTC CCCCCG) was generated

via identical methods as previously described [11]. H2B-mNeon lentivirus was previously described [11]. TET-p53<sup>R175H</sup> was generated as follows: p53(R175H) was amplified through PCR from pCMV-Neo-Bam-p53<sup>R175H</sup> (Addgene #16436) [29] for insertion into the lentiviral pInducer20 [59] using InFusion Cloning (Clontech Laboratories), replacing the ccdB-cassette flanked by two BstXI sites. Subsequently, mKate2-3xNLS and the P2A cleavage sequence from porcine teschovirus-1 were amplified using PCR for insertion into pInducer20-p53(R175H) between Xho and Nhe. Via overlapping sequences, these two PCR fragments were inserted at once upstream of p53(R175H) (Xho,Nhe) to create pInducer20:mKate2-3xNLS-P2A-p53(R175H) (shortly: TET-p53<sup>R175H</sup>), allowing inducible expression of p53<sup>R175H</sup>, visualized by emerging nuclear red fluorescence. shLuc and shp38 expressing constructs were generated by introducing shRNA sequences (Luciferase: TTACGCTGAGTACTTCGACCTGACCCATCGAAGTACTCAGC; p38: GCCGTATAGGATGTCAGACAA [37] into pInducer10-mir-RUP-PheS (Addgene #44011) [59] between XHO1 and ECOR1.

**Live cell imaging and analysis of mitotic errors.** H2B-mNeon expressing organoids were imaged by means of fluorescent confocal microscopy for 16-24 hours in XYZT-mode every 3-4 minutes at 2.5 $\mu$ M Z-intervals using a spinning-disc confocal microscope (Nikon/Andor CSU-W1 with Borealis Illumination), 40x water-immersion objective (1.15NA) or 30x silicon-immersion (1.05NA). The microscope was equipped with a climate chamber constantly kept at 37°C, 5% CO<sub>2</sub>. Acquired movies were processed as previously described [11] and analyzed manually using ImageJ and NIS-elements software.

**FISH and Immunofluorescence imaging.** Organoids were disrupted into small cell clumps by means of trypsinization and plated in 2D on glass-bottom plates (Ibidi). After three to seven days, organoids were fixed in Carnoy's fixative (25% acetic acid, 75% methanol) and stained for centromeres using TelC-Cy3 (F1002, PNABio) according to manufacturer's recommendations. For spreads, organoids were blocked in mitosis using nocodazole, disrupted by trypsinization and dropped on glass microscope slides and subsequently processed as above. For immunofluorescence, cells were

fixed in 4% formaldehyde, permeabilized with 0.2% Triton TX-100 (Sigma) or 0.5% NP-40 (Sigma), blocked with 3% BSA, stained with primary antibodies overnight at 4°C and stained with secondary antibodies for 2 hours at RT. DNA was detected by adding propidium iodide to the before-last washing step. Primary antibodies: RIF1 (1:500, Bioke),  $\gamma$ H2AX (1:1000, Biolegend), 53BP1 (1:1000, Santa Cruz). Images were acquired using a deconvolution system (Deltavision Elite; Applied Precision/GE Healthcare) using a 60x/1.4NA objective (Olympus) and post-acquisition processed into deconvolved maximum intensity projections using SoftWorx6.0 (Applied Precision/GE Healthcare) and analyzed manually using ImageJ and NIS Elements software.

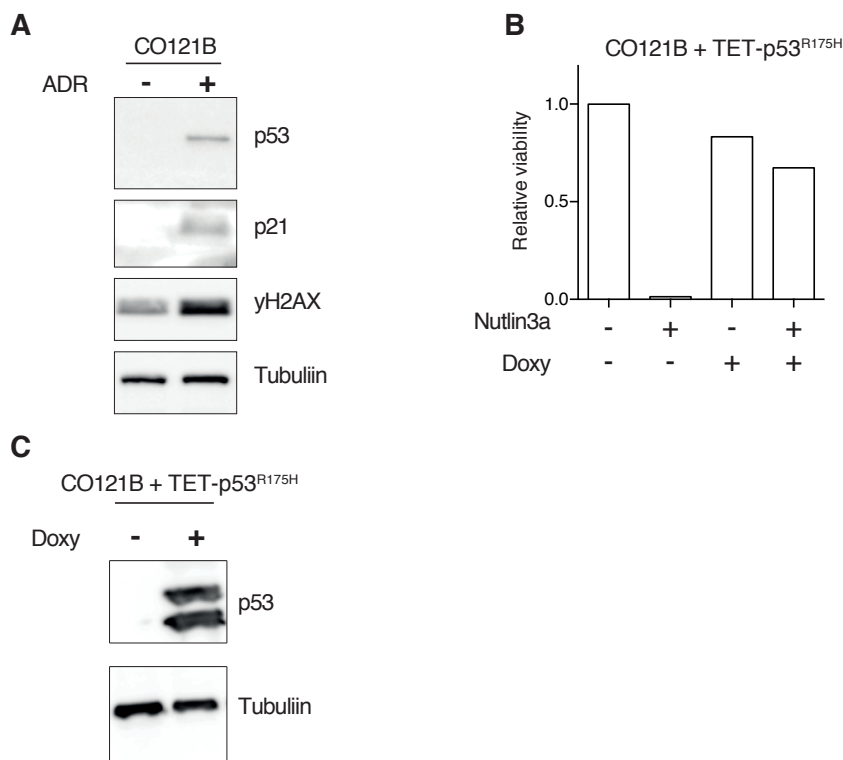
**Immunoblotting.** Proteins from cell lysates were size-separated on SDS-Page gel and transferred to nitrocellulose membranes using a Trans-Blot Turbo system (Biorad). Membranes were blocked with 5% milk and incubated with primary antibodies overnight at 4°C. Secondary antibody incubation was performed for 2 hours at RT and detection was done via chemiluminescence. Primary antibodies: Tubulin (1:10,000, Sigma), p53 (1:1000, Cell Signaling), p21 (1:500, ThermoFisher).

**DNA Fiber assay.** Organoids were seeded 3 days prior to the experiment. 24 hours before the labelling of the fibres, p38i was added to the medium. The organoids were pulse-labelled for 20 minutes by addition of 25  $\mu$ M 5-Chloro-2'-deoxyuridine (CldU, Sigma-Aldrich) to the medium, washed with warm medium three times, and subsequently pulse-labelled for 20 minutes by addition of 250  $\mu$ M 5-Iodo-2'-deoxyuridine (IdU, Sigma-Aldrich). Replication was then stopped by addition of ice-cold PBS. Next, the organoids were trypsinized to obtain a single cell suspension. Single cells were lysed on a microscope slide, which was tilted to spread the DNA. Slides were air-dried and fixed in Carnoy's fixative for 10 minutes. To detect the DNA fibers, the slides were incubated in 2.5M HCl for 75 minutes. Next, slides were incubated for one hour with rat-anti-BrdU (1:1000, Abcam BU1/75 ICR1) and mouse-anti-BrdU (1:250, BD Biosciences B44) and subsequently 2 hours with the Alexa Fluor 488-conjugated goat-anti-rat and Alexa Fluor 594-conjugated goat-anti-mouse antibodies (1:1000, Invitrogen). Images of at least 3 replicate slides were obtained with a Leica DM4000B microscope equipped with a Leica DFL 3000G camera. IdU track length was measured blindly using ImageJ

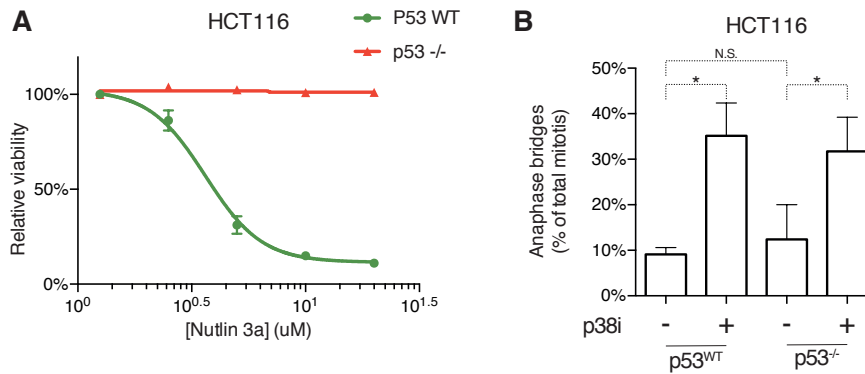
software. The IdU track length was only measured in ongoing replication forks, where a single CldU signal preceded the IdU signal. Statistical analysis was done by a Kruskal-Wallis test, followed by the Dunn's multiple comparison test.

**Cell viability assays.** To measure cell viability, the Cell TiterGlo (Promega) assay was performed according to manufacturer's recommendations.

## Supplemental Data



**Supplemental Figure S1: Generation of a p53 proficient organoid line expressing p53<sup>R175H</sup>.** A) Western blot showing p53 activity by DNA-damage induction in an organoid line derived from an adenoma from a FAP patient (CO121B). Samples were treated for 8 hours with adriamycin (ADR, 10 $\mu$ M) or control (DMSO). B) Relative viability of CO121B infected with a lentiviral construct encoding a doxycycline (Doxy) inducible expression of p53<sup>R175H</sup> and treated with Nutlin3a (10 $\mu$ M for 7 days) or control (DMSO). Viability was judged from Cell TiterGlo assay and normalized to control. N=1. C) Western blot indicating overexpression of p53 upon doxycycline induction after 24 hours. The double bands for p53 likely result from ubiquitination of p53 to mediate its degradation.



**Supplemental Figure S2: Inhibition of p38 induces anaphase bridges in HCT116 cells.** A) Relative viability of HCT116-p53<sup>WT</sup> and HCT116-p53<sup>-/-</sup> treated with Nutlin3a to demonstrate p53 pathway functionality and loss respectively. Viability was judged from Cell TiterGlo assay and normalized to DMSO control (which is shown as the lowest concentration in the graph). Error bars depict S.D. of three independent experiments. B) Quantification of anaphase bridges in movies from HCT116-p53<sup>WT</sup> and HCT116-p53<sup>-/-</sup> cells treated for seven days with p38i or control (DMSO). Statistics as in 1C. \*p<0.05. \*\*p<0.005.

**Supplemental video 1:** Example movie of Triple-p53<sup>WT</sup> organoids used for quantifications of mitotic errors in figure 1A.

**Supplemental video 2:** Example movie of Triple-p53<sup>KO</sup> organoids, cultured in the absence of p38i, used for quantifications of mitotic errors in figure 2A.

**Supplemental video 3:** Example movie of Triple-p53<sup>KO</sup>/p38i organoids used for quantifications of mitotic errors in figure 2A.

**Supplemental video 4:** Example movie of Triple-p53<sup>KO</sup>/shp38(not induced) organoids used for quantifications of mitotic errors in figure 2D.

**Supplemental video 5:** Example movie of Triple-p53<sup>KO</sup>/shp38(dox induced) organoids used for quantifications of mitotic errors in figure 2D.

All supplementary videos are available via:

<https://www.youtube.com/channel/UC4e49VyC2RWUCgAD-HB0aPQ?>



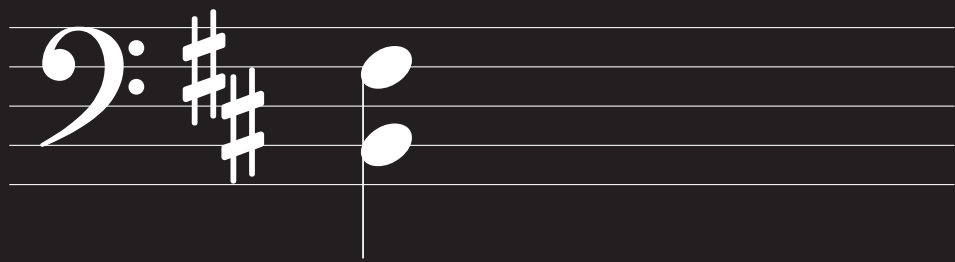
## References

1. Cancer Genome Atlas, N., *Comprehensive molecular characterization of human colon and rectal cancer*. Nature, 2012. **487**(7407): p. 330-337.
2. Lengauer, C., K.W. Kinzler, and B. Vogelstein, *Genetic instability in colorectal cancers*. Nature, 1997. **386**(6625): p. 623-627.
3. Bakhoum, S.F., et al., *Chromosomal instability drives metastasis through a cytosolic DNA response*. Nature, 2018. **553**(7689): p. 467-472.
4. Davoli, T., et al., *Tumor aneuploidy correlates with markers of immune evasion and with reduced response to immunotherapy*. Science, 2017. **355**(6322).
5. Duijf, P.H.G. and R. Benezra, *The cancer biology of whole-chromosome instability*. Oncogene, 2013. **32**(40): p. 4727-4736.
6. Jamal-Hanjani, M., et al., *Tracking the Evolution of Non-Small-Cell Lung Cancer*. N Engl J Med, 2017. **376**(22): p. 2109-2121.
7. Kops, G.J.P.L., B.A.A. Weaver, and D.W. Cleveland, *On the road to cancer: aneuploidy and the mitotic checkpoint*. Nature reviews. Cancer, 2005. **5**(10): p. 773-785.
8. Sorillo, R., et al., *Mad2-induced chromosome instability leads to lung tumour relapse after oncogene withdrawal*. Nature, 2010. **464**(7287): p. 436-440.
9. van Jaarsveld, R.H. and G.J.P.L. Kops, *Difference Makers: Chromosomal Instability versus Aneuploidy in Cancer*. Trends Cancer, 2016. **2**(10): p. 561-571.
10. Fearon, E.R. and B. Vogelstein, *A genetic model for colorectal tumorigenesis*. Cell, 1990. **61**(5): p. 759-767.
11. Drost, J., et al., *Sequential cancer mutations in cultured human intestinal stem cells*. Nature, 2015. **521**(7550): p. 43-47.
12. Kandoth, C., et al., *Mutational landscape and significance across 12 major cancer types*. Nature, 2014. **502**(7471): p. 333-339.
13. Freed-Pastor, W.A. and C. Prives, *Mutant p53: one name, many proteins*. Genes & Development, 2012. **26**(12): p. 1268-1286.
14. Kasthuber, E.R. and S.W. Lowe, *Putting p53 in Context*. Cell, 2017. **170**(6): p. 1062-1078.
15. Meek, D.W., *The p53 response to DNA damage*. DNA Repair (Amst), 2004. **3**(8-9): p. 1049-56.
16. Roos, W.P., A.D. Thomas, and B. Kaina, *DNA damage and the balance between survival and death in cancer biology*. Nat Rev Cancer, 2016. **16**(1): p. 20-33.
17. Bouffler, S.D., et al., *Spontaneous and ionizing radiation-induced chromosomal abnormalities in p53-deficient mice*. Cancer Research, 1995. **55**(17): p. 3883-3889.
18. Shlien, A., et al., *Excessive genomic DNA copy number variation in the Li-Fraumeni cancer predisposition syndrome*. Proc Natl Acad Sci U S A, 2008. **105**(32): p. 11264-9.
19. Soto, M., et al., *p53 Prohibits Propagation of Chromosome Segregation Errors that Produce Structural Aneuploidies*. Cell Rep, 2017. **19**(12): p. 2423-2431.
20. Davaadelger, B., H. Shen, and C.G. Maki, *Novel roles for p53 in the genesis and targeting of tetraploid cancer cells*. PLoS ONE, 2014. **9**(11): p. e110844.
21. Fujiwara, T., et al., *Cytokinesis failure generating tetraploids promotes tumorigenesis in p53-null cells*. Nature, 2005. **437**(7061): p. 1043-1047.
22. Zack, T.I., et al., *Pan-cancer patterns of somatic copy number alteration*. Nat Genet, 2013. **45**(10): p. 1134-40.
23. Rausch, T., et al., *Genome sequencing of pediatric medulloblastoma links catastrophic DNA rearrangements with TP53 mutations*. Cell, 2012. **148**(1-2): p. 59-71.
24. Hampp, S., et al., *DNA damage tolerance pathway involving DNA polymerase iota and the tumor suppressor p53 regulates DNA replication fork progression*. Proc Natl Acad Sci U S A, 2016. **113**(30): p. E4311-9.
25. Klusmann, I., et al., *p53 Activity Results in DNA Replication Fork Processivity*. Cell Rep, 2016. **17**(7): p. 1845-1857.
26. Fukasawa, K., et al., *Abnormal centrosome amplification in the absence of p53*. Science, 1996. **271**(5256): p. 1744-7.
27. Chan, K.L., et al., *Replication stress induces sister-chromatid bridging at fragile site loci in mitosis*. Nature cell biology, 2009. **11**(6): p. 753-760.
28. Naim, V. and F. Rosselli, *The FANCD pathway and BLM collaborate during mitosis to prevent micronucleation and chromosome abnormalities*. Nature cell biology, 2009. **11**(6): p. 761-768.
29. Baker, S.J., et al., *Suppression of human colorectal carcinoma cell growth by wild-type p53*. Science, 1990. **249**(4971): p. 912-5.
30. Willis, A., et al., *Mutant p53 exerts a dominant negative effect by preventing wild-type p53 from binding to the promoter of its target genes*. Oncogene, 2004. **23**(13): p. 2330-8.

31. Forbes, S.A., et al., *COSMIC: somatic cancer genetics at high-resolution*. *Nucleic Acids Res*, 2017. **45**(D1): p. D777-D783.
32. Fessler, E., et al., *TGFbeta signaling directs serrated adenomas to the mesenchymal colorectal cancer subtype*. *EMBO Mol Med*, 2016. **8**(7): p. 745-60.
33. Bunz, F., et al., *Targeted inactivation of p53 in human cells does not result in aneuploidy*. *Cancer Res*, 2002. **62**(4): p. 1129-33.
34. Simoes-Sousa, S., et al., *The p38alpha Stress Kinase Suppresses Aneuploidy Tolerance by Inhibiting Hif-1alpha*. *Cell Rep*, 2018. **25**(3): p. 749-760 e6.
35. Thompson, S.L. and D.A. Compton, *Proliferation of aneuploid human cells is limited by a p53-dependent mechanism*. *J Cell Biol*, 2010. **188**(3): p. 369-81.
36. Canovas, B., et al., *Targeting p38alpha Increases DNA Damage, Chromosome Instability, and the Anti-tumoral Response to Taxanes in Breast Cancer Cells*. *Cancer Cell*, 2018. **33**(6): p. 1094-1110 e8.
37. Alspach, E., et al., *p38MAPK plays a crucial role in stromal-mediated tumorigenesis*. *Cancer Discov*, 2014. **4**(6): p. 716-29.
38. Gisselsson, D., *Chromosome instability in cancer: how, when, and why?* *Adv Cancer Res*, 2003. **87**: p. 1-29.
39. Mankouri, H.W., D. Huttner, and I.D. Hickson, *How unfinished business from S-phase affects mitosis and beyond*. *The EMBO Journal*, 2013. **32**(20): p. 2661-2671.
40. Germann, S.M., et al., *TopBP1/Dpb11 binds DNA anaphase bridges to prevent genome instability*. *J Cell Biol*, 2014. **204**(1): p. 45-59.
41. Hengeveld, R.C., et al., *Rif1 Is Required for Resolution of Ultrafine DNA Bridges in Anaphase to Ensure Genomic Stability*. *Dev Cell*, 2015. **34**(4): p. 466-74.
42. Ke, Y., et al., *PICH and BLM limit histone association with anaphase centromeric DNA threads and promote their resolution*. *EMBO J*, 2011. **30**(16): p. 3309-21.
43. Liu, Y., et al., *The origins and processing of ultra fine anaphase DNA bridges*. *Curr Opin Genet Dev*, 2014. **26**: p. 1-5.
44. Wang, L.H., et al., *Centromere DNA decatenation depends on cohesin removal and is required for mammalian cell division*. *J Cell Sci*, 2010. **123**(Pt 5): p. 806-13.
45. Burrell, R.A., et al., *Replication stress links structural and numerical cancer chromosomal instability*. *Nature*, 2013. **494**(7438): p. 492-496.
46. Leahy, J.J., et al., *Identification of a highly potent and selective DNA-dependent protein kinase (DNA-PK) inhibitor (NU7441) by screening of chromenone libraries*. *Bioorg Med Chem Lett*, 2004. **14**(24): p. 6083-7.
47. Hickson, I., et al., *Identification and characterization of a novel and specific inhibitor of the ataxia-telangiectasia mutated kinase ATM*. *Cancer Res*, 2004. **64**(24): p. 9152-9.
48. Jobson, A.G., et al., *Cellular inhibition of checkpoint kinase 2 (Chk2) and potentiation of camptothecins and radiation by the novel Chk2 inhibitor PV1019 [7-nitro-1H-indole-2-carboxylic acid {4-[1-(guanidinohydrazono)-ethyl]-phenyl}-amide]*. *J Pharmacol Exp Ther*, 2009. **331**(3): p. 816-26.
49. Huang, C., et al., *p38 kinase mediates UV-induced phosphorylation of p53 protein at serine 389*. *J Biol Chem*, 1999. **274**(18): p. 12229-35.
50. She, Q.B., N. Chen, and Z. Dong, *ERKs and p38 kinase phosphorylate p53 protein at serine 15 in response to UV radiation*. *J Biol Chem*, 2000. **275**(27): p. 20444-9.
51. Mikule, K., et al., *Loss of centrosome integrity induces p38-p53-p21-dependent G1-S arrest*. *Nat Cell Biol*, 2007. **9**(2): p. 160-70.
52. Reinhardt, H.C., et al., *p53-deficient cells rely on ATM- and ATR-mediated checkpoint signaling through the p38MAPK/MK2 pathway for survival after DNA damage*. *Cancer Cell*, 2007. **11**(2): p. 175-89.
53. Crasta, K., et al., *DNA breaks and chromosome pulverization from errors in mitosis*. *Nature*, 2012. **482**(7383): p. 53-58.
54. Janssen, A., et al., *Chromosome segregation errors as a cause of DNA damage and structural chromosome aberrations*. *Science*, 2011. **333**(6051): p. 1895-1898.
55. Ganem, N.J. and D. Pellman, *Linking abnormal mitosis to the acquisition of DNA damage*. *J Cell Biol*, 2012. **199**(6): p. 871-81.
56. Andor, N., et al., *Pan-cancer analysis of the extent and consequences of intratumor heterogeneity*. *Nat Med*, 2016. **22**(1): p. 105-13.
57. Janssen, A. and R.H. Medema, *Genetic instability: tipping the balance*. *Oncogene*, 2013. **32**(38): p. 4459-4470.
58. Fumagalli, A., et al., *Genetic dissection of colorectal cancer progression by orthotopic transplantation of engineered cancer organoids*. *Proc Natl Acad Sci U S A*, 2017. **114**(12): p. E2357-e2364.
59. Meerbrey, K.L., et al., *The pINDUCER lentiviral toolkit for inducible RNA interference in vitro and in vivo*. *Proc Natl Acad Sci U S A*, 2011. **108**(9): p. 3665-70.







# Chapter 5

## **The onset of chromosomal instability is associated with oncogenic transformation in colorectal cancer**

R.H. van Jaarsveld<sup>1</sup>, S. Klaasen<sup>1</sup>, C. Rebel<sup>1</sup>, S. Boj<sup>2</sup>, A. Quirindongo<sup>1</sup> and G.J.P.L. Kops<sup>1</sup>

<sup>1</sup>Oncode Institute, Hubrecht Institute - KNAW and Utrecht University Medical Centre Utrecht, Utrecht, The Netherlands

<sup>2</sup>Hubrecht Organoid Technology (HUB), Yalelaan 62, 3584CM Utrecht, the Netherlands

Manuscript in preparation

## Abstract

The majority of colorectal cancers have an aneuploid karyotype. These chromosomal imbalances result from the missegregation of chromosomes during mitosis. Elevated rates of chromosome missegregation give rise to a phenotype known as chromosomal instability (CIN). Little is known about how and when CIN arises during CRC development. Using 3D live imaging of chromosome segregation, we here measure CIN levels in organoids derived from different stages of CRC progression from a mouse model of CRC as well as from human CRC patient samples. Pre-malignant adenomatous lesions were aneuploid but mostly chromosomally stable, while a more advanced adenoma showed mildly elevated missegregation rates. All primary carcinoma and metastasis-derived organoids, however, displayed substantial CIN. Our data show that CIN is associated with oncogenic transformation and suggests it may contribute to the malignant potential of neoplastic lesions.

## Introduction

The development of cancer is associated with the accumulation of mutations that facilitate the transition from normally functioning cells into cells with oncogenic properties [1]. The entirety of all mutations found in a tumor is referred to as the genomic landscape. These landscapes are formed by ongoing acquisition of new mutations, and cancer cells are therefore considered genetically unstable [2]. Colorectal cancer (CRC) is generally classified into two categories based on the dominant form of genetic instability that shaped the genomic landscape. The first form consists of hypermutated tumors and accounts for ~15% of CRCs. These tumors harbor high numbers of point mutations, mainly resulting from defects in mismatch repair (MMR), which can additionally result in microsatellite instability (MSI, or MIN) [3, 4]. The second form, accounting for the remaining ~85%, has genetic landscapes that are dominated by copy number alterations (CNAs). These tumors are characterized by high levels of CNAs of entire chromosomes, also known as aneuploidy. Aneuploidies are caused by a form of genetic instability in which cells have elevated rates of chromosome missegregation during mitosis. The aneuploid CRCs are therefore referred to as having a chromosomal instability (CIN) phenotype [5, 6]. Besides aneuploidies, chromosome missegregation can also cause structural chromosome aberrations (e.g. translocations, inversions, deletions), chromothripsis and additional DNA damage [7-12].

The development of CRC has long been assumed to follow a stepwise progression known as the adenoma-to-carcinoma sequence [13]. This model is based on the most commonly found mutations in human CRC and their frequencies at different stages of tumor progression. The mutations involve the *APC*, *TP53*, *KRAS* and *SMAD4* genes. While early aberrant crypt foci generally have only mutations in the *APC* gene, full blown carcinomas tend to have all four genes (or genes that function in the same pathways) mutated. Since these genes are mutated most frequently in non-hypermutated CRC [4], the adenoma-to-carcinoma sequence model describes the development of CIN tumors specifically.

A study based on in-depth analysis of regional sequencing of CRCs has recently proposed an alternative route for CRC development. As opposed to stepwise development, this model, coined the ‘Big Bang’ model, proposes that CRC develops from a burst of genomic crisis, creating complex genetic landscapes within a short period of time [14]. According to the model, the period of crisis determines the genetic landscape and tumor genomes subsequently evolve neutrally [15]. Furthermore, it states that some tumors are ‘born to be bad’, i.e. that the malignant properties are acquired early in the formation of the tumor, implying most adenomas will never become cancerous. Indeed, the majority of adenomas do not transition to carcinomas [16]. The Big Bang model is primarily based on the analysis of CNAs and thus suggests that CIN is important for creating the genomic crisis that underlies the early stages of tumorigenesis.

CIN is an important phenotype during the evolution of the majority of CRCs, yet little is known about how and when CIN arises, if CIN gradually develops or is initiated instantaneously, what the level is of CIN (i.e. the rate of chromosome missegregation per chromosome per cell division), or whether this level is constant over the progression of the tumor. Small human adenomas were shown to have allelic imbalances [17]. This was verified by recent regional sequencing, but the adenomas were very homogenous for the CNAs found [14]. In contrast, carcinomas were more genomically heterogenous [14], and ongoing chromosome missegregation has been observed in laboratory cell lines of late-stage CRC [6, 18, 19]. Insights into the timing and extent of CIN may further our understanding of CRC evolution, and potentially aid in the selection of high-risk adenomas. Furthermore, CIN may impact on drug resistance and tumor relapse, and has been proposed by others and us to present therapeutic opportunities [11, 20–23]. Importantly, as we previously discussed [11], measuring CIN should be based on observation of chromosome missegregation during mitosis rather than based on aneuploidy measurements (e.g. FISH, sequencing or metaphase spreads) since karyotypes are strongly shaped by evolutionary forces.

We here set out to determine the onset of CIN in CRC tumorigenesis. We utilized recent advances in three-dimensional, stem cell-based cultures known as organoids [24-26]. We monitored chromosome segregation by live imaging of organoids isolated from different stages of CRC development based on a CRC mouse model as well as in organoids derived from human adenomas, carcinomas and metastases.

## Results

### Mouse colon adenomas are chromosomally stable

To study the involvement of CIN in CRC progression we made use of the  $APC^{+/1638N}$  mouse model. Whereas many CRC mouse models develop high burdens of adenomas that do not progress to carcinomas, mice bearing the  $APC^{+/1638N}$  locus develop small numbers of intestinal tumors that sporadically progress to metastatic carcinomas [27]. When combined with an oncogenic  $KRAS^{G12V}$  mutant, the majority of mice develop carcinomas by the age of three months [28]. This model thus presents a unique opportunity to study CRC cancer progression.

We isolated organoids from two macroscopically visible intestinal tumors as well as from healthy appearing tissue from 12-week-old  $APC^{+/1638N}$  mice. In all cases the isolated organoid lines appeared as mixed populations containing both cryptic and cystic organoids a few days after isolation (Figure 1A). In mouse intestinal organoids, a cystic morphology is associated with loss of  $APC$  function [24]. To verify this, we removed RSPO from the culture medium to promote outgrowth of  $APC$ -deficient organoids specifically, a method we recently applied to select for CRISPR/Cas9-mediated  $APC$  knockout in human colon organoid cultures [29]. Indeed, within three passages after RSPO removal, the organoid lines consisted exclusively of organoids with a cystic morphology, suggesting they had lost  $APC$  function (Figure 1B). Interestingly, some organoids derived from a healthy-looking part of the intestine were able to grow in the absence of RSPO. We therefore consider these organoids (line #62) to represent an early, pre-adenoma lesion. The two lines from adenoma tissue (lines #41 and #42) represent low-risk adenomas, because they do not progress beyond the adenoma stage in this model.

To examine if CIN is a phenotype of these early lesions, we introduced fluorescently labelled Histone 2B (H2B-mNeon) to visualize chromosome segregation during mitosis by time-lapse imaging of living organoids for 16 hours (Figure 1C). All three pre/early adenoma lines showed missegregation rates below 6%, which is comparable to the missegregation rates in a wild type control and in line with background



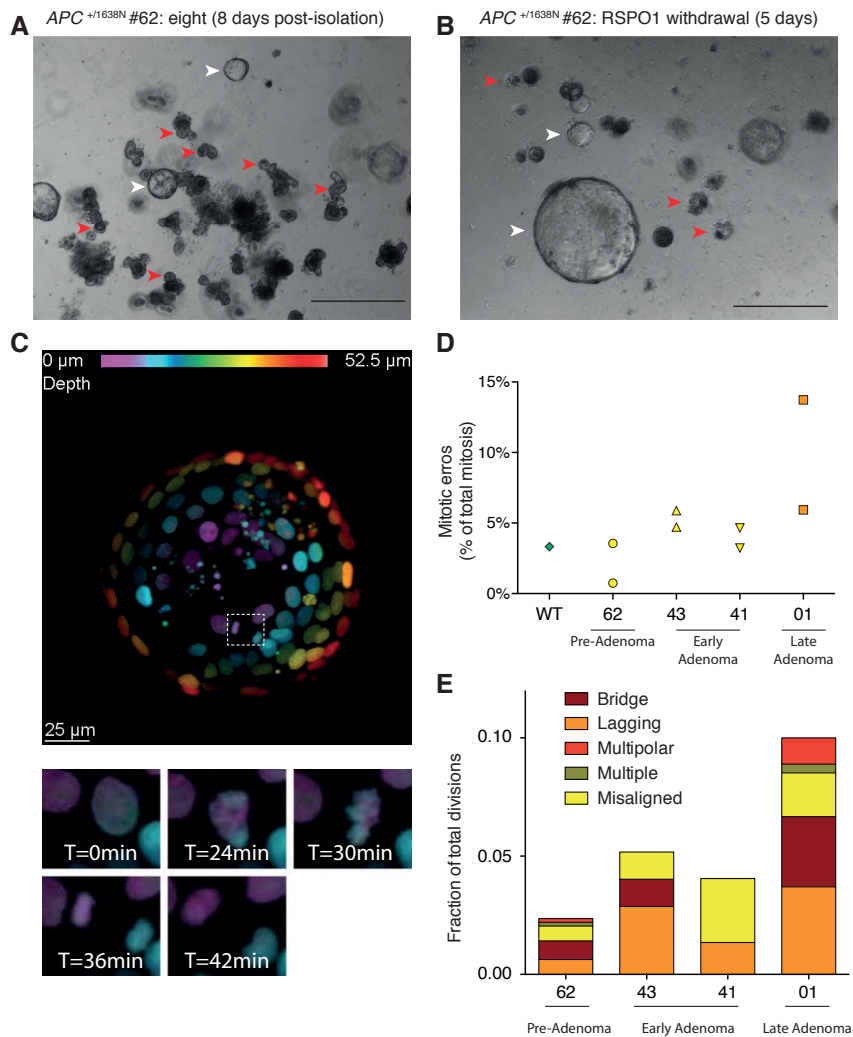


**Figure 1: Adenoma-derived organoids from *APC*<sup>+1638N</sup> mice have low missegregation rates.** A, B) Images from organoids isolated from a healthy appearing part of the small intestine from an eight-week-old *APC*<sup>+1638N</sup> mouse, eight days after isolation, and cultured in complete medium (A) or medium devoid of RSP01 for five days (B). White arrowheads depict cystic organoids, red arrowheads depict cryptic organoids in (A) and dead organoids in (B). Scale bars: 200 $\mu$ m. C) Example taken from a fully processed movie from line 41. Top panel shows the full organoid. H2B-mNeon signals are pseudo-colored according to the Z-layer (top legend) and projected according to the maximum intensity. Bottom panel shows zoomed-in figures from a correct mitosis over different time frames. D) Quantifications of chromosome segregation errors from all mouse-derived organoid lines, including a wild-type, healthy control (WT). Each symbol represents the level of mitotic errors (error/all mitosis) as determined from assessing >60 mitoses per independently established H2B-mNeon-expressing line. E) Quantifications of the types of errors as observed in the movies from (D). Multiple: combination of different types of errors in one event. Fractions can differ slightly from those shown in (D) due to exclusion of experiments with <60 mitoses in (D) but included here.

missegregation rates in chromosomally stable, non-transformed cell cultures and healthy human intestinal organoids [8, 19, 29] (Figure 1D, Supplemental movie 1). The predominant error types were lagging chromosomes and anaphase bridges (Figure 1E), which is consistent with what we observed for the human organoid panel with stepwise accumulation of CRC mutations [29]. We conclude that pre-malignant lesions have low CIN levels in  $APC^{+/1638N}$  mice.

Whereas  $APC^{+/1638N}$  mice mainly develop adenomas, when crossed with mice carrying oncogenic  $KRAS^{G12D}$ , their tumors more commonly develop into invasive carcinomas by 14 weeks [28, 30]. We established an organoid line (line #01) from a tumor of an eight-week-old  $APC^{+/1638N}/KRAS^{G12V}$  mouse, which we consider to represent either a high-risk adenoma or early stage carcinoma. Live imaging of chromosome segregation of H2B-mNeon-expressing organoids revealed up to 14% of cells with mitotic errors, which was ~3.5-fold higher than the low-risk and early lesions (Figure 1D, Supplemental movie 2). Again, the predominant error types were lagging chromosomes and anaphase bridges (Figure 1E). These data therefore indicate that mouse intestinal lesions beyond the early adenoma stage have acquired substantial CIN and suggests that CIN is associated with higher risk of tumor progression.

### **A collection of human colonic organoids from adenomas, carcinomas and metastases**

Our data from the three stages of mouse colorectal cancer formation suggested that CIN increases after the early adenoma stage. We next wondered if this is true also for tumor progression in human cancer. To this end, we collected sets of organoid lines representing different stages of human CRC progression. This collection encompasses organoid lines derived from adenomas from patients with familial adenomatous polyposis coli (FAP) [31], and pairs of matched carcinomas and metastases from end-stage CRC patients.

To characterize the collection of organoids in terms of progression according to the adenoma-to-carcinoma sequence, we subjected each line to selective culture conditions to test if organoids have sustained pathway alterations most commonly associated with CRC progression (i.e. the Wnt, p53 and EGFR) [32]. Continued

proliferation upon WNT and RSPO removal from the culture medium tests for constitutive Wnt pathway activity (e.g. APC mutations), withdrawal of EGF tests for constitutive EGFR signaling (e.g. KRAS mutation), and addition of Nutlin3a tests for loss of p53 pathway function [32]. As expected, healthy colon-derived organoids (lines 03N and p11N) were unable to grow in any of the selection cultures (Figure 2A and B). With the exception of the metastasis-derived line from patient 3 (03M), all tumor lines were resistant to withdrawal of WNT and RSPO (Figure 2C-O), indicating Wnt-

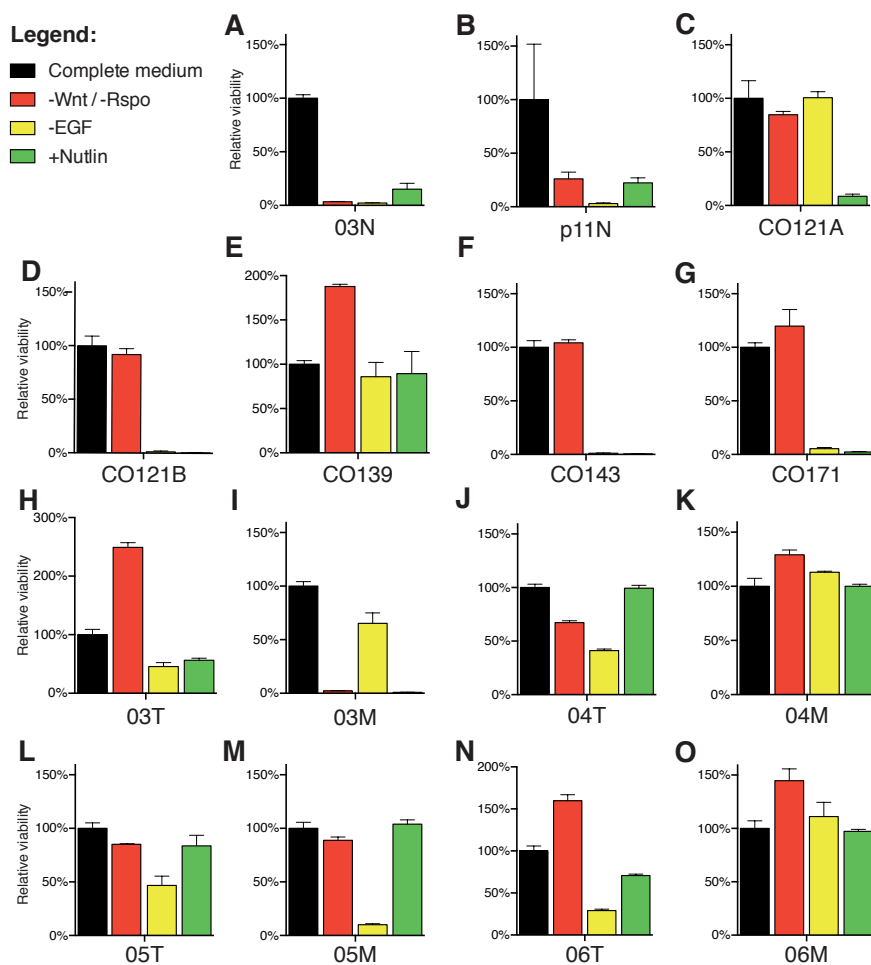


**Figure 2: Functional characterization of oncogenic pathways in human CRC progression organoids.** Relative viability (Cell TiterGlo assay) after medium selection test (see materials and methods) in all human organoid lines used throughout this study. A-B: organoids derived from healthy tissue; C-G: FAP-patient adenoma organoids; H-O: primary tumor (T) and metastasis (M) organoids. Scores were normalized to complete medium scores. Error bars depict S.D. over three independent experiments.

pathway activating mutations in all lines. Three out of five adenomas were unable to grow both in the absence of EGF or presence of Nutlin3a (Figure 2D, F and G), indicating normally functioning EGFR and p53 pathways. In line with a previously reported mutation in *KRAS* [31], CO121A was resistant to EGF withdrawal (Figure 2C). CO139 appeared the most progressed adenoma since it was able to survive in all conditions, indicating alterations in all three pathways tested (Figure 2E). All carcinoma and metastasis-derived lines showed >50% survival in either one or both of the culture selections for alterations to the EGFR and p53 pathways (Figure H-O). These results are in agreement with the adenoma-to-carcinoma sequence and confirm

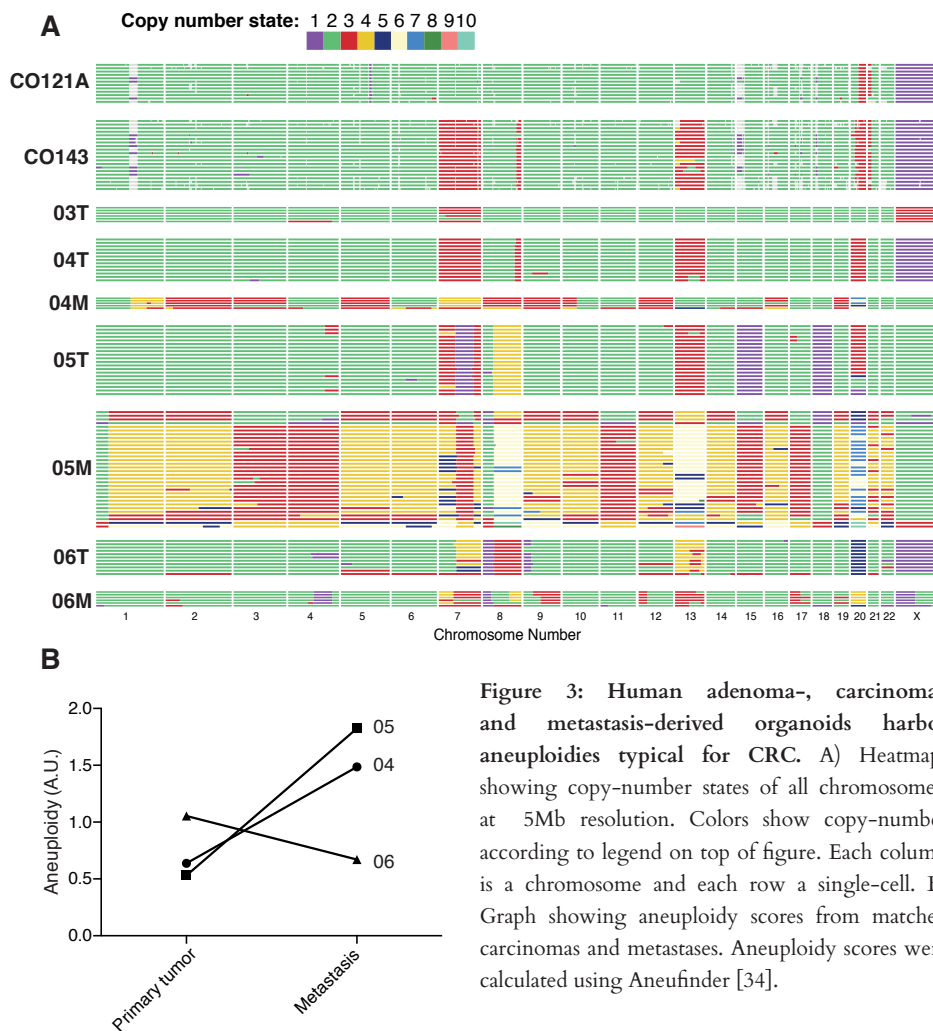


**Figure 3: Human adenoma-, carcinoma- and metastasis-derived organoids harbor aneuploidies typical for CRC.** A) Heatmaps showing copy-number states of all chromosomes, at 5Mb resolution. Colors show copy-number according to legend on top of figure. Each column is a chromosome and each row a single-cell. B) Graph showing aneuploidy scores from matched carcinomas and metastases. Aneuploidy scores were calculated using Aneufinder [34].

that our set of human organoids represent different stages of tumor progression.

### **Human adenoma-, carcinoma- and metastasis-derived organoids harbor aneuploidies typical for CRC**

We next characterized the karyotypes of a subset of the organoid lines. We performed single-cell whole genome sequencing to measure chromosomal copy-numbers for two adenomas and the majority of carcinomas and metastases (Figure 3A). Interestingly, both adenoma lines carried a gain of (a part of) chromosome 20 (Figure 3A). CO143 also had an extra copy of chromosome 13. Gain of chromosome 13 is characteristic for human CRC, and chromosome 20 is also commonly amplified [33]. The characteristic chromosome 13 gain was also seen in the matched primary tumor and metastasis 05T, 05M, 06T and 06M. Interestingly, although organoids from the primary tumor of patient 4 showed this typical chromosome 13 gain, organoids from its matching metastasis did not contain this aneuploidy (Figure 3A). This metastasis therefore either disseminated before chromosome 13 was gained in the primary tumor, lost a copy of chromosome 13 after dissemination, or was derived from a primary tumor subclone with two chromosome 13 copies that we did not sample in our sequencing. The overall number of CNAs however did increase in the metastasis as judged from aneuploidy scores calculated with Aneupfinder [34] (Figure 3B). This increase was also seen in patient 5, where the metastasis seems to have undergone polyploidization (Figure 3A). This could indicate either an increase in chromosomal instability in metastatic cells, selection for specific karyotypes, or chance dissemination of a particular tumor subclone. Of note: organoids from the metastasis of patient 6 had overall reduced aneuploidy when compared to organoids from the primary tumor (Figure 3B).

### **The appearance of CIN coincides with oncogenic transformation**

Knowing overall aneuploidy states, we next wished to examine CIN levels for all the human organoid lines by time-lapse microscopy of chromosome segregation of H2B-mNeon-expressing cells. As observed for the mouse adenoma-derived organoids, human adenoma organoids made few mitotic errors: on average 4.5%, 1.6%, 2.8%

and 3.5% of cells in CO121A, CO121B, CO143 and CO171, respectively, had mitotic errors (Figure 4A, Supplemental movie 3). These CIN levels were slightly higher than the healthy control line (03N, 0.9%; Figure 4A), indicating that adenomas may have a mild CIN phenotype. Interestingly, CO139 (the adenoma line that showed survival on both EGFR and p53 selection media (Figure 2E, Supplemental movie 4)) showed not only the highest CIN levels (average 8.8%; Figure 4A), the missegregations also appeared more severe (i.e. involving more chromosomes) as compared to other adenomas (Figure 4B). Organoid lines derived from primary tumors and metastases showed higher missegregation rates than ones derived from adenomas, with the exception of patient 3 (5.4% missegregations in metastasis; Figure 4A, Supplemental movie 5-7). When comparing CIN levels of all samples from the different progression states (adenoma, carcinoma, metastasis), a significant increase in CIN levels from adenoma to carcinoma was apparent (Figure 4C). Interestingly, the most prominent error were lagging chromosomes and anaphase bridges in all states, suggesting that the predominant underlying defect may have remained the same after initiation of the CIN phenotype (Figure 4B). It thus appears that the induction of CIN is associated with or contributes to oncogenic transformation. Of note: missegregation rates and aneuploidy levels did not correlate (Figure 4D). This underscores our assertion that aneuploidy states cannot be equated to a CIN phenotype [11] and emphasizes the need for separate assessment of CIN and aneuploidy in order to understand karyotype evolution in cancer.

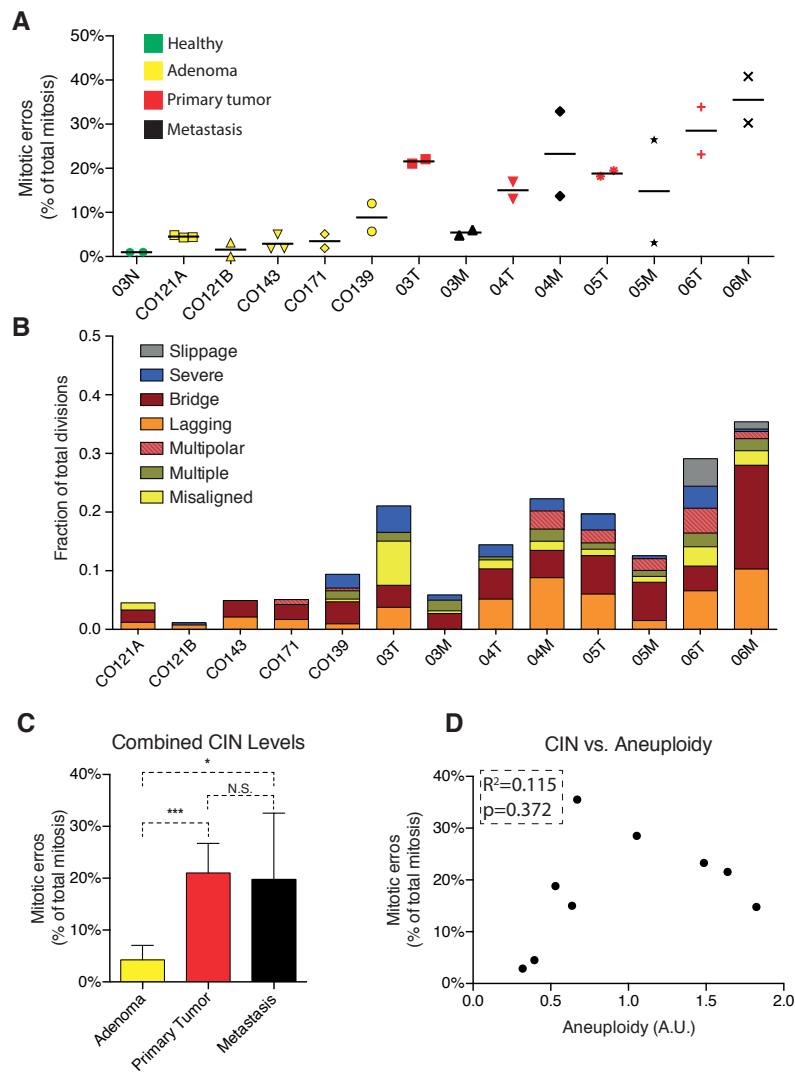


**Figure 4: Chromosomal instability is associated with oncogenic transformation in human colorectal cancer.** A) Quantifications of mitotic errors (error/total mitosis) as judged from live-cell imaging of all lines. Each symbol represents the level of mitotic errors as determined from assessing >60 mitosis in one experiment from two or three independently established H2B-mNeon-expressing lines. Horizontal bars indicated the mean. B) Quantifications of the types of errors as observed in the movies from (A). Multiple: combination of different types of errors in one event. Severe: multiple types of missegregation affecting >8 chromosomes. Slippage: cells exit mitosis without having been through anaphase. Fractions can differ slightly from those shown in (A) due to exclusion of experiments with <60 mitoses in (A) but included here. C) Cumulative analysis of all CIN levels from different progression states as measured in (A). Error bars depict S.D. \* $p<0.05$ , \*\*\* $p<0.0005$ , N.S.: not significant ( $p>0.05$ ). Statistical testing was performed using Prism Graphpad unpaired, two-tailed t-test. CD Scatter plot showing lack of correlation between aneuploidy scores and missegregation rates. Statistical testing performed using Prism Graphpad, correlation.

## Discussion

We here report for the first time a study that evaluates the levels of chromosome missegregation over the course of tumor development. We find that in the  $APC^{+/1638N}$  mouse model, elevated CIN levels are associated with a more advanced adenoma stage. CIN analyses in a set of organoids derived from human colon adenomas and CRC showed that it is associated with oncogenic transformation.

An interesting observation is that adenoma line CO139 has the highest CIN levels of the three human adenomas we examined. This line also appears to be the adenoma that has progressed the farthest, as judged from the pathway function analyses by selective culture conditions. Combined with the observation that the most advanced mouse tumor had the highest CIN level, our results fit with a model in which CIN increases during tumor progression. This is in agreement with the adenoma-to-carcinoma sequence model of CRC development, where the acquisition of CIN could contribute to promoting further progression of the tumor. Our data, however, do not argue against the big bang model for CRC [14]. Our organoid panels may be derived from lesions that are incapable of progressing further due to suboptimal combinations of mutations obtained during the big bang period. For example, low levels of CIN might set a limit in oncogenic potential of an early developing tumor, while early acquisition of high CIN may allow a lesion to become a carcinoma or gain metastatic potential. The latter is in line with the hypothesis that some tumors are 'born to be bad', in which CIN might be a contributing factor [14]. In support of this model, adenomas contain CRC-specific aneuploidies, suggesting that these karyotypes contribute to neoplastic growth but are not sufficient for full oncogenic transformation. A lack of sufficient crisis therefore might have limited the developmental potential of these lesions. Higher CIN levels might enhance the genomic crisis, increasing the chance of creating genotypes that support malignancy. Possibly therefore, elevated CIN levels in carcinomas might represent the tumor-defining crisis moment and have limited contribution on the further development of the tumor.



Aneuploidy has been associated with tumor aggressiveness and holds prognostic value in multiple tumor types [35–39]. Since adenomas can be more aneuploid than carcinomas (03T had the lowest aneuploidy score), but no adenoma had higher CIN levels than any carcinoma, we argue that CIN might be a better predictor than aneuploidy of tumor aggressiveness. As we argued before [11], CIN should be measured by evaluating chromosome missegregations during anaphase rather than inferring CIN from aneuploidy measurements (e.g. by in situ FISH, karyotyping, or genome sequencing). The results presented here underline this notion since we did not find a correlation between aneuploidy and CIN. Direct measurement of CIN in a clinical setting has been limited to the evaluation of anaphase figures in fixed tissue samples, a method that has been used to describe prognostic value for CIN in diffuse large B-cell lymphoma [40]. We here employ a method that is based on time-lapse imaging of tumor-derived organoids to determine CIN levels in tumors. Based on the results presented here, we find that this approach might gain important insights into the contribution of CIN in cancer when applied on larger patient cohorts. Such a study might help understand the contributions of CIN to tumor karyotype evolution and heterogeneity and might reveal clinically valuable insights into the determinants of tumor aggressiveness. A challenge will be to make live imaging of tumor organoids a facile and accessible method.

## Materials and Methods

**Organoid isolation and culturing.** Mouse organoids were isolated from intestines kindly provided by the R. Fodde lab according to previously published methods [24]. Human FAP adenoma organoids were published previously [31]. Healthy line p11N was published previously [29]. Line 03N and all primary tumor and metastasis derived organoids were obtained from the HUB biobank. CRC HUB organoids were established from resected tissue and expanded to generate master (MCB) and working cell banks (WCB) following internal HUB SOP's and LM under stringent QC standards, including the fingerprinting confirmation of organoid origin. WCB vials were provided for the execution of the experiments described here. Mouse organoid cultures were maintained in Matrigel (Corning) and advanced DMEM/F12 (Gibco) supplemented with HEPES (Sigma), Ala-Glu (Sigma), penicillin/streptomycin (Sigma), Noggin conditioned medium, B27 (Gibco), *N*-Acetyl-L-cysteine (Sigma) and EGF (Peprotech). For *APC* wild type lines, the medium was furthermore supplemented with RSPO1 conditioned medium. For human organoid cultures the same medium was used with additional nicotinamide (Sigma) and A-83 (Tocris). For healthy derived organoids, the medium was furthermore supplemented with Wnt3a conditioned medium. All conditioned media were kindly provided by the H. Clevers lab. Expression of H2B-mNeon was achieved by lentiviral infection with a previously published vector [29].

**Live-cell imaging and analysis of mitotic errors.** H2B-mNeon expressing organoids were imaged by means of fluorescent confocal microscopy for 16-24 hours in XYZT-mode every 3-4 minutes at 2.5 $\mu$ M Z-intervals using a spinning-disc confocal microscope (Nikon/Andor CSU-W1 with Borealis Illumination), 40x water-immersion objective (N.A. 1.15). The microscope was equipped with a climate chamber constantly kept at 37°C, 5% CO<sub>2</sub>. Acquired movies were processed as previously described [29] and analyzed manually using ImageJ and NIS-elements software

**Medium selection.** For medium selection tests, organoids were trypsinized to small cell clumps (~1–3 cells) and seeded in medium without WNT and RSPO, without EGF, containing Nutlin3a (10 $\mu$ M, Tocris Bioscience) or control (healthy organoid medium) conditions. Cell viability was measured using Cell TiterGlo (Promega) according to manufacturer's recommendations after 7 days. For Wnt-pathway selection, organoids were split one additional time after 4 days in selection medium.

**Single Cell Sequencing.** For single-cell sequencing, cells were harvested 4h after RO-release by trypsinization. Cells were processed for FACS as described [34] with a minor modification: 10 $\mu$ g/mL Hoechst 34580 was used to quantify DNA content.  $\pm 2N$  nuclei were sorted with a BD FACSJazz (BD Biosciences) in a Hard-Shell 384 wells PCR plate (Bio-Rad) containing 5 $\mu$ L of mineral oil (Sigma-Aldrich) in each well and stored at -20 $^{\circ}$ C until further processing. Cell lysis was performed overnight at 50 $^{\circ}$ C using 0.05 units of Qiagen Protease in 1x NEBuffer 4 (NEB) followed by heat inactivation at 75 $^{\circ}$ C for 20 minutes and 80 $^{\circ}$ C for 5 minutes. The genomic DNA was subsequently fragmented with 100nL 1U NlaIII (NEB) in 1x Cutsmart (NEB) for 60 minutes at 37 $^{\circ}$ C followed by heat inactivation at 80 $^{\circ}$ C for 20 minutes. 100nL of 1 $\mu$ M barcoded double-stranded NlaIII adapters and 100nL of 40U T4 DNA ligase (NEB) in 1x T4 DNA Ligase buffer (NEB) supplemented with 3mM ATP (Invitrogen) was added to each well and ligated overnight at 16 $^{\circ}$ C. After ligation samples were pooled and library preparation was performed as described previously [41]. Libraries were sequenced 1 x 75bp single-end on an Illumina Nextseq 500. The fastq files were mapped to GRCH38 using the Burrows-Wheeler Aligner. The mapped data was analyzed using custom scripts in Python, which parsed for library barcodes, removed reads without an NlaIII sequence and removed PCR-duplicated reads. Copy number analysis was performed as described previously by using Aneufinder [34]. Copy number changes were manually determined using the single cell profiles generated by Aneufinder.

## Supplemental Data

**Supplemental movie 1:** Example movie of organoid line #62

**Supplemental movie 2:** Example movie of organoid line #01

**Supplemental movie 3:** Example movie of organoid line CO121B

**Supplemental movie 4:** Example movie of organoid line CO139

**Supplemental movie 5:** Example movie of organoid line 03M

**Supplemental movie 6:** Example movie of organoid line 04T

**Supplemental movie 7:** Example movie of organoid line 06M

All supplementary videos are available via:

<https://www.youtube.com/channel/UC4e49VyC2RWUCgAD-HB0aPQ?>

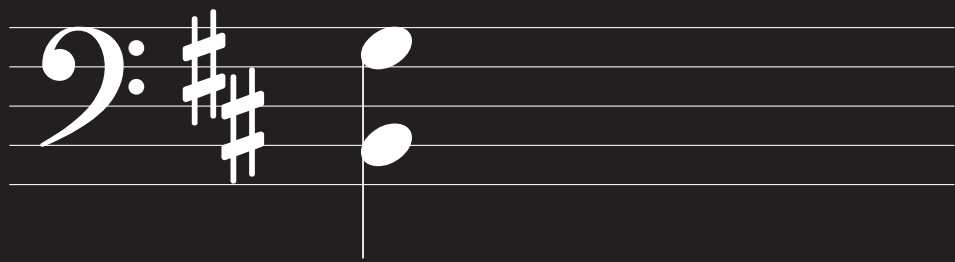


## References

1. Vogelstein, B., et al., *Cancer Genome Landscapes*. Science, 2013. **339**(6127): p. 1546-1558.
2. Negrini, S., V.G. Gorgoulis, and T.D. Halazonetis, *Genomic instability — an evolving hallmark of cancer*. Nature reviews. Molecular cell biology, 2010. **11**(3): p. 220-228.
3. Boland, C.R. and A. Goel, *Microsatellite instability in colorectal cancer*. Gastroenterology, 2010. **138**(6): p. 2073-2087 e3.
4. Cancer Genome Atlas, N., *Comprehensive molecular characterization of human colon and rectal cancer*. Nature, 2012. **487**(7407): p. 330-337.
5. Kops, G.J.P.L., B.A.A. Weaver, and D.W. Cleveland, *On the road to cancer: aneuploidy and the mitotic checkpoint*. Nature reviews. Cancer, 2005. **5**(10): p. 773-785.
6. Lengauer, C., K.W. Kinzler, and B. Vogelstein, *Genetic instability in colorectal cancers*. Nature, 1997. **386**(6625): p. 623-627.
7. Crasta, K., et al., *DNA breaks and chromosome pulverization from errors in mitosis*. Nature, 2012. **482**(7383): p. 53-58.
8. Janssen, A., et al., *Chromosome segregation errors as a cause of DNA damage and structural chromosome aberrations*. Science, 2011. **333**(6051): p. 1895-1898.
9. Soto, M., et al., *p53 Prohibits Propagation of Chromosome Segregation Errors that Produce Structural Aneuploidies*. Cell Rep, 2017. **19**(12): p. 2423-2431.
10. Thompson, S.L. and D.A. Compton, *Proliferation of aneuploid human cells is limited by a p53-dependent mechanism*. J Cell Biol, 2010. **188**(3): p. 369-81.
11. van Jaarsveld, R.H. and G.J.P.L. Kops, *Difference Makers: Chromosomal Instability versus Aneuploidy in Cancer*. Trends Cancer, 2016. **2**(10): p. 561-571.
12. Zhang, C.-Z., et al., *Chromothripsis from DNA damage in micronuclei*. Nature, 2015. **522**(7555): p. 179-184.
13. Fearon, E.R. and B. Vogelstein, *A genetic model for colorectal tumorigenesis*. Cell, 1990. **61**(5): p. 759-767.
14. Sottoriva, A., et al., *A Big Bang model of human colorectal tumor growth*. Nature genetics, 2015. **47**(3): p. 209-216.
15. Williams, M.J., et al., *Identification of neutral tumor evolution across cancer types*. Nat Genet, 2016. **48**(3): p. 238-44.
16. Brenner, H., et al., *Risk of progression of advanced adenomas to colorectal cancer by age and sex: estimates based on 840,149 screening colonoscopies*. Gut, 2007. **56**(11): p. 1585-9.
17. Shih, I.M., et al., *Evidence that genetic instability occurs at an early stage of colorectal tumorigenesis*. Cancer Research, 2001. **61**(3): p. 818-822.
18. Pino, M.S. and D.C. Chung, *The Chromosomal Instability Pathway in Colon Cancer*. Gastroenterology, 2010. **138**(6): p. 2059-2072.
19. Thompson, S.L. and D.A. Compton, *Examining the link between chromosomal instability and aneuploidy in human cells*. The Journal of cell biology, 2008. **180**(4): p. 665-672.
20. Bakhom, S.F., et al., *Numerical chromosomal instability mediates susceptibility to radiation treatment*. Nat Commun, 2015. **6**: p. 5990.
21. Bakhom, S.F. and D.A. Compton, *Chromosomal instability and cancer: a complex relationship with therapeutic potential*. The Journal of clinical investigation, 2012. **122**(4): p. 1138-1143.
22. Janssen, A. and R.H. Medema, *Genetic instability: tipping the balance*. Oncogene, 2013. **32**(38): p. 4459-4470.
23. Sansregret, L., B. Vanhaesebroeck, and C. Swanton, *Determinants and clinical implications of chromosomal instability in cancer*. Nat Rev Clin Oncol, 2018.
24. Sato, T., et al., *Long-term Expansion of Epithelial Organoids From Human Colon, Adenoma, Adenocarcinoma, and Barrett's Epithelium*. Gastroenterology, 2011. **141**(5): p. 1762-1772.
25. Sato, T., et al., *Single Lgr5 stem cells build crypt-villus structures in vitro without a mesenchymal niche*. Nature, 2009. **459**(7244): p. 262-265.
26. van de Wetering, M., et al., *Prospective derivation of a living organoid biobank of colorectal cancer patients*. Cell, 2015. **161**(4): p. 933-945.
27. Fodde, R., et al., *A targeted chain-termination mutation in the mouse Apc gene results in multiple intestinal tumors*. Proc Natl Acad Sci U S A, 1994. **91**(19): p. 8969-73.
28. Alberici, P., et al., *Aneuploidy arises at early stages of Apc-driven intestinal tumorigenesis and pinpoints conserved chromosomal loci of allelic imbalance between mouse and human*. The American journal of pathology, 2007. **170**(1): p. 377-387.
29. Drost, J., et al., *Sequential cancer mutations in cultured human intestinal stem cells*. Nature, 2015. **521**(7550): p. 43-47.
30. Janssen, K.P., et al., *APC and Oncogenic KRAS Are Synergistic in Enhancing Wnt Signaling in Intestinal*

- Tumor Formation and Progression*. Gastroenterology, 2006. **131**(4): p. 1096–1109.
31. Fessler, E., et al., *TGFbeta signaling directs serrated adenomas to the mesenchymal colorectal cancer subtype*. EMBO Mol Med, 2016. **8**(7): p. 745–60.
  32. Fujii, M., et al., *A Colorectal Tumor Organoid Library Demonstrates Progressive Loss of Niche Factor Requirements during Tumorigenesis*. Cell Stem Cell, 2016.
  33. Hoadley, K.A., et al., *Multiplatform analysis of 12 cancer types reveals molecular classification within and across tissues of origin*. Cell, 2014. **158**(4): p. 929–944.
  34. Bakker, B., et al., *Single-cell sequencing reveals karyotype heterogeneity in murine and human malignancies*. Genome Biol, 2016. **17**(1): p. 115.
  35. Carter, S.L., et al., *A signature of chromosomal instability inferred from gene expression profiles predicts clinical outcome in multiple human cancers*. Nature genetics, 2006. **38**(9): p. 1043–1048.
  36. Duijf, P.H.G. and R. Benezra, *The cancer biology of whole-chromosome instability*. Oncogene, 2013. **32**(40): p. 4727–4736.
  37. Duijf, P.H.G., N. Schultz, and R. Benezra, *Cancer cells preferentially lose small chromosomes*. International Journal of Cancer, 2012. **132**(10): p. 2316–2326.
  38. Skirnisdottir, I., et al., *Prognostic importance of DNA ploidy and p53 in early stages of epithelial ovarian carcinoma*. Int J Oncol, 2001. **19**(6): p. 1295–302.
  39. Smid, M., et al., *Patterns and incidence of chromosomal instability and their prognostic relevance in breast cancer subtypes*. Breast Cancer Res Treat, 2011. **128**(1): p. 23–30.
  40. Bakhoun, S.F., et al., *Chromosomal instability substantiates poor prognosis in patients with diffuse large B-cell lymphoma*. Clin Cancer Res, 2011. **17**(24): p. 7704–11.
  41. Muraro, M.J., et al., *A Single-Cell Transcriptome Atlas of the Human Pancreas*. Cell Syst, 2016. **3**(4): p. 385–394 e3.







# Chapter 6

## Individual chromosomes differ in propensity for missegregation in SAC-compromised cells

R.H. van Jaarsveld<sup>1</sup>, S. Klaasen<sup>1</sup>, E.M. Gerrits<sup>1</sup> and G.J.P.L. Kops<sup>1</sup>

<sup>1</sup>Oncode Institute, Hubrecht Institute - KNAW and Utrecht University Medical Centre Utrecht, Utrecht, The Netherlands

Manuscript in preparation

## Abstract

The chance to missegregate during mitosis is assumed to be equal for all chromosomes. No experimental evidence however exists to support this assumption. Non-randomness in chromosome missegregation might contribute to recurrent karyotype aberrations among tumors. We here set out to investigate the chance for each chromosome to missegregate in near-diploid human cells forced to prematurely enter anaphase due to inhibition of the spindle assembly checkpoint (SAC). Using single-cell karyotype sequencing and FISH, we find that certain chromosomes depend more heavily on a functional SAC than others to segregate correctly. A higher probability of missegregation correlates with peripheral location of those chromosomes in the interphase nucleus. We also find that missegregation proportions correlate with a chromosome's dependency on CENP-E, a kinesin motor that promotes efficient congression of peripheral chromosomes, for alignment on the metaphase plate. We therefore propose that peripheral chromosomes need more time to correctly attach to the mitotic spindle, enhancing their propensity for missegregation in SAC-impaired cells.

6

## Introduction

During mitosis cells have to ensure that all duplicated chromosomes are distributed equally over both daughter cells so that each daughter receives an exact copy of the genome. Errors in this process lead to aneuploidy, a state where cells harbor a karyotype that is not an exact multiple of the haploid set. Aneuploidy is associated with reduced cellular fitness, embryonic lethality, growth retardation, aging and cancer [1, 2]. To prevent aneuploidy, several mechanisms are in place to ensure correct chromosome segregation during mitosis [3]. These mechanisms however are not flawless and so chromosome segregation errors occur sporadically to an estimated rate of 0.025% per chromosomes per cell division in healthy cells [4]. Elevated missegregation rates (up to 1% per chromosome per cell division) have been reported to occur in cancer, resulting in a phenotype known as chromosomal instability (CIN) [5]. CIN is believed to contribute to tumorigenesis by facilitating mutation rates beneficial for the evolution of the tumor [3, 6, 7]. On the contrary, CIN has also been proposed to present therapeutic opportunities by increasing missegregation rates that generate aneuploidies and DNA-damage at levels that are no longer compatible with cell survival [7, 8].

Chromosome segregation errors are assumed to be random, meaning that all chromosomes have an equal chance to missegregate. However, chromosomes show great differences on many different aspects, including size, gene density, number of genes, centromere location, nuclear location, and many more. Some of these characteristics might influence the behavior of individual chromosomes during mitosis and thereby might affect their chance to missegregate.

Faithfull chromosome segregation depends on the correct attachment of each chromosome pair to the mitotic spindle, the machinery responsible for physical separation of the chromatids towards both sides of the cell before cytokinesis takes place. These attachments are facilitated by protein rich structures located at the centromeres known as kinetochores [9, 10]. Within a pair of sister chromatids, each kinetochore has to attach to opposite sides of the spindle (bipolar attachment) so that

both sister chromosomes are pulled to opposite sides during anaphase. Only when all chromosomes have attached their kinetochores in a bipolar fashion, cells can progress to anaphase. To prevent premature anaphase onset and subsequent chromosome missegregation, cells harbor a signaling machinery that arrests them at the metaphase-to-anaphase transition until bipolar attachment for all chromosome pairs has been achieved. This time-buying mechanism is known as the spindle-assembly checkpoint (SAC) and is essential to prevent chromosome missegregation [10, 11]. The SAC is orchestrated by its master kinase Mps1 (Mono polar spindle 1) [12]. Inhibition or depletion of MPS1 compromises the SAC and so cells progress to anaphase in the absence of complete alignment and bipolar attachment. Disturbing MPS1 function thus results in shortened mitotic timing and increased chromosome missegregation [13].

6

Here we set out to determine if there is a bias in chance to missegregate among individual chromosomes when the SAC is weakened. We make use of MPS1 inhibition to shorten mitotic timing and induce chromosome missegregation. Utilizing recent advances in single-cell sequencing (single-cell karyotype sequencing; scKaryoSeq) techniques, as well as elaborate validation using classical FISH approaches, we demonstrate that certain chromosomes tend to missegregate more than others. This bias likely results from peripheral nuclear localization of these chromosomes during interphase, increasing the time these chromosomes need to align and attach bipolarly.

## Results

### An optimized protocol for synchronous mitotic progression in RPE cells

To determine the chance for an error in segregation of each individual chromosome, we set out to measure the karyotypes of cells after they had been synchronously passed through an error-prone mitosis. To achieve this, we used the karyotypically stable, non-transformed RPE1 cells, allowing any karyotype deviation to be directly related back to a missegregation event. In addition, we optimized a cell-cycle synchronization protocol that allowed us to generate a high percentage of cells that had undergone a single round of missegregation maximally 4 hours before harvesting (Figure 1A). We achieved synchronization at the G2/M boundary by using a sequential G1-G2 block protocol. Briefly, we used RO-3306 (a CDK1 inhibitor) [14] to block cells at the G2/M boundary, after which they were released into mitosis in the presence of a low dose of an MPS1 inhibitor (MPS1i: Compound 5 (Cpd-5)) [15] to abolish the SAC and induce premature, error-prone anaphase. To ensure that the RO-3306 block was relatively brief (RPE1 cells tend to slip through this block or die after prolonged times at the G2/M transition point (data not shown)), we made cells synchronously progress to the G2/M block by release from a prior palbociclib-induced G1 block. Palbociclib (a CDK4/6 inhibitor) [16] enabled G1 synchronization without directly affecting DNA replication/damage, as is the case when using other G1/S synchronization procedures (e.g. thymidine or aphidicolin) [17-19]. To find the right dose of MPS1i that causes missegregations without inducing swift, post-mitotic cell death, we titrated MPS1i and analyzed chromosome segregation error rates by live imaging of asynchronous populations. A concentration of 62.5nM achieved mild missegregations in >90% of cells by accelerating the onset of anaphase, as expected (Figure 1B and C). Combining our full synchronization protocol with MPS1i or control (DMSO) resulted in ~70% of cells in G1 four hours after release from the RO-3306 block (Figure 1D). At this timepoint we did not observe any cell death (Figure 1E), confirming that any subsequent karyotype analysis will not be biased by selection of specific, surviving karyotypes. Furthermore, the synchronization procedure per se

did not induce missegregation, and did not impact on the frequency of errors induced by MPS1i (Figure 1F). Our synchronization procedure thus allowed us to measure a potential missegregation bias in the absence of selection and in a controlled fashion.

### **Single-cell sequencing and FISH reveal missegregation bias for a subset of chromosomes**

We next used single-cell karyotype sequencing (scKaryoseq) to determine the karyotypes of individual cells that passed through an error-prone mitosis. The scKaryoseq approach is based on a previously published pipeline [20] with some changes (see materials and methods section). Sequencing results were analyzed using the AneuFinder software [21] to map copy-number changes and display single-cell karyotypes (Figure 2A and B). Of note: although scKaryoSeq assessed genome copy number states at 2Mb bins, the data generally displayed consistent copy number variations for all bins in a chromosome, as expected from a single round of missegregations (Figure 2B and C). In concordance with prior findings [4, 13] and our live-cell imaging data (Figure 1B), RPE1 cells maintained a stable karyotype when passed through mitosis unchallenged (Figure 2A). As expected, mild inhibition of MPS1 resulted in a karyotypically heterogenous population (Figure 2B), with on average 5.8 deviations from the normal karyotype per cell. In all likelihood therefore, our procedure had induced ~6 chromosome missegregations per cell.

If individual chromosomes have an equal chance of missegregation, each chromosome should account for 1/23 (4.35%) of all measured gains and losses. Interestingly however, we observed great variety in missegregation proportions among chromosomes (Figure 2C). These results show that some chromosomes depend more heavily on a functional SAC for correct segregation than others. We did not find significant differences in gains versus losses per individual chromosomes, which supports the notion that our approach measured chromosome missegregation in the absence of selection.

To confirm that the observed bias resulted from differences in behavior during mitosis, we performed the same synchronization procedure but now fixed the cells shortly after RO-3306 release. This enabled us to analyze anaphase figures by FISH

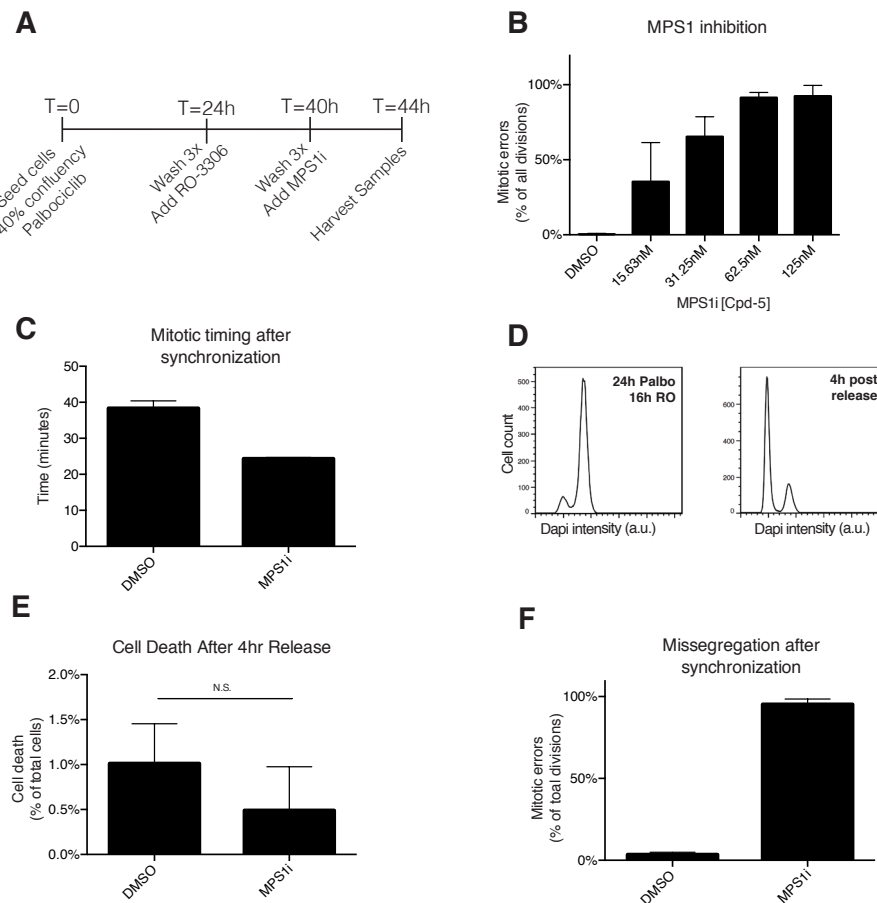


**Figure 1: A synchronized chromosome missegregation protocol for RPE1 cells.** A) Timeline of the synchronization procedure as used throughout this study. B) Titration of MPS1 inhibitor (Cpd-5; MPS1i). RPE1 cells were infected with H2B-mNeon expressing lentivirus in order to visualize chromosome segregation. MPS1i was added 1 hour before start of the movie. Cells were imaged every 4 minutes for 16 hours and movies were analyzed manually. Error bars show standard deviation (S.D.) over three independent experiments. C) Mitotic timing as judged by DNA condensation to anaphase onset. Cells were released after the full synchronization protocol. Movie started maximally 5 minutes after wash-out of RO-3306 and cells were imaged every 4 minutes for 4,5 hours. Error bars show S.D. of 3 independent experiments. D) Cell cycle profiles of cell populations at the moment before release into mitosis and 4 hours after release. Shown is one representative out of 3 experiments. E) Quantifications of cell death 4 hours after release. Cell death was scored from live-cell imaging data based on morphology changes of H2B-mNeon. Movies same as (C). Error bars show S.D. of three independent experiments. Statistical testing was done using Prism Graphpad; unpaired, two-tailed t-test,  $p > 0.05$ . F) Quantifications of chromosome missegregation after the full synchronization protocol. Movies same as (C). Error bars show S.D. of 3 independent experiments.

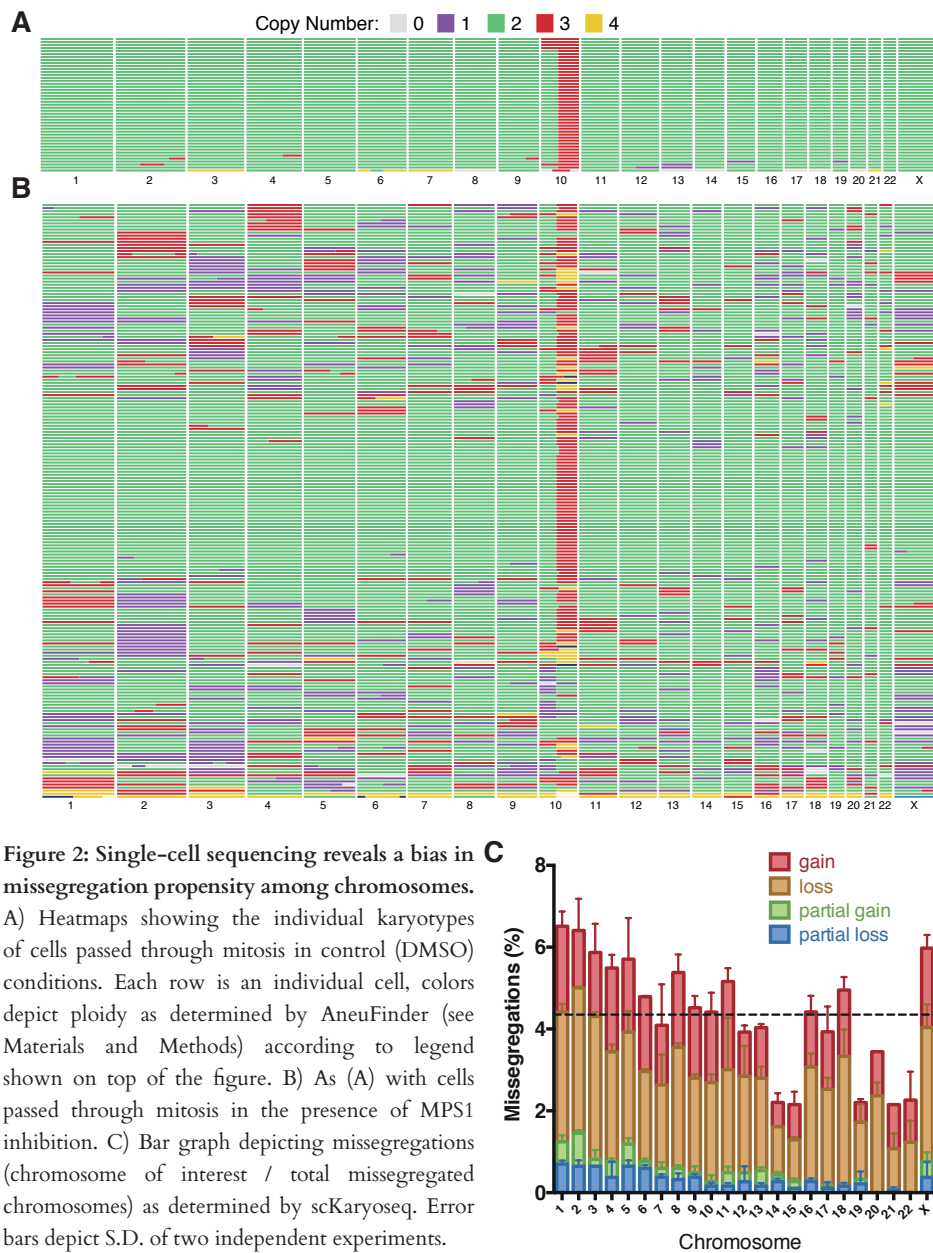


**Figure 2: Single-cell sequencing reveals a bias in missegregation propensity among chromosomes.** A) Heatmaps showing the individual karyotypes of cells passed through mitosis in control (DMSO) conditions. Each row is an individual cell, colors depict ploidy as determined by AneuFinder (see Materials and Methods) according to legend shown on top of the figure. B) As (A) with cells passed through mitosis in the presence of MPS1 inhibition. C) Bar graph depicting missegregations (chromosome of interest / total missegregated chromosomes) as determined by scKaryoseq. Error bars depict S.D. of two independent experiments.

to identify the chromosomes that had not segregated correctly. Based on DAPI-staining, we counted all chromosomes that were clearly missegregating, and whether they were positive for the (chromosome-specific) FISH signal (Figure 3A and B). We performed this analysis for a subset of chromosomes (Figure 3B), which revealed



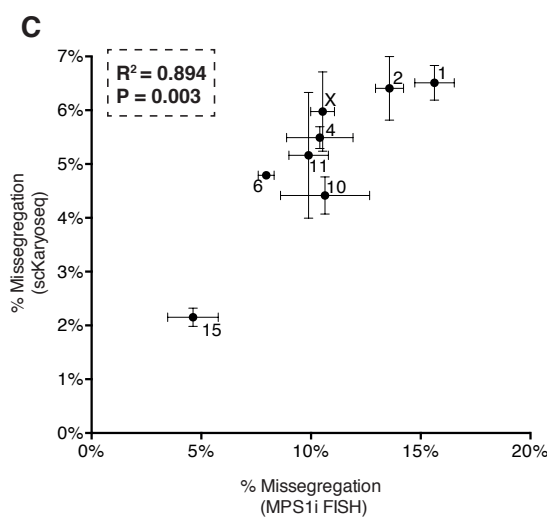
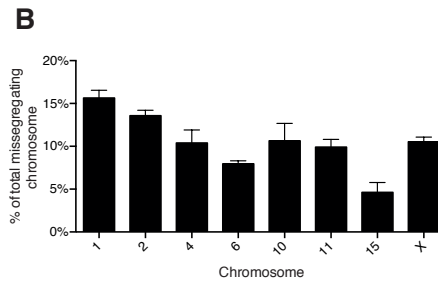
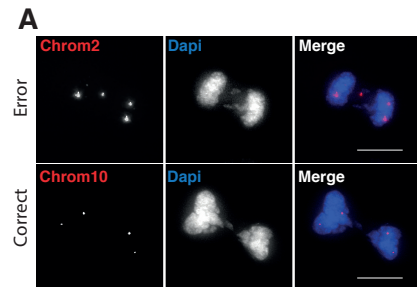


**Figure 3: FISH analysis confirms bias in missegregation propensity among chromosomes.** A) An example of an anaphases that missegregates the chromosome of interest (COI; chromosome 2, upper panel) and an example that segregates the COI correctly (chromosome 10, lower panel). Scale bars: 10  $\mu$ m. B) Quantifications of (A). >100 missegregating chromosomes were analyzed per chromosome per replicate. Error bars show S.D. of three independent experiments C) Scatter plot indicating a correlation between the scKaryoSeq data from Figure 2C (Y-axis) and the FISH data from Figure 3B (X-axis). Pearson correlation coefficient and p-value were calculated using Prism Graphpad correlation test, two-tailed.

a similar trend as found by scKaryoSeq (Figure 3B and C). Of note: the differences in missegregation proportions as measured by scKaryoSeq (Figure 2C) and FISH (Figure 3B) is explained by limitations of the FISH-based measurements. Based on DAPI we can only identify missegregating chromosomes if they are not moving with the bulk DNA-packs, resulting in an underestimation of the total missegregations. Indeed, on average, we find less missegregating chromosomes based on DAPI as we do with scKaryoSeq (4.5 and 6 chromosomes per cell, respectively). We thus conclude that the observed bias resulted from chromosome segregation errors, and that individual chromosomes differ in propensity to missegregate when the SAC is impaired.

## Missegregation bias correlates with interphase nuclear organization

Having shown that certain chromosomes depend more than others on a functional SAC for their correct segregation, we next asked whether this bias could be explained by a trait intrinsic to the chromosomes. There was no obvious correlation between missegregation proportions and gene density, centromere size or centromere ratio (centromere size / total chromosome size) (data not shown). However, chromosome size did correlate with missegregation proportions (Figure 4A). We nevertheless considered size to be an unlikely cause for the missegregation bias, for two reasons. First, chromosomes 14 and 15 missegregate less than their size would predict according to the correlation (Figure 4A). Second, RPE1 cells harbor a fusion of one X chromosome to the q-arm of chromosome 10 that causes an increase of ~60% in size for chromosome X. However, both the normal X and X:10q fusion had near-identical missegregation rates (Figure 4B).

During interphase, chromosomes are located in restricted areas known as chromosomal territories [22]. Larger chromosomes tend to be located more closely to the nuclear lamina and thus farther away from the center of the nucleus, and this appears to be conserved across cell types [23]. Importantly, this correlation is not strict: some small chromosomes can be peripheral and some relatively large ones can be internal. We found a correlation between previously published [24] chromosomal territory to nuclear center distances (CT-CN) and missegregation proportions (Figure 4C). Importantly, the correlation is stronger than the one we found for chromosome size.

We hypothesized that a more peripheral nuclear location before mitotic onset might increase the chance of those chromosomes to be at the periphery of the mitotic spindle at the onset of mitosis and that this would increase the time for those chromosomes to achieve bipolar attachment. A forced premature anaphase by SAC impairment could in this way bias the missegregation of peripheral chromosomes. To test this hypothesis, we let cells enter mitosis in the presence of an inhibitor of the kinesin motor CENP-E (CENP-Ei; GSK923295). CENP-E activity is needed to move peripheral polar chromosomes towards the metaphase plate during pro-metaphase [25-27]. Inhibition

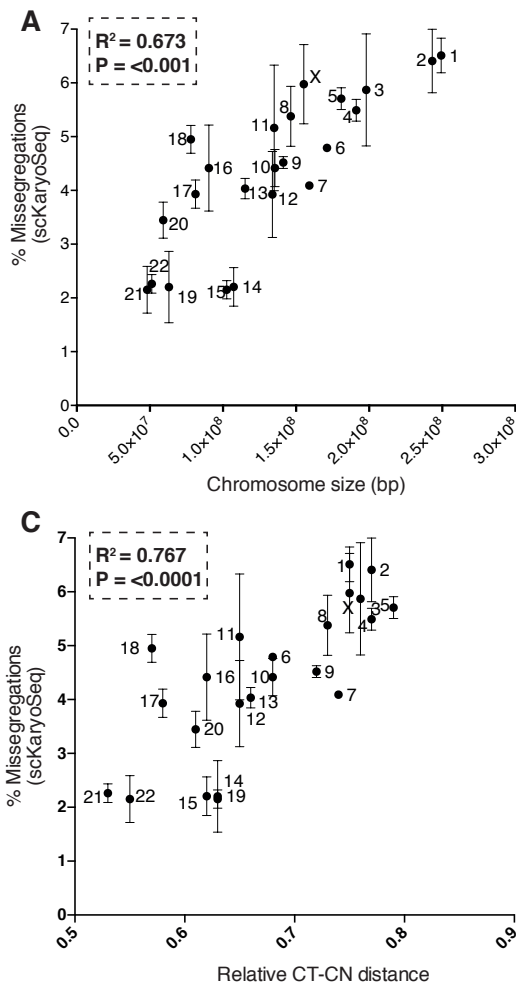


**Figure 4: Misregulation propensity is associated with interphase localization of chromosomes.** A) Scatter plot showing the correlation between chromosome size (X-axis; size in megabase, mb) and missegregations as measured by scKaryoSeq, data from Figure 2C. Statistics as in Figure 3C. B) Total observed missegregations of the X chromosome divided into the normal and X:10q fusion. Differences or not significant as tested by a two-tailed t-test ( $p > 0.05$ ). C) Scatter plot showing the correlation between chromosomal territory location to nuclear center distance (CT-CN; relative values: 0 = located at nuclear center, 1 = maximally peripheral. Data from [24] and missegregations from Figure 2C. Statistics as in Figure 3C.

of CENP-E thus causes peripheral polar chromosomes to remain stuck near spindle poles [28]. We used FISH to quantify the proportions of each polar chromosome over the total number of polar chromosomes in CENPE-E inhibited cells (Figure 5A and B) and found that the chromosomes displaying a bias for missegregation in our SAC-impaired cells also were more frequently present near spindle poles upon CENP-E inhibition (Figure 5C). We therefore propose a model in which a more peripheral nuclear location during interphase increases a chromosome's time to alignment and bipolar attachment during mitosis, which in turn increases its dependency on a functional SAC for its correct segregation.

## Discussion

It has long been assumed that individual chromosomes have an equal chance to undergo missegregation during an erroneous mitosis. However, here we describe a bias in missegregation among chromosomes when the SAC is impaired. Missegregation proportions are associated with a more peripheral localization of chromosomes in the interphase nucleus as well as with a dependency on CENP-E to achieve chromosome alignment to the metaphase plate. We propose a model in which the nuclear location before mitotic onset determines the position of a chromosome relative to the nascent mitotic spindle. A more peripheral location positions chromosomes on the astral sides of the spindle poles during early mitosis. This in turn increases their dependency on CENP-E-mediated transport to the metaphase plate, resulting in more time needed for these chromosomes to achieve alignment and bipolar attachment. In conditions where the SAC is impaired, anaphase is initiated before the peripherally localized chromosomes can achieve biorientations, resulting in increased missegregation as compared to more centrally located chromosomes.

Confirmation of this model requires experimental validation in which the chromosomal territories during interphase are disrupted before mitotic onset. This organization is facilitated by lamina-associated domains (LADs): chromosomal regions consisting mainly of heterochromatin that associate with the nuclear lamina [29]. Disturbing the heterochromatin state of LADs has been shown to alter the location of chromosomal domains in the nucleus [30]. Our model predicts that by this approach the missegregation bias is neutralized, assuming that the new nuclear organization is random. Similarly, arresting cells for a few hours in mitosis by means of spindle disruption (e.g. nocodazole treatment) should also change chromosomal organization, and thus missegregation frequencies, once those cells are allowed to re-build a spindle and continue division.

Recent reports have found that in specific conditions or model organisms, a missegregation bias for specific chromosomes can occur [31, 32]. For example, when inducing missegregations after release from a prolonged mitotic arrest, chromosome

1 appeared to be more vulnerable to premature loss of cohesion and subsequent missegregation than other chromosomes [32]. In another study, cells of indian muntjac deer, which have only three chromosomes with very large kinetochores, missegregated chromosome 3+X more frequently when CENP-E activity was compromised. This bias was attributed to its extremely large kinetochore, which was proposed to rely more heavily on CENP-E-dependent alignment than others [31]. Since we don't see a correlation of missegregation frequencies with centromere size in human cells and don't allow time for cohesion loss, the mechanism of bias when cells go through an accelerated mitosis is different. It would be interesting to see how perturbation of different mitotic processes results in different biases and how these relate to each other. Such insights might have implications in how we interpret disease related aneuploidies and might reveal which defects underlie them.

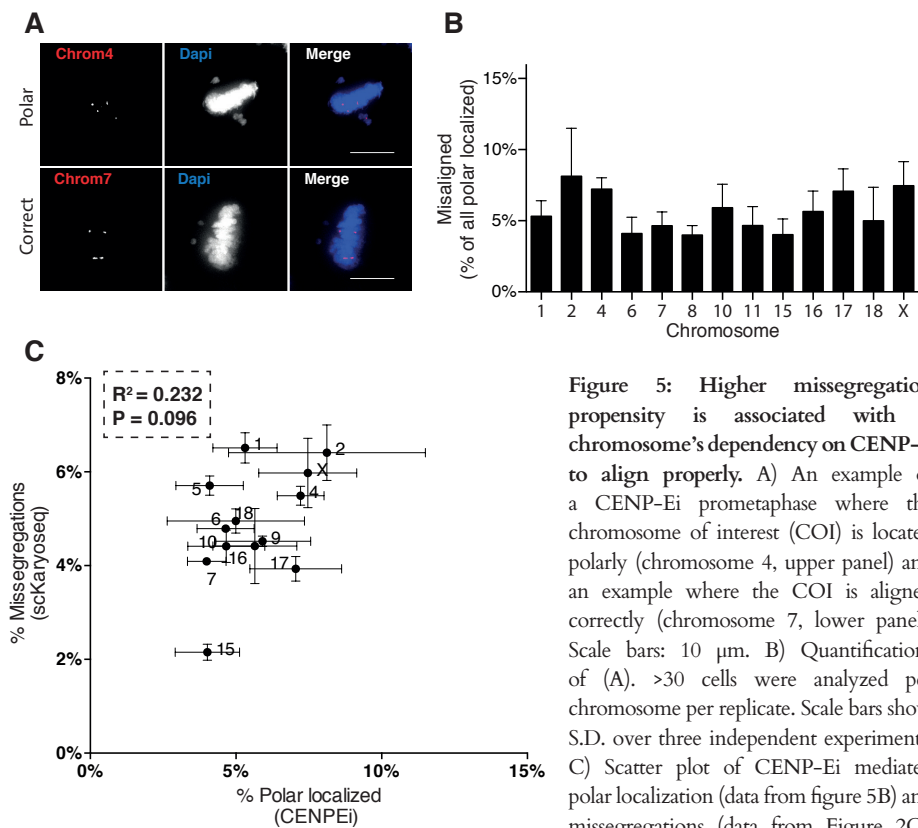


**Figure 5: Higher missegregation propensity is associated with a chromosome's dependency on CENP-E to align properly.** A) An example of a CENP-Ei prometaphase where the chromosome of interest (COI) is located polarly (chromosome 4, upper panel) and an example where the COI is aligned correctly (chromosome 7, lower panel). Scale bars: 10  $\mu$ m. B) Quantifications of (A). >30 cells were analyzed per chromosome per replicate. Scale bars show S.D. over three independent experiments. C) Scatter plot of CENP-Ei mediated polar localization (data from figure 5B) and missegregations (data from Figure 2C). Statistics as in Figure 3C.

## Materials and Methods

**Cell lines.** Cells were maintained at 37°C and 5% CO<sub>2</sub>. RPE1 (ATCC) cells were cultured in DMEM/F12 (Sigma) supplemented with Ala-Gln (Sigma), penicillin/streptomycin (Sigma) and 8% Fetal Bovine Serum (Sigma).

**Cell treatments.** For synchronization, RPE1 cells were plated at 40% confluency in 250nM palbociclib (Selleck Chemicals). After 24 hours cells were washed three times with warm (37°C) medium and cultured for 16 hours in RO-3306 (Tocris, 5μM). After three washes with warm (37°C) medium supplemented with DMSO (control) or Mps1 inhibitor (Compound 5, 62.5nM) [15], cells were processed depending on subsequent analysis. For chromosome alignment assays, cells were arrested using RO-3306 for 16 hours, washed three times using warm medium and subsequently put in CENP-E inhibitor (GSK923295, Selleck Chemicals, 150nM) for 2 hours.

**FACS.** Cells were harvested by trypsinization for 5 minutes at 37°C. Cells were fixed in ice-cold 70% ethanol while vortexing and stored at -20°C until further processing. Cells were washed with PBS and stained with 1μg/mL Hoechst 34580 in PBS for 1 hour at room temperature. Flow cytometry was performed on a BD FACSCanto II (BD Biosciences) and the data was analysed using FlowJo 7.

**FISH.** FISH probes were obtained from Cytocell. Cells were fixed using Carnoy's fixative (25% acetic acid, 75% methanol) and stained according to manufacturer's recommendations. Images were acquired using a deconvolution system (Deltavision Elite; Applied Precision/GE Healthcare) using a 60x/1.4NA objective (Olympus) and post-acquisition processed into deconvolved maximum intensity projections using SoftWorx6.0 (Applied Precision/GE Healthcare). Images were analyzed manually using ImageJ software.

**Live-cell imaging.** For time-lapse live-cell imaging, RPE1 cells were infected with a previously published lentivirus expressing H2B-mNeon [33] to visualize chromosome segregation. Cells were seeded in glass-bottom culturing plates and imaged at 3 to 4-minute intervals in XYZ-mode using a microscope (Nikon Eclipse

Ti) equipped with a climate chamber to keep cells at 37°C and 5% CO<sub>2</sub> throughout the experiment. Pictures were taken every 4 minutes. Chromosome missegregation and cell fate were analyzed manually based on maximal projection movies from the H2B signals using ImageJ or NIS-Elements software.

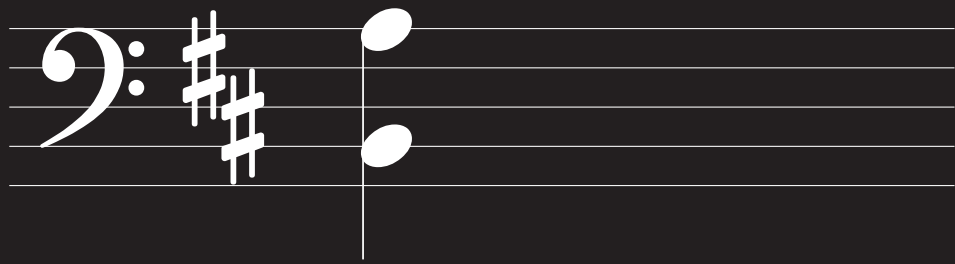
**Single-cell sequencing.** For single-cell sequencing, cells were harvested 4h after RO-release by trypsinization. Cells were processed for FACS as described [21] with a minor modification: 10µg/mL Hoechst 34580 was used to quantify DNA content. ±2N nuclei were sorted with a BD FACSJazz (BD Biosciences) in a Hard-Shell 384 wells PCR plate (Bio-Rad) containing 5µL of mineral oil (Sigma-Aldrich) in each well and stored at -20°C until further processing. Cell lysis was performed overnight at 50°C using 0.05 units of Qiagen Protease in 1x NEBuffer 4 (NEB) followed by heat inactivation at 75°C for 20 minutes and 80°C for 5 minutes. The genomic DNA was subsequently fragmented with 100nL 1U NlaIII (NEB) in 1x Cutsmart (NEB) for 60 minutes at 37°C followed by heat inactivation at 80°C for 20 minutes. 100nL of 1µM barcoded double-stranded NlaIII adapters and 100nL of 40U T4 DNA ligase (NEB) in 1x T4 DNA Ligase buffer (NEB) supplemented with 3mM ATP (Invitrogen) was added to each well and ligated overnight at 16°C. After ligation samples were pooled and library preparation was performed as described previously [34]. Libraries were sequenced 1 x 75bp single-end on an Illumina Nextseq 500. The fastq files were mapped to GRCH38 using the Burrows-Wheeler Aligner. The mapped data was analyzed using custom scripts in Python, which parsed for library barcodes, removed reads without an NlaIII sequence and removed PCR-duplicated reads. Copy number analysis was performed as described previously by using Aneufinder [21]. Copy number changes were manually determined using the single cell profiles generated by Aneufinder.

## References

1. Orr, B., K.M. Godek, and D. Compton, *Aneuploidy*. *Current Biology*, 2015. **25**(13): p. R538-R542.
2. Santaguida, S. and A. Amon, *Short- and long-term effects of chromosome mis-segregation and aneuploidy*. *Nature reviews. Molecular cell biology*, 2015. **16**(8): p. 473-485.
3. Kops, G.J.P.L., B.A.A. Weaver, and D.W. Cleveland, *On the road to cancer: aneuploidy and the mitotic checkpoint*. *Nature reviews. Cancer*, 2005. **5**(10): p. 773-785.
4. Thompson, S.L. and D.A. Compton, *Examining the link between chromosomal instability and aneuploidy in human cells*. *The Journal of cell biology*, 2008. **180**(4): p. 665-672.
5. Lengauer, C., K.W. Kinzler, and B. Vogelstein, *Genetic instability in colorectal cancers*. *Nature*, 1997. **386**(6625): p. 623-627.
6. Funk, L.C., L.M. Zasadil, and B.A. Weaver, *Living in CIN: Mitotic Infidelity and Its Consequences for Tumor Promotion and Suppression*. *Dev Cell*, 2016. **39**(6): p. 638-652.
7. van Jaarsveld, R.H. and G.J.P.L. Kops, *Difference Makers: Chromosomal Instability versus Aneuploidy in Cancer*. *Trends Cancer*, 2016. **2**(10): p. 561-571.
8. Janssen, A. and R.H. Medema, *Genetic instability: tipping the balance*. *Oncogene*, 2013. **32**(38): p. 4459-4470.
9. Foley, E.A. and T.M. Kapoor, *Microtubule attachment and spindle assembly checkpoint signalling at the kinetochore*. *Nat Rev Mol Cell Biol*, 2013. **14**(1): p. 25-37.
10. Sacristan, C. and G.J. Kops, *Joined at the hip: kinetochores, microtubules, and spindle assembly checkpoint signaling*. *Trends Cell Biol*, 2015. **25**(1): p. 21-8.
11. Musacchio, A., *The Molecular Biology of Spindle Assembly Checkpoint Signaling Dynamics*. *Curr Biol*, 2015. **25**(20): p. R1002-18.
12. Pachis, S.T. and G. Kops, *Leader of the SAC: molecular mechanisms of Mps1/TTK regulation in mitosis*. *Open Biol*, 2018. **8**(8).
13. Janssen, A., G.J. Kops, and R.H. Medema, *Elevating the frequency of chromosome mis-segregation as a strategy to kill tumor cells*. *Proc Natl Acad Sci U S A*, 2009. **106**(45): p. 19108-13.
14. Vassilev, L.T., et al., *Selective small-molecule inhibitor reveals critical mitotic functions of human CDK1*. *Proc Natl Acad Sci U S A*, 2006. **103**(28): p. 10660-5.
15. Koch, A., et al., *Molecular basis underlying resistance to Mps1/TTK inhibitors*. *Oncogene*, 2016. **35**(19): p. 2518-28.
16. Toogood, P.L., et al., *Discovery of a potent and selective inhibitor of cyclin-dependent kinase 4/6*. *J Med Chem*, 2005. **48**(7): p. 2388-406.
17. Chan, Y.W., K. Fugger, and S.C. West, *Unresolved recombination intermediates lead to ultra-fine anaphase bridges, chromosome breaks and aberrations*. *Nat Cell Biol*, 2018. **20**(1): p. 92-103.
18. Chan, K.L., et al., *Replication stress induces sister-chromatid bridging at fragile site loci in mitosis*. *Nature cell biology*, 2009. **11**(6): p. 753-760.
19. Darzynkiewicz, Z., et al., *Cell synchronization by inhibitors of DNA replication induces replication stress and DNA damage response: analysis by flow cytometry*. *Methods Mol Biol*, 2011. **761**: p. 85-96.
20. Mooijman, D., et al., *Single-cell 5hmC sequencing reveals chromosome-wide cell-to-cell variability and enables lineage reconstruction*. *Nat Biotechnol*, 2016. **34**(8): p. 852-6.
21. Bakker, B., et al., *Single-cell sequencing reveals karyotype heterogeneity in murine and human malignancies*. *Genome Biol*, 2016. **17**(1): p. 115.
22. Cremer, T. and C. Cremer, *Chromosome territories, nuclear architecture and gene regulation in mammalian cells*. *Nat Rev Genet*, 2001. **2**(4): p. 292-301.
23. Sun, H.B., J. Shen, and H. Yokota, *Size-dependent positioning of human chromosomes in interphase nuclei*. *Biophys J*, 2000. **79**(1): p. 184-90.
24. Bolzer, A., et al., *Three-dimensional maps of all chromosomes in human male fibroblast nuclei and prometaphase rosettes*. *PLoS Biol*, 2005. **3**(5): p. e157.
25. Barisic, M., et al., *Kinetochore motors drive congression of peripheral polar chromosomes by overcoming random arm-ejection forces*. *Nat Cell Biol*, 2014. **16**(12): p. 1249-56.
26. Rieder, C.L., *Kinetochores are transported poleward along a single astral microtubule during chromosome attachment to the spindle in newt lung cells*. *The Journal of Cell Biology*, 1990. **110**(1): p. 81-95.
27. Wood, K.W., et al., *CENP-E is a plus end-directed kinetochore motor required for metaphase chromosome alignment*. *Cell*, 1997. **91**(3): p. 357-366.
28. Ding, X., et al., *Probing CENP-E function in chromosome dynamics using small molecule inhibitor syntelin*. *Cell Res*, 2010. **20**(12): p. 1386-9.
29. van Steensel, B. and A.S. Belmont, *Lamina-Associated Domains: Links with Chromosome Architecture, Heterochromatin, and Gene Repression*. *Cell*, 2017. **169**(5): p. 780-791.
30. Kind, J., et al., *Single-cell dynamics of genome-nuclear lamina interactions*. *Cell*, 2013. **153**(1): p. 178-92.
31. Drpic, D., et al., *Chromosome Segregation Is Biased by Kinetochore Size*. *Curr Biol*, 2018. **28**(9): p.



- 1344-1356 e5.
32. Worrall, J.T., et al., *Non-random Mis-segregation of Human Chromosomes*. Cell Rep, 2018. 23(11): p. 3366-3380.
  33. Drost, J., et al., *Sequential cancer mutations in cultured human intestinal stem cells*. Nature, 2015. 521(7550): p. 43-47.
  34. Muraro, M.J., et al., *A Single-Cell Transcriptome Atlas of the Human Pancreas*. Cell Syst, 2016. 3(4): p. 385-394 e3.



# **Chapter 7**

## **Summary & Discussion**

## Summary

The development of colorectal cancer (CRC) is associated with the accumulation of genetic mutations that provide cells with malignant properties. Cancer cells carry defects in genome surveillance mechanisms that lead to genetic instability, providing increased chance to generate the mutations needed for malignant transformation. One of the main manifestations of genetic instability is aneuploidy, a karyotype that is not a multiple of the haploid set. Elevated chromosome segregation errors during mitosis underlie the accumulation of aneuploidy in CRC, and this reduced mitotic fidelity gives rise to a specific form of genetic instability known as chromosomal instability (CIN). This thesis encompasses a series of studies that aim to understand the causes and consequences of CIN in CRC development.

In **chapter 2** we provide an in-depth discussion concerning current literature on aneuploidy and CIN in cancer biology. We discuss how aneuploidy and CIN are fundamentally different traits and how each differently influence different aspects of cancer biology. Therefore, we emphasize the need to study CIN and aneuploidy individually and to that end CIN should be measured not based on aneuploidies but rather based on the measurement of chromosome missegregation itself. We finally provide a theoretical framework based on the hormesis concept to hypothesize how aggravating CIN might be a therapeutically exploitable option in treating CIN tumors.

**Chapter 3** describes the first study that employs the CRISPR/Cas9 technique in combination with organoid cultures. We combine both techniques to develop an artificial CRC progression model by introducing the most commonly mutated genes in CRC that are associated with the adenoma-to-carcinoma sequence. Studying the resulting set of genetically engineered tumor progression organoids confirmed that mutation of all four genes is needed for full malignant transformation. Based on time-lapse imaging of the progression set, we furthermore find that loss of p53 induces CIN in colon organoids.

We continue to use the set of progression organoids in **chapter 4** to decipher the role of p53 in preventing chromosome segregation errors. We find that loss of p53 renders cells dependent on p38 activity to prevent a specific form of mitotic error that we term ‘bulky anaphase bridges’ (BABs). BABs are associated with DNA-damage and are dependent on active DNA-damage signaling in G2. Finally, we show that p53 deficient, CRC patient derived organoids depend on active p38 to prevent excessive CIN as well. This study therefore reveals previously unanticipated roles for p53 and p38 in preventing genetic instability by limiting missegregation rates. Furthermore, the interaction between p53 and p38 might provide therapeutic opportunities based on CIN aggravation by p38 inhibition in p53 deficient tumors.

The study described in **chapter 5** is the first to assess chromosome segregation errors over the course of tumor progression. Assessment of CIN in organoids derived from benign, pre-malignant and malignant tissues from mice and men revealed that CIN is associated with malignant transformation. CIN levels do not increase from primary tumor to metastasis and do not correlate with aneuploidy scores.

In **chapter 6** we address the question whether each chromosome has an equal chance to missegregate when cells are forced to enter anaphase prematurely. We find that a more peripheral location in the interphase nucleus correlates with increased missegregation proportions, revealing a previously unanticipated relation between interphase nuclear organization and mitotic behavior of chromosomes.

## Discussion

### Organoids as a model system in mitosis and cancer research

The development of organoid cultures has provided a leap forward in *in vitro* tissue modeling. The multicellular and three-dimensional nature of organoids provides major advances over classical two-dimensional cell cultures in that it allows for the assessment of cell behavior in a context that more closely resembles the tissues from which they originate. One other important improvement of organoids over classical cell lines is that organoids can potentially be grown indefinitely without the need for immortalization.

In terms of mitosis research, a main advantage of organoids resides in the three-dimensional structure, which potentially allows for investigating the involvement of spindle positioning on chromosomes segregation and how neighboring cells might influence this position. Indeed, the three-dimensional context has been associated with improved mitotic fidelity [1], suggesting improvements over classical cell cultures. Furthermore, the multicellular and differentiated nature of organoids allows for the assessment of chromosome segregation - and mitosis in general - in specific cell types, most notably stem cells.

Besides improvements in modeling physiological conditions, organoids have also been successfully implemented in studying cancer. Organoids have been grown from tumors originating from a variety of organs, including colon [2-4], prostate [5], breast [6], pancreas [7] and liver [8]. In the context of cancer research, organoids provide multiple advances over classical cell lines. For instance, organoids have improved initiation rates (i.e. the engraftment efficiency is higher) when taken into culture from primary tumors as compared to two-dimensional culture systems and since organoids can be grown from many healthy tissues, they provide the possibility to include matched healthy controls [9]. These properties combined provide the basis for chapters 3 and 5 to conduct studies on CRC progression that would not have been possible without the ability to efficiently grow healthy and pre-malignant

tissues *in vitro*. However, chapter 4 demonstrates that under certain circumstances the culture conditions needed to maintain healthy tissue-derived organoids in culture, potentially induce unintended side-effects. In this specific case, inhibition of p38, which is essential to maintain organoids derived from healthy colon [2], induces CIN in a p53 null background. As with any study, this example highlights the importance of evaluating findings in independent model systems, and organoid-based studies are no exception.

### **The causes for CIN in human cancer**

Maintaining a stable karyotype depends on the complete duplication of chromosomes and subsequent correct segregation in mitosis. Both processes are however complex and therefore many pathways are in place to ensure that they are executed correctly and cells only progress in the cell cycle when all conditions for proper execution of the next step have been met. Since maintaining a stable karyotype depends on so many processes, it is not surprising that alterations in many different mechanisms have been proposed to cause CIN in human cancer. These mechanisms include replication stress [10], cohesion defects [11, 12], mutation or altered expression of SAC components [13-16], altered microtubule dynamics [17], supernumerary centrosomes [18, 19] and the presence of DNA-damage and associated signaling during mitosis [20-22].

In chapter 4 we describe how combined loss of p53 and p38 gives rise to increased chromosome missegregation, most likely by allowing mitotic entry in the presence of DNA-damage. The aberrant DNA structures subsequently hold together the sister chromatids to form anaphase bridges. Since such missegregations can result in chromosome breakage [23, 24] and thus additional DNA-damage, a scenario emerges in which mitotic entry in the presence of DNA-damage initiates a vicious cycle of chromosome breakage and missegregation. The association of chromosome missegregation with the formation of micronuclei which subsequently predispose to chromothripsis possibly presents an additional aggravation of the cycle [25]. A vicious cycle would however predict that eventually all tumor cells make mitotic errors in every division but missegregation rates typically range from ~10%-40% in CRC organoids (Chapter 5 figure 4A). Multiple explanations might account for this discrepancy. First,

cells can eventually be cleared from the population due to cell death resulting from severe missegregations. Second, the cycle depends on maintaining damage over the cell cycle to the next mitosis. DNA-damage repair might however efficiently repair foci within this time frame. If this is a stochastic process, the vicious cycle might be discontinued within a limited number of cell cycles. Third, missegregation does not always result in chromosome breakage or damage [26], providing another source for stochastic interruption of the cycle. Finally, the percentages might represent a sub-population of cells within the organoids, possibly stem cells, that are more prone to missegregation. In light of these explanations, it would be interesting to conduct long-term imaging experiments that assess mitotic fidelity over subsequent generations, preferably in combination with live-cell markers for DNA damage (e.g. based on the tudor domain of 53BP1) [27] and for cell types (e.g. stem-cell markers) [28]. Performing such experiments in tumor-derived organoids might clarify the mechanisms behind CIN in CRC. In the context of the p53/p38 interaction, these experiments might reveal the source of DNA-damage leading to anaphase bridge formation as well as clarify why we find anaphase bridges consistently in ~25% of mitotic events (Chapter 4, figures 1A, 1D, 1F, 2A, 2D).

### **Chromosomal Instability in Colorectal Cancer Progression**

One major question that is addressed in this thesis is when during CRC development CIN arises. We find that CIN is associated with malignant transformation based on the assessment of CIN levels in benign and malignant tissues (Chapter 5) and based on an artificial CRC progression model (Chapter 3). Importantly however, CIN itself is insufficient for malignant transformation since  $APC^{KO}/KRAS^{G12D}/TP53^{KO}$  colon organoids are as CIN but non-invasive, while  $APC^{KO}/KRAS^{G12D}/TP53^{KO}/SMAD4^{KO}$  organoids are equally CIN but do form carcinomas [29, 30]. These results can be interpreted in the light of the two main CRC progression models: stepwise progression according to the adenoma-to-carcinoma sequence [31] and genomic crisis-mediated tumor formation according to the big bang model [32].

The adenoma-to-carcinoma sequence states that CRC progresses from healthy tissue to malignant in a stepwise manner. Each step is associated with additional mutations



that provide the acquisition of new oncogenic traits. CIN would provide a genetic instability background that potentially aids in accumulating the mutations needed to progress to the next stage. However, we find that benign adenomas are chromosomally stable (that is: missegregation rates that are similar to healthy cells), yet they already carry aneuploidies characteristic of CRC. This might be explained in two different ways. First, adenomas might have gradually acquired aneuploidies by the slightly elevated rates of chromosome missegregation. Second, the karyotypes of adenomas can be formed by a single erroneous mitosis. In the latter case, per definition, CIN has never been present since the missegregation occurred only in one generation (Chapter 2). The adenoma might subsequently acquire CIN in later stages to facilitate its progression to the carcinoma state. Either way, according to our results, CIN is not present in benign tumors and the adenoma-to-carcinoma sequence therefore predicts that CIN is either present at restricted times during progression and/or acquired at the moment of malignant transformation.

Interpretation of our results in light of the big bang model however suggests a different contribution of CIN to CRC development. This model states that the malignant potential of colorectal tumors is defined at an early stage of tumor formation by means of a short period of genomic crisis. Since CIN is only present in malignant tissue, this model suggests that the presence or generation of CIN at the moment of the genomic crisis is essential in providing malignant potential. The contributions of CIN to further progression are therefore probably limited, however CIN might provide malignant properties by mechanisms beyond genetic mutation [33]. The absence of CIN during genomic crisis -or the lack of CIN induction by the crisis- would leave the tumor with limited oncogenic potential and it will therefore not progress beyond the adenoma stage. The possibility that CIN can be acquired later to provide the acquisition of malignant behavior can however not be excluded, although evidence for this should have been detected by multiregional sequencing [32].

Our data are thus not conclusive in defining the moment when CIN arises during tumor development but do show a relation between CIN and oncogenic transformation. Several approaches can help to further elucidate the contributions

of CIN to tumorigenesis. One such approach would be to generate inducible and reversible induction of CIN in pre-malignant tissues and assess malignant potential in different timing scenarios, for instance in a xenograft model. This can be achieved by inducible expression of shRNAs targeting genes essential for correct chromosome segregation (e.g. *TTK*, *Mps1*). Such an approach might reveal if CIN is sufficient to transform benign lesions into malignant tumors and, if so, whether ongoing CIN is necessary to maintain malignant potential.

Combining this approach with the artificial tumor progression model (Chapter 3) can give additional insights into the contributions and timing of CIN in tumor progression. For instance, Triple- $p53^{WT}$  mutant organoids are chromosomally stable and non-malignant (chapter 4) [30]. It would be interesting to see whether induction of CIN in these organoids gives them malignant properties. These experiments might furthermore elucidate the role of p53 in preventing malignant transformation, since loss of p53 induces both CIN and malignant potential (chapter 3 and 4). This raises the question if CIN induced by p53 loss contributes to oncogenic transformation or is merely a passenger event that coincides with p53 loss. The results presented in chapter 4 suggest that additional modifications can prevent excessive CIN induction by p53 loss, for instance by alterations in the p38 or ATM pathways, providing a possibility to study p53 tumor suppressor function independent of CIN induction.

### **Clinical Implications of CIN in CRC**

CRC survival declines drastically with advanced tumor stage [34]. Early detection is therefore essential in reducing CRC associated mortality. Understanding how CRC develops can therefore provide important insights into early detection and distinguishing between high and low-risk lesions. As described in chapter 5, CIN might specifically mark high-risk adenomas. It would therefore be interesting to conduct a study in which material from surgically resected adenomas is tested for CIN in combination with pathological staging to confirm whether high-risk adenomas indeed are more frequently CIN. Since ethical reasons prohibit prognostic studies in human, a prognostic study based on the *APC<sup>+ / 1638N</sup>* mouse model in which tumor CIN levels are determined by means of biopsy-derived organoid cultures would

give important insights into the relation between CIN and metastatic potential. It is important to note that this approach and the data presented in this thesis possibly assesses non-hypermuted CRC specifically. Additional parameters, such as mutation load or microsatellite instability, might therefore be essential in combination with CIN assessment.

As described in chapter 2, CIN might provide opportunities for developing novel anti-cancer therapies. The findings in this thesis provide additional potential approaches to this idea. First, the observation that p53 renders cells dependent on p38 activity to limit chromosome missegregation levels opens the possibility to treat p53 deficient tumors specifically with CIN-enhancing therapies by p38 targeting drugs. This approach might benefit from additional DNA-damaging agents since the anaphase bridges that form after combined p53 and p38 loss likely result from DNA-damage foci (Chapter 4). Whether elevated missegregation levels by p38 inhibition indeed reduce viability of p53 deficient tumors however remains to be determined.

Inhibitors of SAC components provide a promising approach for CIN aggravating therapeutic strategies as well. The missegregation bias described in chapter 6 might provide ways to improve patient stratification for such therapies. In general, the efficacy of CIN-enhancing therapeutics will depend on the combined toxicity resulting from missegregation associated DNA-damage and the generation of severe aneuploidies. Since complete loss of a chromosome is likely the most lethal form of aneuploidy (due to loss of essential genes), SAC-inhibition based strategies will be most efficient in tumors that already lost a copy of a commonly missegregating chromosome. Whereas one of the daughter cells dies as a result of complete loss of that chromosome, the other cell still suffers from the DNA-damaging component of toxicity. Furthermore, the newly acquired karyotype is likely to be sub-optimal, further reducing cellular fitness. The common loss of chromosome 3p in kidney tumors [35] present such a possibility and evaluating the sensitivity of those tumors to SAC inhibition could therefore provide interesting insights in patient stratification of CIN-based therapeutic strategies.

Finally, the observation that peripheral chromosomes depend more on the SAC for their correct segregation than others suggests that enhancing peripheral localization of chromosomes in the interphase nucleus increases missegregation rates when the SAC is impaired. Interphase nuclear organization is facilitated by the interaction of the nuclear lamina with lamina-associated domains (LADs) [36]. Since the interaction of LADs with the lamina is dependent on the heterochromatin state of LADs [37], increasing the general heterochromatin state by means of HDAC inhibitors relocates chromosomes to a more peripheral location [38]. It would be interesting to see whether combined inhibition of HDACs and MPS1 enhances chromosome missegregation and CIN-induced toxicity.

## Concluding Remarks

Recent efforts in whole-genome sequencing of cancer have led to the realization that cancer is a complex, multi-genic, heterogeneous disease that will not be cured by one common approach. Instead, each tumor has to be assessed individually to design optimal treatment strategies, an approach now widely known as ‘personalized medicine’. The majority of studies aiming to design a personalized therapeutic approach focus on the development of drugs targeting one specific mutation. The CIN-based approach proposed in this thesis presents a different approach to personalized medicine, since the biomarker that would predict treatment efficacy is a phenotype instead of a genotype. CIN might present an excellent biomarker since it is mostly absent in non-malignant tissues and so CIN-targeting therapeutic strategies, especially when enhancing CIN in malignant cells specifically, promise great potential in cancer treatment.

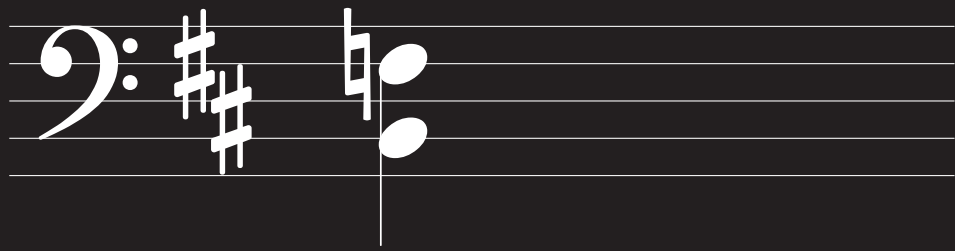
Finally, studies that compare benign and malignant tumors, as presented here, have the unique possibility to define the essential alterations to develop oncogenic behavior. Since those alteration define what makes a cell a cancer cell, identifying them will be most informative for many aspects of cancer biology. It is my conviction that truly understanding the alterations that facilitate oncogenic transformation will be the root to developing new and improved strategies in cancer prevention, detection and in therapy.

## References

1. Knouse, K.A., et al., *Chromosome Segregation Fidelity in Epithelia Requires Tissue Architecture*. Cell, 2018. **175**(1): p. 200–211 e13.
2. Sato, T., et al., *Long-term Expansion of Epithelial Organoids From Human Colon, Adenoma, Adenocarcinoma, and Barrett's Epithelium*. Gastroenterology, 2011. **141**(5): p. 1762–1772.
3. Fujii, M., et al., *A Colorectal Tumor Organoid Library Demonstrates Progressive Loss of Niche Factor Requirements during Tumorigenesis*. Cell Stem Cell, 2016.
4. van de Wetering, M., et al., *Prospective derivation of a living organoid biobank of colorectal cancer patients*. Cell, 2015. **161**(4): p. 933–945.
5. Gao, D., et al., *Organoid cultures derived from patients with advanced prostate cancer*. Cell, 2014. **159**(1): p. 176–87.
6. Sachs, N., et al., *A Living Biobank of Breast Cancer Organoids Captures Disease Heterogeneity*. Cell, 2018. **172**(1–2): p. 373–386 e10.
7. Boj, S.F., et al., *Organoid models of human and mouse ductal pancreatic cancer*. Cell, 2015. **160**(1–2): p. 324–38.
8. Broutier, L., et al., *Human primary liver cancer-derived organoid cultures for disease modeling and drug screening*. Nat Med, 2017. **23**(12): p. 1424–1435.
9. Drost, J. and H. Clevers, *Organoids in cancer research*. Nat Rev Cancer, 2018. **18**(7): p. 407–418.
10. Burrell, R.A., et al., *Replication stress links structural and numerical cancer chromosomal instability*. Nature, 2013. **494**(7438): p. 492–496.
11. Barber, T.D., et al., *Chromatid cohesion defects may underlie chromosome instability in human colorectal cancers*. Proc Natl Acad Sci U S A, 2008. **105**(9): p. 3443–8.
12. Zhang, N., et al., *Overexpression of Separase induces aneuploidy and mammary tumorigenesis*. Proc Natl Acad Sci U S A, 2008. **105**(35): p. 13033–8.
13. Cahill, D.P., et al., *Mutations of mitotic checkpoint genes in human cancers*. Nature, 1998. **392**(6673): p. 300–3.
14. Schvartzman, J.-M., et al., *Mad2 is a critical mediator of the chromosome instability observed upon Rb and p53 pathway inhibition*. Cancer Cell, 2011. **19**(6): p. 701–714.
15. Sotillo, R., et al., *Mad2 overexpression promotes aneuploidy and tumorigenesis in mice*. Cancer Cell, 2007. **11**(1): p. 9–23.
16. Sotillo, R., et al., *Mad2-induced chromosome instability leads to lung tumour relapse after oncogene withdrawal*. Nature, 2010. **464**(7287): p. 436–440.
17. Bakhroum, S.F., G. Genovese, and D.A. Compton, *Deviant kinetochore microtubule dynamics underlie chromosomal instability*. Curr Biol, 2009. **19**(22): p. 1937–42.
18. Ganem, N.J., S.A. Godinho, and D. Pellman, *A mechanism linking extra centrosomes to chromosomal instability*. Nature, 2009. **460**(7252): p. 278–82.
19. Silkworth, W.T., et al., *Multipolar spindle pole coalescence is a major source of kinetochore mis-attachment and chromosome mis-segregation in cancer cells*. PLoS One, 2009. **4**(8): p. e6564.
20. Bakhroum, S.F., et al., *DNA-Damage Response during Mitosis Induces Whole-Chromosome Mis-segregation*. Cancer discovery, 2014. **4**(11): p. 1281–1289.
21. Canovas, B., et al., *Targeting p38alpha Increases DNA Damage, Chromosome Instability, and the Anti-tumoral Response to Taxanes in Breast Cancer Cells*. Cancer Cell, 2018. **33**(6): p. 1094–1110 e8.
22. Degryareva, N.P., et al., *Chronic oxidative DNA damage due to DNA repair defects causes chromosomal instability in Saccharomyces cerevisiae*. Mol Cell Biol, 2008. **28**(17): p. 5432–45.
23. Crasta, K., et al., *DNA breaks and chromosome pulverization from errors in mitosis*. Nature, 2012. **482**(7383): p. 53–58.
24. Janssen, A., et al., *Chromosome segregation errors as a cause of DNA damage and structural chromosome aberrations*. Science, 2011. **333**(6051): p. 1895–1898.
25. Zhang, C.-Z., et al., *Chromothripsis from DNA damage in micronuclei*. Nature, 2015. **522**(7555): p. 179–184.
26. Amaral, N., et al., *The Aurora-B-dependent NoCut checkpoint prevents damage of anaphase bridges after DNA replication stress*. Nat Cell Biol, 2016. **18**(5): p. 516–26.
27. Beckta, J.M., S.C. Henderson, and K. Valerie, *Two- and three-dimensional live cell imaging of DNA damage response proteins*. J Vis Exp, 2012(67).
28. Oost, K.C., et al., *Specific Labeling of Stem Cell Activity in Human Colorectal Organoids Using an ASCL2-Responsive Minigene*. Cell Rep, 2018. **22**(6): p. 1600–1614.
29. Drost, J., et al., *Sequential cancer mutations in cultured human intestinal stem cells*. Nature, 2015. **521**(7550): p. 43–47.
30. Fumagalli, A., et al., *Genetic dissection of colorectal cancer progression by orthotopic transplantation of engineered cancer organoids*. Proc Natl Acad Sci U S A, 2017. **114**(12): p. E2357–e2364.

31. Fearon, E.R. and B. Vogelstein, *A genetic model for colorectal tumorigenesis*. Cell, 1990. **61**(5): p. 759-767.
32. Sottoriva, A., et al., *A Big Bang model of human colorectal tumor growth*. Nature genetics, 2015. **47**(3): p. 209-216.
33. Bakhoum, S.F., et al., *Chromosomal instability drives metastasis through a cytosolic DNA response*. Nature, 2018. **553**(7689): p. 467-472.
34. Brenner, H., M. Kloor, and C.P. Pox, *Colorectal cancer*. Lancet, 2014. **383**(9927): p. 1490-1502.
35. Hoadley, K.A., et al., *Multiplatform analysis of 12 cancer types reveals molecular classification within and across tissues of origin*. Cell, 2014. **158**(4): p. 929-944.
36. van Steensel, B. and A.S. Belmont, *Lamina-Associated Domains: Links with Chromosome Architecture, Heterochromatin, and Gene Repression*. Cell, 2017. **169**(5): p. 780-791.
37. Kind, J., et al., *Single-cell dynamics of genome-nuclear lamina interactions*. Cell, 2013. **153**(1): p. 178-92.
38. Taddei, A., et al., *Reversible disruption of pericentric heterochromatin and centromere function by inhibiting deacetylases*. Nat Cell Biol, 2001. **3**(2): p. 114-20.







# **Addendum**

**Nederlandse Samenvatting  
Nederlands Curriculum Vitae  
List of Publications  
Dankwoord**

## Nederlandse samenvatting

Kanker ontstaat als cellen in ons lichaam eigenschappen verwerven die hen in staat stellen ongecontroleerd en buiten hun normale niche te groeien. Deze eigenschappen ontwikkelen zich als gevolg van mutaties in het DNA. Het DNA codeert –in de vorm van genen– voor de productie van eiwitten, welke vervolgens de vele functies van de cel tot uitvoering brengen. Al het DNA in een cel wordt collectief het genoom genoemd en het humane genoom bestaat uit 46 grote DNA-moleculen, de zogeheten chromosomen. Mutaties in het genoom ontstaan als cellen fouten maken bij de duplicatie of verdeling van het genoom, beiden noodzakelijk om de toekomstige dochtercellen van alle benodigde en correcte informatie te voorzien.

De mutaties die bijdragen aan de ontwikkeling van kanker komen in vele vormen voor. Eén van die vormen is aneuploidie, de staat waarin een cel een aantal chromosomen heeft dat afwijkt van de gebruikelijke 46. Aneuploidie ontstaat als een cel tijdens de celdeling niet in staat is om beide dochtercellen van een exacte kopie van het genoom (oftewel 46 chromosomen) te geven. Cellen die herhaaldelijk fouten maken in de verdeling van de chromosomen tijdens de celdeling worden chromosomaal instabiel (kortweg CIN) genoemd. Vele typen kanker, waaronder de meerderheid van de dikke darmtumoren, zijn aneuploid en CIN.

Het onderzoek in dit proefschrift richt zich op het ontstaan van aneuploidie en CIN in dikkedarmkanker (colorectale kanker). Ongeveer 80% van de colorectaal tumoren zijn aneuploid. Zoals in hoofdstuk 2 staat beschreven, betekent dat echter niet dat deze tumoren ook per se CIN zijn. Een mogelijk scenario is namelijk dat vroeg gedurende de ontwikkeling van de tumor de cellen fouten hebben gemaakt tijdens de celdeling, maar deze fouten in een later stadium niet meer maken. De aanwezigheid van aneuploidie in een cel wil dus niet per se betekenen dat deze ook CIN is. De belangrijkste conclusie van hoofdstuk 2 is daarom dat CIN alleen te bepalen is door het visualiseren van de verdeling van chromosomen gedurende de celdeling. Dit vormt de basis voor de methodologie voor de rest van dit proefschrift, waarin CIN bestudeerd wordt op basis van visualisatie van de verdeling van chromosomen tijdens de celdeling.

&

Op basis van het mutatiespectrum kunnen colorectaal tumoren ingedeeld worden in twee klassen: Een hoog aantal puntmutaties die de codering van genen veranderen of een hoog aantal veranderingen in het aantal kopieën dat van ieder gen aanwezig is. Die laatste manifesteert zich met name als aneuploidie en beslaat ongeveer 80% van alle colorectaal tumoren. Een belangrijk model voor de ontwikkeling van deze tumoren beschrijft hoe de acquisitie van mutaties in vier genen (*APC*, *KRAS*, *TP53* en *SMAD4*) de basis vormt voor de ontwikkeling van deze tumoren. Hoe en wanneer CIN en aneuploidie ontstaan en bijdragen aan de ontwikkeling van deze tumoren is echter onbekend. In hoofdstuk 3 wordt deze vraag behandeld. Daartoe is een model ontwikkeld waarin gezond darmweefsel wordt gekweekt en genetisch gemanipuleerd om de vier genen stuk voor stuk te muteren. Vervolgens wordt er gekeken hoe deze (combinaties van) mutaties de celdeling beïnvloeden. We concluderen dat de acquisitie van mutaties in *TP53* verantwoordelijk zijn voor het ontstaan van CIN. *TP53* codeert voor het eiwit p53 en is het meest gemuteerde gen in alle humane tumoren. De functie van p53 richt zich voornamelijk op het beschermen van het genoom tegen de acquisitie van mutaties. Onze bevindingen zijn nieuw omdat het een rol suggereert voor p53 in het voorkomen van het maken van fouten in de celdeling die nieuwe mutaties kunnen veroorzaken, in plaats van het beschermen van cellen die al mutaties hebben verworven.

Deze potentiële nieuwe functie van p53 wordt verder onderzocht in hoofdstuk 4, waarin de exacte bijdrage van *TP53* mutaties aan CIN wordt bekeken. We beschrijven afhankelijkheid voor de functionaliteit van een ander eiwit, p38, om CIN te voorkomen als p53 functie verloren is. Verlies van de functionaliteit van beide eiwitten (p53 en p38) resulteert in een specifieke vorm van fouten genaamd anaphase bruggen. Deze bruggen manifesteren zich als een streng DNA dat de twee grote pakken DNA die zich scheiden tijdens de celdeling (gedurende de zogenaamde anaphase) verbindt. Deze bruggen worden gekenmerkt door de aanwezigheid van eiwitten die betrokken zijn bij de herkenning en reparatie van DNA-schade en inhibitie van deze mechanismen resulteert in vermindering van het aantal bruggen. Een waarschijnlijk scenario is daarom dat het verlies van p53 en p38 resulteert in het starten van de celdeling terwijl er nog schade aanwezig is in het genoom, wat



vervolgens resulteert in een anaphase brug doordat het reparatiemechanisme de strengen DNA bij elkaar houdt.

De aanwezigheid van aneuploidie in veel eindstadium tumoren doet vermoeden dat CIN belangrijk is voor de ontwikkeling van colorectaal kanker. Het punt wanneer tijdens de ontwikkeling CIN ontstaat is echter onbekend. Daarnaast zijn veel goedaardige tumoren (adenomen) ook aneuploid wat suggereert dat aneuploidie en CIN op zichzelf geen kanker veroorzaken. Om inzicht te krijgen in de timing van CIN gedurende de ontwikkeling van colorectaal kanker, alsmede de contributie tot het ontwikkelen van kwaadaardige tumoren, hebben we in hoofdstuk 5 een verzameling aangelegd van goed- en kwaadaardige tumoren van muismodellen en humane patiënten. We vinden dat kwaadaardige tumoren verhoogde CIN-levels hebben ten opzichte van gezond weefsel en goedaardige tumoren. We concluderen dat CIN geassocieerd is met de ontwikkeling van kanker. Het is echter nog onbekend of CIN een goedaardig gezwel kan transformeren tot kwaadaardig indien de CIN zich in een later stadium ontwikkeld. Daarmee passen onze vindingen in beide van de twee belangrijkste modellen ten aanzien van de ontwikkeling van colorectaal kanker: geleidelijke, stapsgewijze ontwikkeling van gezond weefsel, via goedaardig tot kwaadaardig gezwel; of, een korte periode van genetische crisis die het maligne potentieel (potentie tot de ontwikkeling van kwaadaardigheid) van een tumor definieert.

&

In hoofdstuk 7 adresseren wij vervolgens de vraag of alle chromosomen een gelijke kans hebben om in de verkeerde dochtercel terecht te komen indien cellen fouten maken tijdens de deling. Daartoe forceren we cellen om fouten te maken door inhibitie van een eiwit (MSP1) dat essentieel is om de celdeling correct te laten verlopen. We vinden dat na een foute deling bepaalde chromosomen vaker betrokken zijn bij de fout (een missegregatie) dan andere. De verhoogde kans op missegregatie is geassocieerd met een locatie van die chromosomen aan de randen van de celkern vlak voor aanvang van het delingsproces. We stellen een model voor dat stelt dat chromosomen die verder van het midden van de celkern verwijderd liggen bij aanvang van de celdeling, meer tijd nodig hebben om aan de eisen voor correcte segregatie te voldoen.

## Discussie

De onderzoeken in dit proefschrift richten zich op CIN tijdens de ontwikkeling van colorectaal tumoren. We laten zien dat verlies van p53 de ontwikkeling van CIN kan veroorzaken. Echter, het proces is ingewikkeld zoals blijkt uit de nauwe betrokkenheid van andere eiwitten zoals, p38 en DNA-reparatie mechanismen. Nader onderzoek zal moeten uitwijzen of het verlies van p53 een wijdverspreid mechanisme is dat leidt tot de ontwikkeling van CIN in humane kanker. De vindingen van hoofdstuk 5 suggereren dat de aanwezigheid van CIN kan duiden op een tumor met verhoogd maligne potentieel. Een uitgebreid onderzoek naar de relatie tussen hoog en laag risico adenomen en de aanwezigheid van CIN daarin kan belangrijke inzichten geven in de bijdrage van CIN aan maligne transformatie en kan resulteren in klinische implementaties om het risico van premaligne tumoren te bepalen. Hoofdstuk 6 baant ten slotte de weg vrij voor nader onderzoek naar de bijdrage van CIN aan de vorming van typische aneuploïdïen die voorkomen in vele soorten kanker. Dergelijke studies kunnen inzicht geven in wat de bijdrage van deze aneuploïdïen is aan het maligne gedrag van deze tumoren, alsmede in de invloed van evolutionaire processen op de vorming van een tumor.



## Curriculum Vitae

Richard Hermanus van Jaarsveld werd op 3 juni 1987 geboren te Woerden. In 2005 behaalde hij zijn VWO diploma aan het Kalsbeek College te Woerden. Na een jaar de bachelor Farmaceutische Wetenschappen aan de Vrije Universiteit te Amsterdam te hebben gevolgd, begon hij in 2006 met de bachelor Biomedische Wetenschappen, tevens aan de Vrije Universiteit te Amsterdam. Na deze in 2010 te hebben afgerond begon hij aan de master Oncology, tevens aan de Vrije Universiteit te Amsterdam. Tijdens deze master heeft hij zijn eerste stage volbracht aan het Cancer Centre Amsterdam in de groep van prof. dr. C. R. Jimenez onder begeleiding van dr. M. de Wit. Tijdens deze stage heeft hij onderzoek gedaan naar de aanwezigheid van eiwitten die indicatief zijn voor maligne transformatie in dikkedarmkanker in exosomen. Zijn tweede stage heeft Richard vervuld in het Centre for Molecular Medicine te Wenen, Oostenrijk in de groep van dr. S. Nijman onder begeleiding van dr. M. Smida. Gedurende deze stage heeft hij bijgedragen aan drug screens, gericht op nieuwe therapeutische mogelijkheden voor longkanker en gebaseerd op het concept van synthetische letaliteit. Tevens heeft Richard een literatuurstudie geschreven over de toepassingen van het syntetische letaliteit concept voor de behandeling van kanker. Richard verkreeg zijn master Oncology in 2013 en in mei van dat jaar begon hij als promovendus in de groep van prof. dr. G.J.P.L. Kops in het UMC Utrecht en per september 2015 in het Hubrecht Instituut. Het in dit proefschrift beschreven onderzoek is gedurende de periode in de groep van prof. dr. G.J.P.L. Kops, van mei 2013 tot en met oktober 2018, uitgevoerd.



## List of Publications

Drost, J., **van Jaarsveld, R.H.**, Ponsioen, B., Zimmerlin, C., et al. (2015). Sequential cancer mutations in cultured human intestinal stem cells. *Nature* 521, 43–47.

**van Jaarsveld, R.H.** and Kops, G.J.P.L. (2016). Difference Makers: Chromosomal Instability versus Aneuploidy in Cancer. *Trends Cancer* 2, 561–571.

Bolhaqueiro, A.C.F., **van Jaarsveld, R.H.**, et al. (2018). Live imaging of cell division in 3D stem-cell organoid cultures. *Methods in Cell Biology* 145, 91–106.



## Dankwoord

For your convenience I have put all names in **bold**, so you don't have to read all this to see if you're in it. If not, I'm sorry, believe me when I say I am also grateful towards your support the past years but I completely forgot to put you in the list. So this one's for you: thanks to **those forgotten!**

**Geert**, jouw passie en enthousiasme voor biologie en wetenschap in het algemeen zorgt ervoor dat eenieder die in jouw omgeving mag werken nog net iets meer plezier heeft om onderzoek te doen. Ik wil je bedanken voor de vrijheid en het vertrouwen dat je me hebt geschonken om mijn projecten op mijn eigen manier in te vullen.

Mijn commissie leden, **Hugo** en **Alain**. Bedankt voor jullie interesse in en feedback op mijn traject als PhD student. Jullie positiviteit ten opzichte van mijn projecten was een soms welkome duw in de rug. Hugo, jij in het bijzonder bedankt voor het instrueren van mij als organoid-kweek-robot in de vroege fase van mijn promotietraject. Tevens wil ik alle leden van de leescommissie (**Rene**, **Susanne** en **Marcel**) hartelijk danken voor hun tijd en interesse in mijn werk.

&

Dit proefschrift had niet tot stand kunnen komen zonder een aantal waardevolle samenwerkingen. **Bas**, bedankt voor vele zaken, maar met name de uren samen achter de microscoop met een gierende blues gitaar op de achtergrond. Ik hoop dat we elkaar ook in de toekomst nog op de hoogte zullen houden van onze nieuwste muzikale ontdekkingen. **Jarno**, dat ik mocht aansluiten bij jouw project is een essentiële zet binnen mijn promotietraject gebleken, dat moge duidelijk zijn uit de hoofdstukken 3 en 4. Bedankt dat je mij die mogelijkheid hebt gegeven en ik wens je alle succes en geluk met je eigen lab. **Riccardo** en **Matthias**, bedankt voor het materiaal dat ik dankzij jullie heb kunnen toevoegen aan hoofdstuk 5. **Marcel** en **Nathalie**, een DNA-fiber assay is nog niet zo makkelijk dus ik prijs me gelukkig dat ik dat dankzij jullie niet helemaal zelf heb hoeven uitvoeren. **Jan Paul** en medewerkers, de FAP-adenomas zijn een essentieel onderdeel geworden van mijn proefschrift, bedankt voor het beschikbaar stellen van dit materiaal.



Vervolgens wil ik hen bedanken met wie ik dagelijks heb mogen samenwerken. Allereerst **Wilma**, bijna tegelijk begonnen en nu bijna tegelijk klaar. Zonder onze koffiepauzes had ik nooit zover gekomen, bedankt voor het aanhoren van mijn (wetenschappelijke) frustraties en ik wil je alvast alle succes wensen in Schotland. **Claudia**, bedankt voor alle hulp en ondersteuning die je hebt geboden, ik hoop dat je op je nieuw ingeslagen weg je plek vindt. **Antoinette**, een PhD student kan zich geen betere labmanager wensen. Ik wens je alle geluk met de grondige verandering in je carrière.

Mannen van de Mancave, **Ajit, Bas, Sjoerd, Spiros** en **Timo**, bedankt voor een fijne sfeer op kantoor waar altijd ruimte was voor een serieuze wetenschappelijk discussie en altijd ondersteuning om de juiste figuren te vinden. Ajit, ik hoop dat de hondjes je kunnen bijhouden tijdens het uitlaten. Heel veel succes met je eigen bedrijf. Bas, bijzonder bedankt voor alle spierpijn na het squashen, maar nog iets meer voor de broodjes kroket die we daarmee bij elkaar verdiend hebben. Sjoerd, bedankt voor een fijne samenwerking en ik hoop dat we het snel tot een fantastisch einde kunnen brengen. Spiros, please forgive me for all the inappropriate jokes I made and all the best for finishing your PhD and future career. Timo, bedankt voor je support als ik weer eens met ImageJ klem zat, en we moeten nog een keertje een etentje plannen, prik jij even een datum?

**Nannette**, voor een wetenschapspurist als jij is het niet altijd even makkelijk in het moderne wetenschappelijke klimaat. Des te meer respect heb ik voor jouw oog voor detail. We zien elkaar snel weer in ons mooie Woerden. **Carlos**, spreek je tegenwoordig al Nederlands? Probably not, so: you must be the kindest guy I ever met and will meet. Please don't hesitate to contact me if you want to complain about how terrible it is to analyze missegregations, I would love to join in. **Banafsheh**, bijzonder om te zien hoe verschillend mensen tegen het leven aan kunnen kijken, maar soms zou ik juist iets meer Bana moeten zijn. **Eelco**, jouw oneindige interesse in alles wat wetenschap is, is uitzonderlijk. Ik hoop dat je carrière je ver brengt, want wetenschappers zoals jij ben ik te weinig tegen gekomen. **Vincent**, je bent by-far de beste astroloog die ik ken, heel veel geluk aan de andere kant van de wereld! **Pim**,

&



altijd fijn om iemand in de groep te hebben die van een slap kletspraatje houdt. Ik hoop dat je nog lang door mag jeppen (zo zeg je dat toch?). **Jingchao**, thank you for your puzzling type of humor and all the best with your projects. **Anko**, jammer dat we uiteindelijk nooit samen muziek hebben gemaakt, wie weet komt dat nog in de toekomst! Newbies **Kim**, **Nico**, **Bastiaan** en **Emine**, I wish you all the best for your time in the Kops Lab and beyond. Thanks as well to all former lab members with whom I have worked with: **Richarda**, **Deborah**, **Alexandra**, **Wilco**, **Tale**, **Xiaorong**, **Joris**, I wish you all the very best. **Manja**, I have missed your energizing presence in the lab ever since you left. I hope we can play Lingo soon again.

Bedankt ook **Mattie** voor ontelbare kopjes koffie in ons vertrouwde HvdB en memorabele avondjes stappen. Tot snel in Berlijn!

**Elianne**, jouw stageproject bleek niet het makkelijkste te zijn. Des te meer bewondering heb ik voor jouw doorzettingsvermogen. Zonder jouw bijdrage had hoofdstuk 6 nooit van de grond gekomen.

Bedankt **Litha** voor je ondersteuning in de laatste maanden, met jouw support hoeft geen promovendus in het Hubrecht zich druk te maken over de administratie.

**Marjan**, zonder jouw deskundige ondersteuning had dit boekje er heel anders uit gezien. Bedankt voor je hulp. **Cees Willem**, een kleine, maar niet onbelangrijke bijdrage aan mijn cover, bedankt! Tot snel op een van onze altijd gezellige etentjes.

Zoals de titel van dit proefschrift doet vermoeden, heeft muziek een belangrijke plek in mijn leven. Muziek maken met vrienden samen is dan ook het meest dierbare moment van ontspanning. Bedankt **Cor**, **Joost**, **Maarten**, **Michel** en **Nick** voor het bieden van deze uitlaatklep. Ik hoop dat er nog vele gezellige repetitieavonden en optredens in het verschiet mogen liggen.

Bedankt ook mijn biljartmaten **Ad**, **Daan** en **Jac** voor de altijd gezellige competitieavonden en in het bijzonder de potjes 10-over-rood na afloop.

**Stephan en Renate**, bedankt voor altijd een goed -of slecht- gesprek onder het genot van een drankje en potje darts.

**Koen en Guido**, ooit zijn wij samen aan ons academische avontuur begonnen. Nu, op de climax van dit avontuur, kunnen jullie niet onvermeld blijven. Bedankt voor een bijzondere vriendschap.

Mannen van K', **Diego, Erik, Gerben en Jeroen**, even aan de bar over niks praten is altijd een goede manier om de zinnen te verzetten, bedankt daarvoor.

**Jelmer en Vasco**, onze roadtrip vond plaats op een cruciaal punt in mijn promotietraject. Bedankt voor deze nodige afleiding en mooie herinneringen. Bedankt ook voor de avonden spiegeltje-krak en balletje-tik en vooral bedankt dat jullie jullie zijn.

Mijn lieve paranimfen, mijn zussen, **Judith en Karin**. Het is niet toevallig dat ik jullie achter mij wil hebben staan op dit belangrijke moment in mijn leven. Ik voel me gezegend met jullie aan mijn zijde.

Lieve **Mam**, niet altijd de makkelijkste zoon, maar hier sta ik dan. Eerlijk is eerlijk, zonder jouw spreekwoordelijke schoppen onder de kont had ik hier nooit gekomen, dus als er iemand bedankt moet worden ben jij het. Bedankt ook voor je onvoorwaardelijke steun, begrip, liefde en zorg. Je bent een moeder uit duizenden.

Last but not least, my dear **Camilla**. It is safe to say that without you, I would have not made it to this point. Thank you for your love and support. I am convinced we are heading towards a bright future together and nothing can stay in our way as long as we're together. I love you till the moon and back, and a bit more.

&

